SYNTHESIS AND CHARACTERIZATION OF RUTHENIUM MALTOLATO, SULFOXIDE, AND NITROIMIDAZOLE COMPLEXES AS POTENTIAL ANTICANCER AGENTS

by

Adam Wu

B. Sc. (Hons.), The University of British Columbia, 2000

A THESIS SUBMITTED IN PARTIAL FULFILMENT
OF THE REQUIREMENTS FOR THE DEGREE OF

MASTER OF SCIENCE

in

THE FACULTY OF GRADUATE STUDIES
(Department of Chemistry)

We accept this thesis as conforming to the required standard

THE UNIVERSITY OF BRITISH COLUMBIA
October, 2002

In presenting this thesis in partial fulfilment of the requirements for an advanced degree at the University of British Columbia, I agree that the Library shall make it freely available for reference and study. I further agree that permission for extensive copying of this thesis for scholarly purposes may be granted by the head of my department or by his or her representatives. It is understood that copying or publication of this thesis for financial gain shall not be allowed without my written permission.

Department of Chemistry

The University of British Columbia
Vancouver, Canada

Date NOV. 7, 2002

DE-6 (2/88)

Abstract

The anticancer properties of Ru sulfoxide and imidazole complexes, including *cis*-$RuCl_2(DMSO)_3(DMSO)$, *trans*-$RuCl_2(DMSO)_4$, and [*trans*-$Ru(Im)(DMSO)Cl_4]^-$ have previously been studied by other groups (DMSO and DMSO = S-bonded and O-bonded dimethylsulfoxide, respectively; Im = imidazole). This thesis work concerns the use of Ru maltolato complexes in this regard; maltol (3-hydroxy-2-methyl-4-pyranone), being a non-toxic, water-soluble food additive, is suitable for biological use.

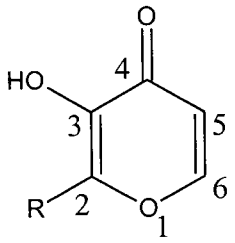

R = Me, maltol (Hma);
R = Et, ethylmaltol (Hetma)

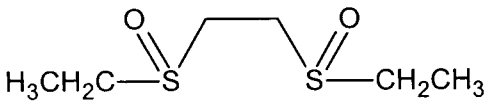

BESE

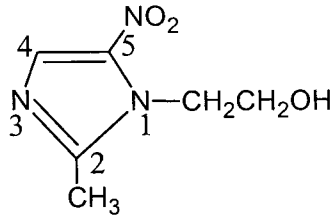

metronidazole (metro)

Several Ru^{II} bis(maltolato) and bis(ethylmaltolato) complexes with ancillary monodentate and bidentate sulfoxide ligands (DMSO, TMSO, and BESE) have been synthesized and well characterized, as well as a Ru^{II} BESE-metronidazole complex, $RuCl_2(BESE)(metro)_2$ (TMSO = tetramethylenesulfoxide, BESE = 1,2-bis(ethylsulfinyl)ethane, metro = metronidazole). Some Ru^{III} maltolato complexes have also been synthesized in order to compare their anticancer activities to those of related Ru^{II} complexes. The Ru complexes were characterized by a variety of spectroscopic techniques, including NMR, UV-vis, IR, and MS; elemental analysis and solution conductivity data were also collected. Cyclic voltammetry was used to determine the reduction potentials of various Ru complexes. X-ray crystallographic structures were determined for *cis*-$Ru(ma)_2$(*S,R*-BESE), *trans*-$RuCl_2$(*R,R*-BESE)$(metro)_2$, and *trans*-$[Ru(ma)_2(metro)_2](CF_3SO_3)$ (ma = maltolato). The sulfoxide ligands are exclusively S-bonded as observed in the IR and ^1H NMR spectra, and in the first two X-ray structures.

Of the complexes tested, $Ru(ma)_3$ and $Ru(etma)_3$ (etma = ethylmaltolato) exhibit the best anticancer activities against human breast cancer cells (MDA435/LCC6) in the *in*

vitro MTT assay (a colorimetric determination of cancer cell viability), in terms of the lowest IC_{50} values of 150 and 80 μM, respectively, IC_{50} being the drug concentration that kills 50 % of the cancer cells relative to the control. The Ru^{II} maltolato-sulfoxide complexes also showed some anticancer activities, with $Ru(etma)_2(DMSO)_2$ being the most potent (IC_{50} = 470 μM). The ethylmaltolato complexes are generally more effective than the corresponding maltolato complexes. Further anticancer testing of Ru maltolato complexes is encouraged from these preliminary results.

Table of Contents

List of Figures

List of Tables

List of Symbols and Abbreviations

acac	acetylacetonate/acetylacetonato
AMP	adenosine 5′-monophosphate
Anal.	analysis
ApG	3′→5′-adenylyl guanosine monophosphate
asym.	asymmetric
ATP	adenosine 5′-triphosphate
BBSE	1,2-bis(butylsulfinyl)ethane
BESE	1,2-bis(ethylsulfinyl)ethane
BETE	3,6-dithiaoctane
BMSE	1,2-bis(methylsulfinyl)ethane
BMSP	1,3-bis(methylsulfinyl)propane
BPSE	1,2-bis(propylsulfinyl)ethane
BPSP	1,3-bis(propylsulfinyl)propane
br	broad
Bu	butyl
Calcd	calculated
CD	circular dichroism
CHO cells	Chinese hamster ovary cells
CMP	cytidine 5′-monophosphate
COD	1,5-cyclooctadiene
conc.	concentrated
CV	cyclic voltammetry
d	doublet
2D COSY	two-dimensional correlation spectroscopy
2′-dA	2′-deoxyadenosine
dApG	3′→5′-deoxy(adenylyl guanosine monophosphate)
2′-dC	2′-deoxycytidine
2′-dG	2′-deoxyguanosine

5′-dGMP	deoxyguanosine 5′-monophosphate
dGpA	3′→5′-deoxy(guanylyl adenosine monophosphate)
dGpG	3′→5′-deoxy(guanylyl guanosine monophosphate)
DMEM	Dulbecco's modified Eagle's medium
DMF	*N,N*-dimethylformamide
DMSO	dimethylsulfoxide
DM<u>S</u>O	S-bonded dimethylsulfoxide
DMS<u>O</u>	O-bonded dimethylsulfoxide
DNA	deoxyribonucleic acid
2′-dT	2′-deoxythymidine
$E_{½}$	electrochemical half-wave potential
EDTA	ethylenediaminetetraacetate
ES	electrospray
Et	ethyl
etma	ethylmaltolate/ethylmaltolato
FBS	fetal bovine serum
$FeCp_2$	ferrocene
$FeCp^*_2$	bis(pentamethylcyclopentadienyl)iron(II)
GMP	guanosine 5′-monophosphate
GpA	3′→5′-guanylyl adenosine monophosphate
h	hour
hfac	1,1,1,5,5,5-hexafluoroacetylacetonate/1,1,1,5,5,5-hexafluoroacetylacetonato
HPCE	high performance capillary electrophoresis
HPLC-MS	high performance liquid chromatography-mass spectrometry
IC_{50}	initial concentration where 50 % of the cells die
Im	imidazole
Ind	indazole
IR	infrared
J	coupling constant (Hz)

LD_{50}	the dosage that kills 50 % of the organism
LR	low resolution
LSIMS	liquid secondary ion mass spectrometry
m	multiplet
M	molar (mol L^{-1})
ma	maltolate/maltolato
Me	methyl
2-MeIm	2-methylimidazole
5-MeIm	5-methylimidazole
metro	metronidazole
min	minute
mol	mole
MS	mass spectrometry
MTT	3-(4,5-dimethylthiazol-2-yl)-2,5-diphenyltetrazolium bromide
n	normal
NAMI	Na[*trans*-Ru(Im)(DMSO)Cl_4]
NAMI-A	(ImH)[*trans*-Ru(Im)(DMSO)Cl_4]
3-NBA	3-nitrobenzylalcohol
N-MeIm	N-methylimidazole
NMR	nuclear magnetic resonance
4-NO_2Im	4-nitroimidazole
5-NO_2Im	5-nitroimidazole
ORTEP	Oakridge Thermal Ellipsoid Program
p	para
PBS	phosphate-buffered saline solution
p-cymene	*para*-isopropyltoluene
Ph	phenyl
ppm	part per million
q	quartet
RNA	ribonucleic acid

r.t.	room temperature
s	singlet
SCE	saturated calomel electrode
SER	sensitizer enhancement ratio
sym.	symmetric
t	triplet
tert	tertiary
THF	tetrahydrofuran
TLC	thin layer chromatography
TMP	thymidine 5′-monophosphate
TMSO	tetramethylenesulfoxide
TM<u>S</u>O	S-bonded tetramethylenesulfoxide
TOF	time of flight
UV-vis	ultraviolet-visible
v	very
δ	chemical shift (ppm)
ε_{max}	extinction coefficient (L mol^{-1} cm^{-1})
Λ_M	molar conductance (Ω^{-1} cm^2 mol^{-1})
λ_{max}	wavelength of maximum absorbance (nm)
μ	bridging coordination mode
ν	wavenumber (cm^{-1})

Key to Numbered Complexes

1 *cis*-$RuCl_2(DMSO)_3(DMSO)$

2 *trans*-$RuCl_2(DMSO)_4$

3 $(ImH)[trans\text{-}Ru(Im)_2Cl_4]$

4 $(IndH)[trans\text{-}Ru(Ind)_2Cl_4]$

5 $Na[trans\text{-}Ru(Im)(DMSO)Cl_4]$

6 $(ImH)[trans\text{-}Ru(Im)(DMSO)Cl_4]$

7 *cis*-$RuCl_2(TMSO)_4$

8 $RuCl_2(DMSO)_2(4\text{-}NO_2Im)_2$

9 *cis*-$RuCl_2(BESE)(DMSO)(DMSO)$

10 $[RuCl_2(p\text{-cymene})]_2(\mu\text{-BESE})$

11 $Ru(ma)_2(DMSO)_2$

12 $Ru(etma)_2(DMSO)_2$

13 $Ru(ma)_2(TMSO)_2$

14 $Ru(etma)_2(TMSO)_2$

15 $[RuCl(H_2O)(BESE)]_2(\mu\text{-}Cl)_2$

16 *cis*-$RuCl_2(BESE)_2$

17 *cis*-$Ru(ma)_2(BESE)$

18 *cis*-$Ru(etma)_2(BESE)$

19 $RuCl_2(BESE)(metro)_2$

20 $RuCl_2(BESE)(4\text{-}NO_2Im)_2$

21 $RuCl_2(metro)_4$

22 $RuCl_2(4\text{-}NO_2Im)_4$

23 *mer*-$Ru(ma)_3$

24 *mer*-$Ru(etma)_3$

25 *trans*-$[Ru(ma)_2(metro)_2](CF_3SO_3)$

26 *trans*-$[Ru(etma)_2(metro)_2](CF_3SO_3)$

Key to Ligand Structures

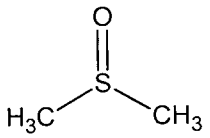

DMSO

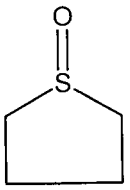

TMSO

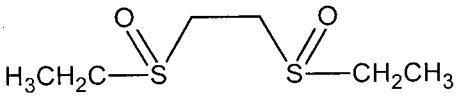

BESE

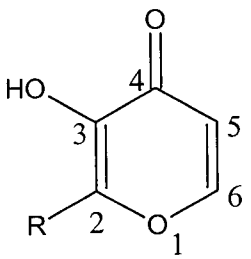

R = Me, maltol (Hma);
R = Et, ethylmaltol (Hetma)

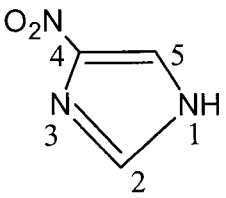

4-nitroimidazole
(4-NO_2Im)

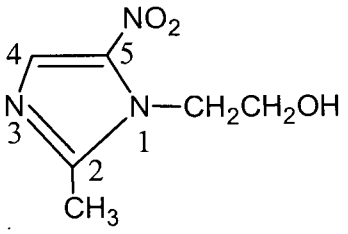

metronidazole
(metro)

Acknowledgements

I would like to thank my supervisor, Prof. Brian James, for his off-hand approach throughout this project. I thank him for giving me lots of freedom, lab space, and funding for the research. I also acknowledge Prof. Kirsten Skov from the BC Cancer Research Center for collaboration in the *in vitro* biological testing.

I thank Dr. Craig Pamplin for his guidance throughout my years of graduate work. He is an ideal mentor who provided help, in terms of showing me many cool lab techniques any time of the day. I also thank him for proofreading my thesis. I thank David Kennedy for all his research ideas, although most of them did not work as well as proposed. I thank Dr. Chi-Wing Tsang for teaching me how to collect ^{1}H 2D COSY NMR spectra, and also for being my loyal lunch buddy for two years. I hope his JACS dream will one day come true.

I thank Prof. Gábor Besenyei for showing me how to grow crystals the "size of an elephant"; unfortunately the method only works for selected Pd complexes. I thank Bronwyn Gillon and Kevin Ralloff for fun lunch pastimes and entertaining pool games. I thank Raymond Lam for being a great coffee buddy in my first year of study. I hope he will make big bucks in the business side of chemistry (rather than the synthesis side).

I thank Lynsey Huxham for assistance with the MTT assay, Jennifer Hutcheon for preparing the "soon to be killed" human breast cancer cells, Krisztina Paal for letting me use the plate reader, and Helen Wright for lending me the $800 multi-channel pipet. I also thank Dr. Elena Polishchuk and Mona Rizvi for their wonderful help in the Biological Services.

I thank David Green of the Orvig group for supplying abundant maltol and ethylmaltol. I thank Tracey Stott of the Wolf group for her generous help in using the CV instrument. I thank Dr. Brian Patrick for solving my crystal structures, and for training me to have lots of patience to wait for my turn. I thank the NMR technicians, Marietta Austria and Lianne Diarge, for their invaluable NMR assistances. I thank the MS technicians, Lina Madilao and Marshall Lapawa, very much for running my samples. I also thank Lina for teaching me to operate the ES ion trap. I would like to acknowledge Dr. Gunther Eigendorf and Dr. Yun Ling for their generous help. I thank the now-retired

Peter Borda for running EA samples and for encouraging me to make sure that my samples are pure and abundant. I thank the SFU EA technician, M. K. Yang, for doing an excellent job analyzing my samples.

I acknowledge my Ru predecessors: Peter Chan, Donald Yapp, Elizabeth Cheu, Ian Baird (whose elemental analyses contain plenty and variety of solvents), and again Lynsey Huxham for their thick-thesis works. I acknowledge the present James group members: Júlio Rebouças, Paolo Marcazzan, Maria Ezhova, Jo Ling Foo, Guibin Ma, and Jenkins Tsang for their presences.

This thesis is dedicated to my family,

and to those who have inspired me enormously throughout this work:

Fédéric Chopin, Felix Mendelssohn, Camille Saint-Saëns, Max Bruch, and the

impetuoso, Henry Charles Litolff.

CHAPTER 1

Introduction to Ruthenium Chemistry and Anticancer Research

1.1 Preamble

A cancer or malignant tumor is the abnormal growth of cells caused by mutations which can be triggered by mutagens such as radiation and chemicals.[1] Cancerous cells differ from normal cells by many different phenotypic changes: rapid division rate, invasion of new cellular territories, higher metabolic rate, and modified shape. A cancer cell does not arise from a single mutation; a series of sequential mutations must occur within a single cell for it to become cancerous.[1] This leads to uncontrolled proliferation and the invasive destruction of healthy neighboring cells, and may eventually give rise to metastases, the spread of a cancerous tumor.

Metal-based anticancer drugs originated in 1965 with the discovery by Rosenberg *et al.* of cell division inhibition in *Escherichia coli* by electrolysis products formed at a platinum electrode.[2] Platinum complexes, including the well-known cisplatin (Figure 1.1), were found to inhibit sarcoma 180 and leukemia L1210 in mice,[3] and cisplatin was approved for the treatment of testicular and ovarian cancer in 1978.[4] However, the severe toxicity of cisplatin has led to a search for other potent Pt derivatives. These included carboplatin, which is less toxic and has been approved for clinical use, and orally active AMD473 and JM216 (Figure 1.1).

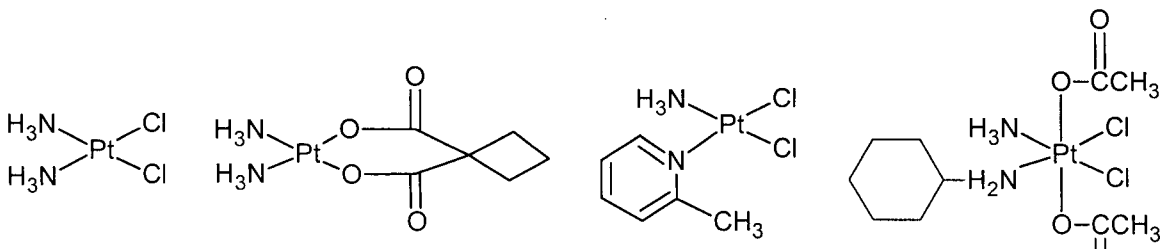

Figure 1.1 Structures of cisplatin, carboplatin, AMD473, and JM216.

References on page 25

The general mechanism of cancer growth inhibition involves the binding of the Pt complexes to DNA.[5] Cisplatin, for example, undergoes chloride dissociation in water to give monoaquo and diaquo species that are "active" toward DNA. The Pt center can bind to two adjacent guanine bases at their N_7 positions to form an adduct of intrastrand crosslink. This causes a bend in the overall DNA structure and inhibits DNA replication in cancer cells.

Because of the success of Pt anticancer drugs, the search for other metal-based drugs is continuing. Only a narrow range of tumors can be treated with cisplatin, while other Pt drugs, although less toxic, are only active in the same range of tumors.[4] Some tumors show natural resistance to cisplatin, while others develop resistance after the initial treatment. As a result, the anticancer research of Ru complexes was initiated in the 1970s in the hope of combating other kinds of tumors, as well as Pt-resistant ones. The remainder of this introduction is devoted to a discussion of potential Ru anticancer complexes.

1.2 Ruthenium(II) Sulfoxide Complexes: *Cis*-$RuCl_2(DMSO)_3(DMSO)$ and *Trans*-$RuCl_2(DMSO)_4$

1.2.1 Synthesis, Structure, and Aqueous Chemistry

The anticancer research of Ru complexes started in the early 1970s. *Cis*-$RuCl_2(DMSO)_3(DMSO)$ (**1**) was first synthesized by James *et al.* in 1971, where DMSO and DMSO represent S- and O-bonded dimethylsulfoxide, respectively.[6] The synthesis was greatly simplified by Evans *et al.* in 1973.[7] The structure was determined by Mercer and Trotter in 1975,[8] and has also been published by other groups.[9,10] The structure illustrates the ambidentate nature of DMSO by showing three S-bonded DMSO ligands in a facial configuration and one O-bonded DMSO, as previously observed in the IR and ^1H NMR spectra.[6,7] The initial interest in the James group was to synthesize Ru sulfoxide complexes as olefin hydrogenation catalysts.[11] However in 1975, Monti-Bragadin *et al.* reported *in vitro* testing of **1** that possessed mutagenic activity in bacteria by interacting with DNA.[12] Complex **1** was therefore proposed as a potential antitumor substance because of its comparable mutagenic activity to that of cisplatin.

References on page 25

The synthesis and X-ray structure of *trans*-$RuCl_2(DMSO)_4$ (**2**) were reported by Alessio *et al.* in 1988.[10] Complex **2** was synthesized by photochemical isomerization of the thermodynamically more stable *cis*-isomer (**1**) in DMSO. The structure of **2,** which shows four S-bonded DMSOs, was also published by Jaswal *et al.* following a new synthetic method.[13] The aqueous chemistry of **1** and **2** is shown in Figure 1.2.[10]

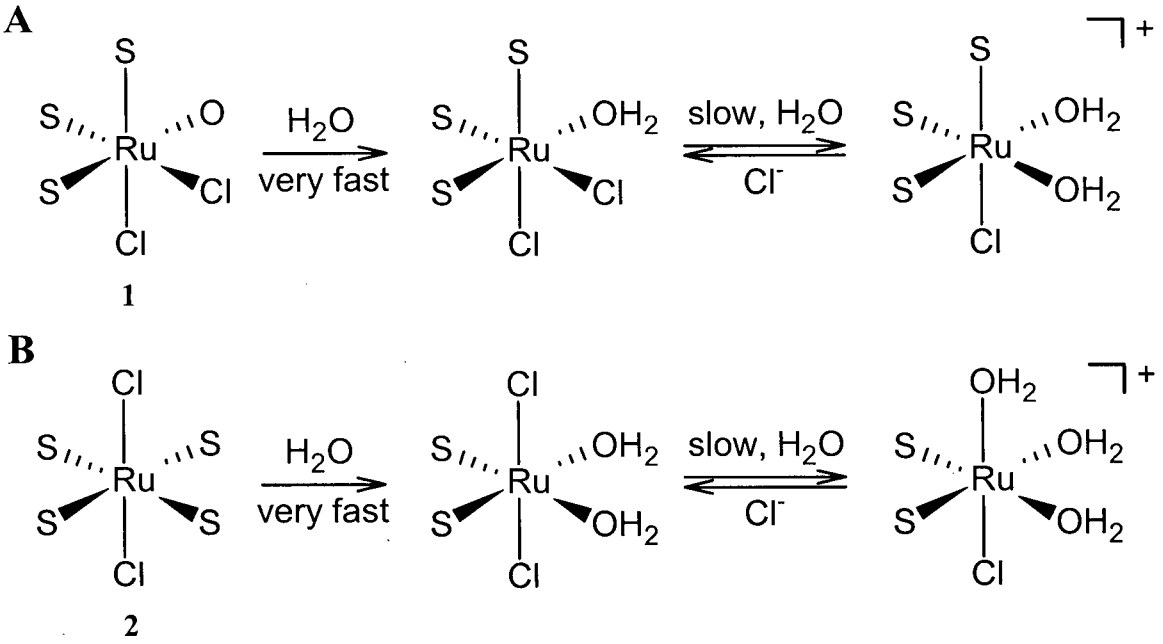

Figure 1.2 The aqueous chemistry of *cis*-$RuCl_2(DMSO)_3(DMSO)$ (**1**) (A) and *trans*-$RuCl_2(DMSO)_4$ (**2**) (B), where S and O represent S- and O-bonded DMSOs, respectively (adapted from ref. 10).

The O-bonded DMSO in **1** is immediately replaced by H_2O when the complex is dissolved in aqueous solutions.[10] Slow chloride dissociation then occurs over 10 h at 25 °C or 3 h at 37 °C to give a 1:1 electrolyte. On the other hand, two adjacent S-bonded DMSOs in **2** are immediately replaced by H_2O upon dissolution of the complex in water, and then a similar chloride displacement takes place. The dissociation of chloride for both species is inhibited in 150 mM NaCl (extracellular concentration), but not in 3 mM NaCl (intracellular concentration). This implies that **1** and **2** convert into monoaquo and *cis*-

References on page 25

diaquo neutral species, respectively, outside the cell. Once inside the cell, the neutral species will lose a chloride to form cationic complexes capable of DNA binding.

1.2.2 Anticancer Bioassays

The *in vivo* testing of **1** was undertaken by Sava *et al.* using mice bearing Lewis lung carcinoma, B16 melanoma, and MCa mammary carcinoma.[14] Equitoxic dosages were administered for cisplatin and **1** (0.52 and 610 mg/kg/day, respectively). The result indicated that **1** was as effective as cisplatin against primary tumor growth and lung metastases, and was significantly less toxic (LD_{50} = 1000 mg/kg for **1** and 0.94 mg/kg for cisplatin). It was hoped that Ru drugs would overcome the toxic side-effects of cisplatin, while contributing comparable anticancer activity.

The *in vivo* testing of **1** and **2** was subsequently reported in mice bearing Lewis lung carcinoma.[10] Equitoxic dosages were administered (700 for **1** and 37 mg/kg/day for **2**). Both species were partially active against primary tumor growth, but more effective against lung metastases. Because **2** was administered at a 20-fold lower dosage, the *trans*-isomer was more toxic and potent than the *cis*-isomer. Similar anticancer results were obtained for testing bromo and iodo derivatives of **1** and **2**.[10,15]

Further *in vivo* testing was reported by Coluccia *et al.* using mice bearing P388 and P388/DDP leukemia; the latter was a subline made resistant to cisplatin.[16] Both **1** and **2** showed significant activity against P388 leukemia, although the survival time of mice treated with the Ru drugs was not as pronounced as those treated with cisplatin. The percent reduction of peritoneal tumor growth treated with cisplatin, **1**, and **2** was 99, 62, and 30 %, respectively. Thus, cisplatin was more effective than the Ru drugs in P388 leukemia. However, the reverse was observed for P388/DDP leukemia. This implies that **1** and **2** can treat cisplatin-resistant tumors.

1.2.3 DNA Binding Studies

In 1982, Farrell and De Oliveira demonstrated the reaction between **1** and two equivalents of adenine or guanine (Figure 1.3) in DMSO to generate Ru-purine adducts, of which $[Ru(adenine)_2(DMSO)_3(DMSO)]Cl_2$ was isolated analytically pure.[17] The IR spectral data indicated the retention of the S- and O-bonded DMSOs, but the ^1H NMR

References on page 25

signals of H_2 and H_8 of adenine were not clearly resolved. The binding site was tentatively assigned as between Ru and the N_7 position of adenine, based on the ^1H NMR data of an analogous Rh complex, $RhCl_3(adenine)(DMSO)_2$.

Figure 1.3 Structures of adenine (left) and guanine showing their N_7 binding sites.

Cauci *et al.* reported the reaction between **1** and double-stranded DNA, poly(dGdC) and poly(dAdT) in aqueous solutions.[18] Complex **1** preferably bound to adenine and guanine bases over the pyrimidine ones. The binding site was tentatively assigned as between Ru and the N_7 positions of the purines, although binding between Ru and the adenine N_1 position was considered possible.

Alessio *et al.* reported on the reaction between **2** and deoxyguanosine 5′-monophosphate (5′-dGMP, Figure 1.4) in water to give two diastereoisomeric monoadducts, $[RuCl(H_2O)(DMSO)_2(5'\text{-dGMP})]^-$, while no bis-adduct was observed.[19] The Ru center was chelated between the N_7 guanine moiety and the 5′-phosphate of 5′-dGMP, as deduced from the ^1H and ^{31}P NMR spectra, and the monoadducts exhibited opposite chirality at the Ru center, as observed in the CD spectra. However, the monoadduct structures were not assigned because of many possible isomeric forms. An analogous reaction between **1** and 5′-dGMP, reported by Tian *et al.*, resulted in the formation of two diastereoisomeric monoadducts, $[RuCl(DMSO)_3(5'\text{-dGMP})]^-$, with opposite chirality (Figure 1.5).[20] The phosphate binding inhibited the formation of a bis(5′-dGMP) complex in both **1** and **2.** A better model is required to study possible intrastrand crosslinking between Ru and adjacent guanine bases; presumably, the phosphodiester group in DNA should exhibit less affinity for binding Ru.[20]

References on page 25

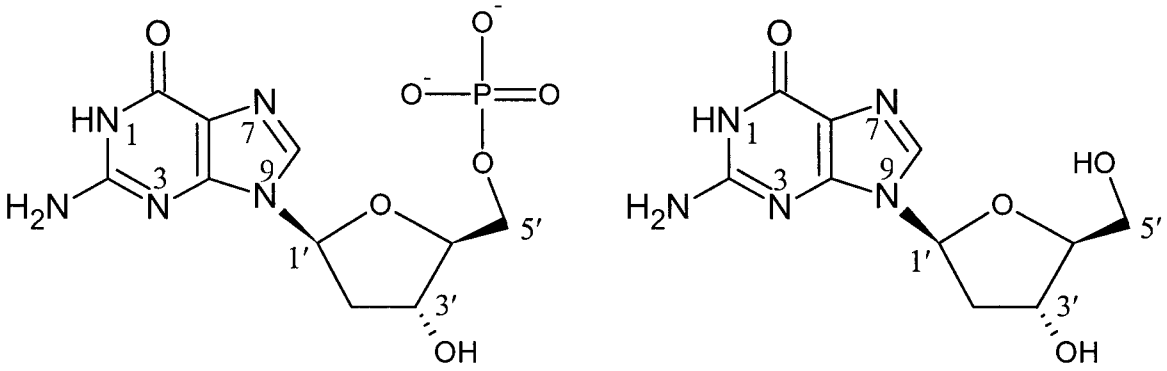

5′-dGMP 2′-dG

Figure 1.4 Structures of deoxyguanosine 5′-monophosphate (5′-dGMP) and 2′-deoxyguanosine (2′-dG) showing the N_7 binding site.

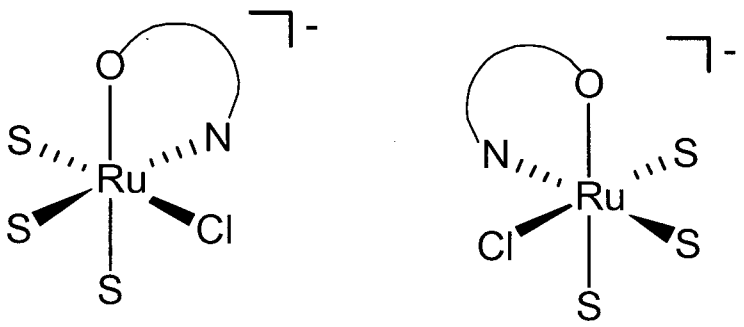

Figure 1.5 Structures of the diastereomers, $[RuCl(DMSO)_3(5'\text{-dGMP})]^-$, formed by the reaction of *cis*-$RuCl_2(DMSO)_3(DMSO)$ (**1**) and 5′-dGMP, where S represents S-bonded DMSO, and N—O represents the chelation of the N_7 guanine moiety and the 5′-phosphate of 5′-dGMP (adapted from ref. 20).

Cauci *et al.* reacted **2** with 2′-deoxyguanosine (2′-dG, Figure 1.4) in water and observed two diastereoisomeric monoadducts (**MI** and **MII**) and one bis-adduct (**B**) (Figure 1.6).[21] Complex **2** immediately formed the *cis*-diaqua species in water (cf. Figure 1.2), and the coordination of a 2′-dG through the N_7 site generated an intermediate from which chloride dissociation gives **MI** and **MII;** these can also be formed from the

References on page 25

reaction of the *fac*-triaquo species and 2′-dG (Figure 1.6). The coordination of the second 2′-dG to either **MI** or **MII** gave **B.** The absence of the 5′-phosphate in 2′-dG is thought to allow the formation of the bis-adduct.

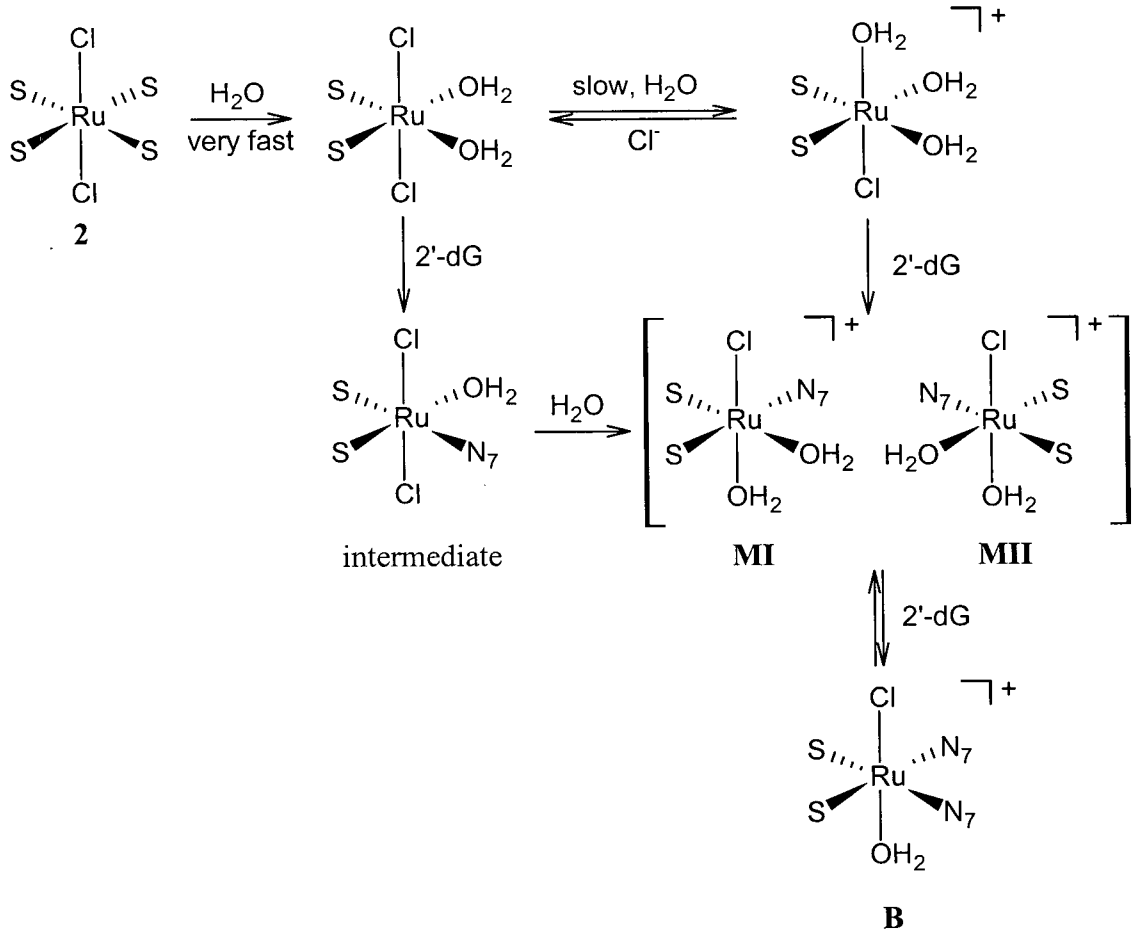

Figure 1.6 Reaction pathways between *trans*-$RuCl_2(DMSO)_4$ (**2**) and 2′-deoxyguanosine (2′-dG) in water, where S and N_7 represent S-bonded DMSO and N_7-coordinated 2′-dG, respectively. **MI** and **MII** are the diastereoisomeric monoadducts, and **B** is the bis-adduct (adapted from ref. 21).

Davey *et al.* have also reported on the reactions of **1** and **2** with nucleosides in water.[22] The reaction between **1** and 2′-dG gave **MI, MII,** and **B** products identical to those formed in the reaction of **2** with 2′-dG (see above). The O-bonded DMSO in **1** was

References on page 25

immediately displaced by H_2O, which was then displaced by 2′-dG (Figure 1.7). Subsequent dissociations of a DMSO and a chloride formed a pair of diastereoisomeric monoadducts (**MI** and **MII**), to which further coordination of 2′-dG gave the bis-adduct (**B**).

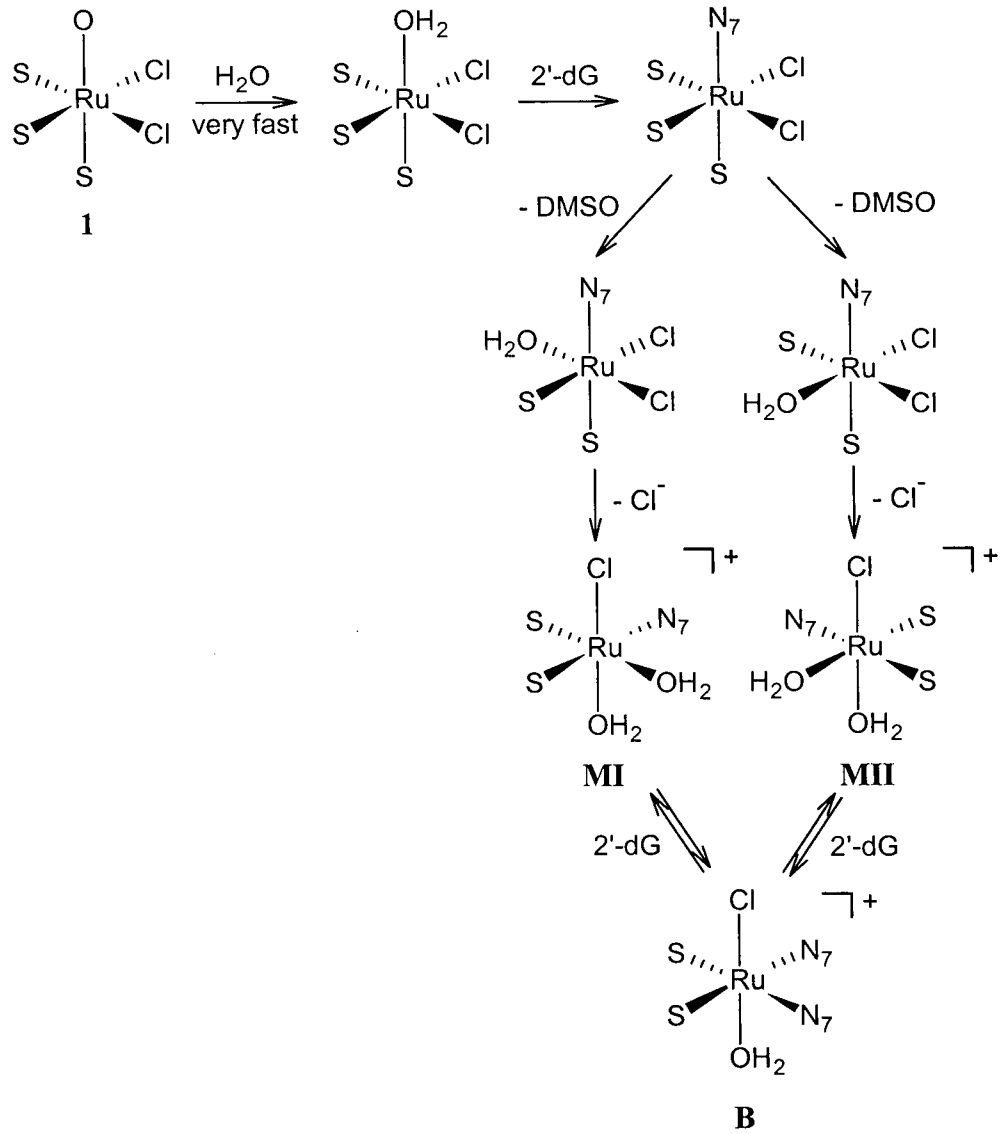

Figure 1.7 Reaction pathways between *cis*-$RuCl_2(DMSO)_3(DMSO)$ (**1**) and 2′-deoxyguanosine (2′-dG) in water, where S and O represent S- and O-bonded DMSOs, respectively. N_7 represents N_7-coordinated 2′-dG. **MI, MII,** and **B** were identical to products formed in the reaction between *trans*-$RuCl_2(DMSO)_4$ (**2**) and 2′-dG (adapted from ref. 22).

References on page 25

Complexes **1** and **2** both react with 2′-deoxyadenosine (2′-dA, Figure 1.8) to form a complex containing a single nucleoside ligand.[22] The binding site was assigned as N_1. The reaction between **2** and 2′-dA yielded a pair of diastereomers, while **1** and 2′-dA gave a mixture of products. Coordination between Ru and the N_1 atom would be unlikely in DNA because N_1 is involved in Watson-Crick hydrogen-bonding. A Ru complex may initially bind at the N_7 of the adenine base or at an adjacent guanine base to perturb the hydrogen-bonding and open up the N_1 site. Complexes **1** and **2** showed little or no reactivity towards 2′-deoxycytidine (2′-dC) and 2′-deoxythymidine (2′-dT).

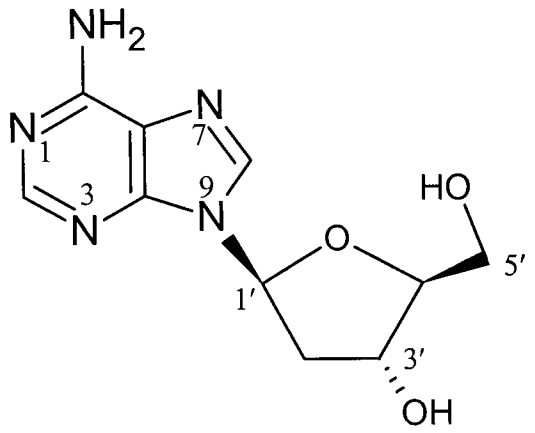

Figure 1.8 The structure of 2′-deoxyadenosine (2′-dA) showing the N_1 binding site.

Esposito *et al.* reported the reaction between **2** and dGpG, a dimeric structure of two 2′-dG joined by a phosphodiester (Figure 1.9).[23] An intrastrand crosslink between Ru and the two N_7-coordinated guanine moieties was observed, similar to that formed by cisplatin. This implies a similar anticancer mechanism in **2** despite the differences in coordination geometry. Ru binding would introduce a bend in the overall DNA structure to inhibit DNA replication and eventually lead to cell death.

Anagnostopoulou *et al.* reported the interaction of **1** and **2** with 3′ to 5′ nucleotides: GpA, dGpA, ApG, dApG (Figure 1.9), and d(CCTGGTCC).[24] GpA and ApG have a 2′-hydroxy group on their ribose sugars, while dGpA and dApG have a 2′-hydrogen. Both **1** and **2** react with a dinucleotide resulting in the formation of the same

References on page 25

major product of intrastrand crosslink. All binding sites were assigned between the Ru and the N_7 of the purine moiety. Complex **2** was found to be about 20 times more reactive than **1**; this may be related to the 20-fold greater toxicity of **2** comparing to **1** in previous cancer testing.[10] Reacting **1** and **2** with d(CCTGGTCC) gave similar G, G intrastrand binding as in the reaction of dGpG.[23]

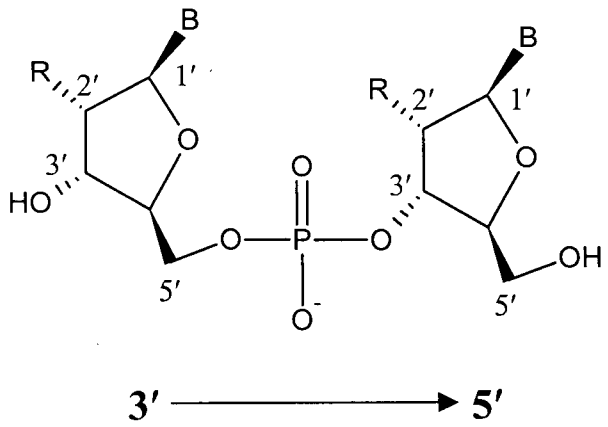

Figure 1.9 The structure of a dinucleotide showing 3′ to 5′ direction. B represents a purine base (A or G). GpA and ApG have a 2′-hydroxy group (R = OH), while dGpA and dApG have a 2′-hydrogen (R = H).

Nováková *et al.* have reported on irreversible binding of **1** and **2** with natural, double-helical DNA in cell-free media, and the binding rate of **2** was considerably greater than that of **1**.[25] Intrastrand crosslinking between neighboring purine residues was observed, with also a small amount (~1 %) of interstrand crosslinking. The DNA adduct of **2** inhibited RNA synthesis, a process performed by DNA-dependent RNA polymerases, while the adduct of **1** did not. Both Ru complexes modified the DNA conformation in a non-denaturational manner.

1.3 The Ruthenium(III) Imidazole Complex: (ImH)[*trans*-$Ru(Im)_2Cl_4$]

1.3.1 Synthesis, Structure, and Aqueous Chemistry

In 1987, Keppler *et al.* published the synthesis and structure of (ImH)[*trans*-$Ru(Im)_2Cl_4$] (**3**) made by reacting a mixture of $RuCl_3{\cdot}3H_2O$ and HCl in EtOH with excess imidazole (Im = imidazole).[26] The aqueous chemistry of **3,** elucidated by ^1H NMR spectroscopy, proceeded via stepwise aquation.[27] The initial disappearance of **3** with loss of a chloride followed pseudo-first-order kinetics in the formation of a monoaquo species. Two more species, tentatively assigned as *cis*- and *trans*-diaquo complexes, were formed by a second aquation, but an associated drop in pH suggested deprotonation of coordinated H_2O to give a hydroxo complex. A further study by the same group supported the aquation pathway shown in Figure 1.10.[28] The second chloride dissociation occurs in water, but not in extracellular chloride concentration (150 mM). The lower chloride concentration (3 mM) inside the cell would presumably induce the second chloride dissociation, forming *trans*-$Ru(Im)_2Cl_2(H_2O)(OH)$, which is more labile and capable of DNA-binding. Anderson and Beauchamp also reported the solution chemistry of **3** and (4-NO_2ImH)[*trans*-Ru(5-NO_2Im)$_2Cl_4$].[29]

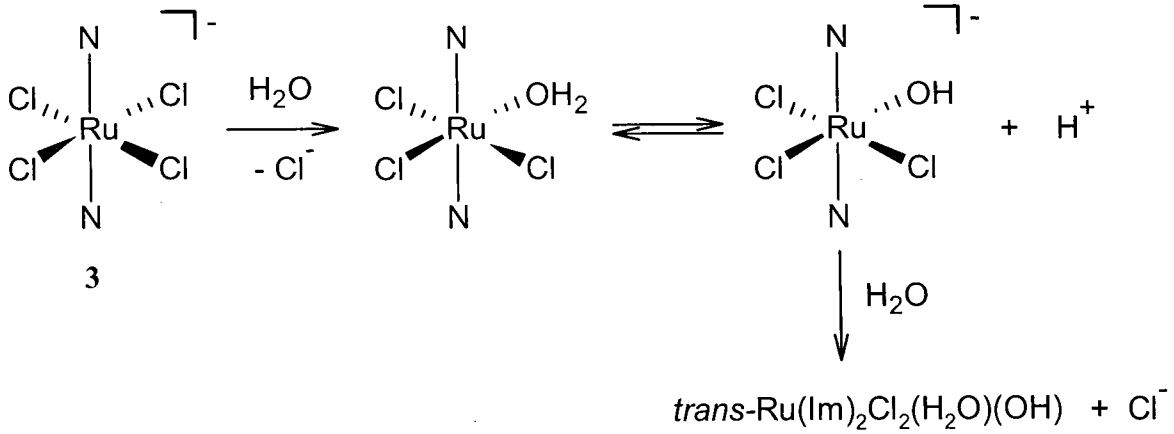

Figure 1.10 The aqueous chemistry of (ImH)[*trans*-$Ru(Im)_2Cl_4$] (**3**) (the imidazolium cation is not shown), where N represents coordinated imidazole (adapted from ref. 28).

1.3.2 Anticancer Bioassays

Preliminary *in vivo* testing of **3** suggested promising anticancer activity in mice bearing P388 Leukemia, Walker 256 carcinosarcoma, and sarcoma 180.[26] Complex **3**

References on page 25

(Figure 1.11) exhibited activity comparable to that of cisplatin, increasing the lifespan of mice and inhibiting tumor growth. It was also more active than methyl-substituted imidazole (1, 2, or 4-Me) derivatives. Earlier testing demonstrated that **3** was effective against chemically induced, colorectal tumor in rats, which cannot be treated with cisplatin.[30] Complex **3** exhibited 80 % tumor growth inhibition compared to the 37 % inhibition by treatment with 5′-deoxy-5-fluorouridine, a classical chemotherapeutic agent against colorectal cancer. Analogues of **3,** $(ImH)_2[Ru(Im)Cl_5]$ and (IndH)[*trans*-$Ru(Ind)_2Cl_4$] (**4,** Figure 1.11), were synthesized and tested in the P388 Leukemia model, and indicated good anticancer activity (Ind = indazole).[31,32] The sodium salt of **4** was later synthesized to improve its water-solubility.[33]

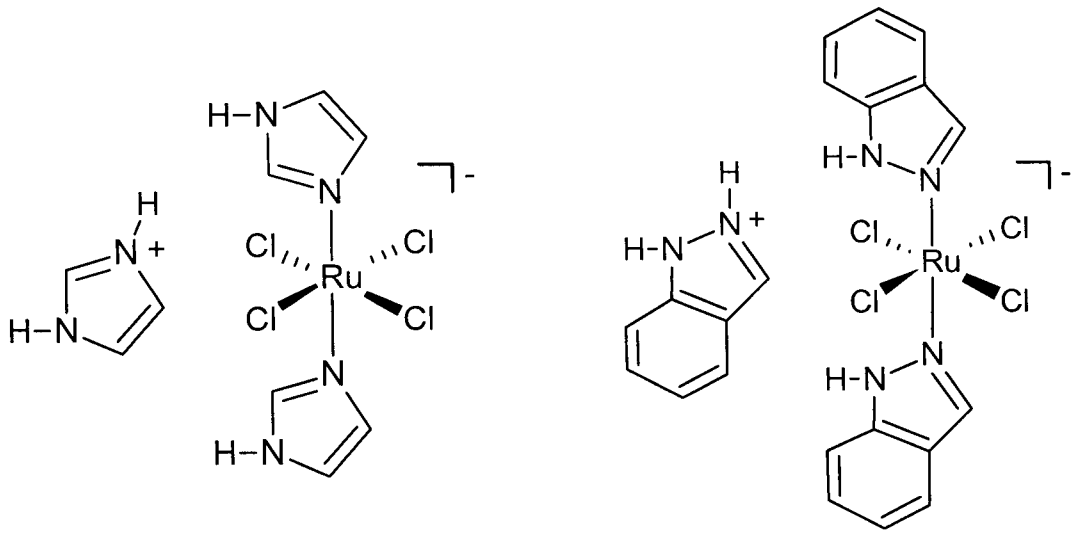

3 **4**

Figure 1.11 Structures of (ImH)[*trans*-$Ru(Im)_2Cl_4$] (**3**) and (IndH)[*trans*-$Ru(Ind)_2Cl_4$] (**4**).

1.3.3 Human Serum Protein-Binding Studies

Keppler's group have also studied the binding of **3** and **4** to human serum apotransferrin, a protein capable of binding and transporting Fe^{3+} into the cell.[34] The rate of binding of **3** was much slower than that of **4** (5 h for **3** and a few minutes for **4** at 37 °C). The Ru complexes reversibly bind to apotransferrin at a ratio of 2:1 at the two Fe^{3+}

References on page 25

binding sites. The coordinated Ru moiety can be displaced in the presence of competing ferric nitrilotriacetate or at a lower pH by the presence of citrate or adenosine 5′-triphosphate (ATP). The binding of the Ru^{3+} (like Fe^{3+}) also requires the presence of bicarbonate (HCO_3^-), and no dissociation of coordinated imidazole was observed. Tumor cells need a higher supply of iron, and therefore require greater transferrin activity. The *in vivo* binding of **3** and **4** to apotransferrin may represent a potential drug delivery system analogous to the transport of Fe^{3+}, where Ru complexes can be transported through the cell membrane and released intracellularly to enhance their anticancer activities.[34]

The binding of **3** and **4** to crystals of human apolactoferrin was then studied by using X-ray crystallographic analyses to gain insight into transferrin-mediated delivery of the Ru complexes.[35] The protein can reversibly bind to two Fe^{3+} ions together with two CO_3^{2-} ions, and was chosen to be a study model. The Ru complexes were capable of binding to two histidine residues (His 253 and His 597) at the specific metal binding sites, without significant loss of their heterocyclic ligands. Complex **3** is also capable of binding to albumin, a major human serum protein.[36]

1.3.4 Reaction of (ImH)[*trans*-Ru(Im)$_2$Cl$_4$] with *L*-Histidine and *L*-Glutathione

Keppler and coworkers have reported on the reaction between **3** and *L*-histidine (Figure 1.12), which generates $[RuCl_2(histidine)_4]Cl$ isolable at pH 4-5, but its structure remains uncertain.[37] The presence of a ν(Ru-O) IR band (518 cm^{-1}) suggested binding through the carboxylate. Histidyl imidazoles (pK_a ~6) remain protonated at pH 4-5 and were considered to be irresponsible of binding Ru. Above pH 5, a mixture of unidentified products was observed.

Reaction between **3** and *L*-glutathione (Figure 1.12) resulted in the reduction of Ru^{III} to Ru^{II}, and the imidazoles of **3** were no longer coordinated.[37] Coordination of glutathione was apparently through the sulfur, followed by a reduction of the Ru^{III} that labilizes the release of imidazoles. It had long been suggested that Ru^{III} complexes may be useful prodrugs that are activated by *in vivo* reduction to form the more active DNA-binding Ru^{II} complexes.[38] Glutathione is certainly a potential *in vivo* reducing agent.

References on page 25

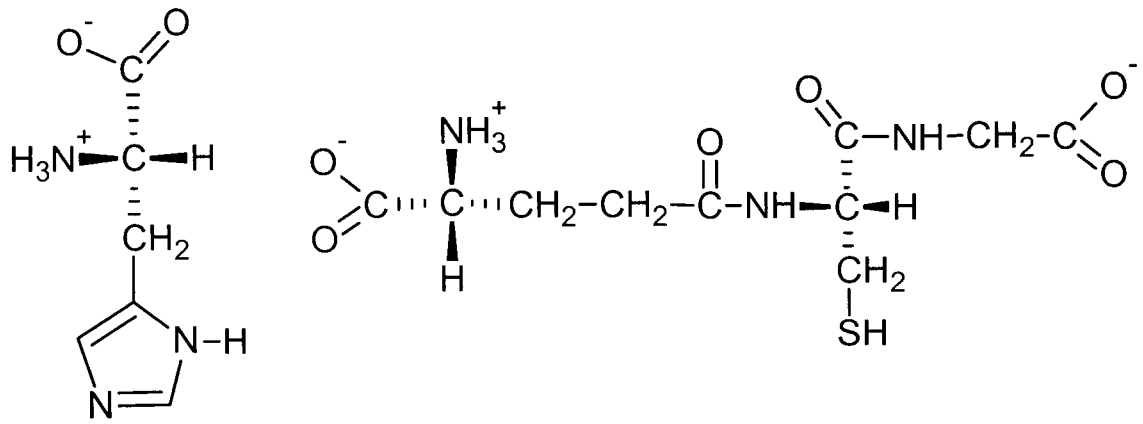

Figure 1.12 Structures of *L*-histidine (left) and *L*-glutathione (γ-Glu-Cys-Gly).

1.3.5 Recent Studies Using HPCE and HPLC-MS

In 2001, the Keppler group investigated the hydrolysis of **3** and **4** by means of high performance capillary electrophoresis (HPCE) and high performance liquid chromatography-mass spectrometry (HPLC-MS).[39] The hydrolytic decomposition of **3** followed pseudo-first-order kinetics with half-life of about 2 h at 37 °C, and was independent of pH. The pseudo-first-order kinetics were also observed in **4,** but the rate was pH-dependent with half-lives from 5.4 h (pH 6.0) to <0.5 h (pH 7.4). HPLC-MS detected the products, $[RuCl_2(MeCN)_2(Im)_2]^+$ from **3** and $[RuCl_4(MeCN)_2]^-$ from **4** using $MeCN/H_2O$ (70:30) as the mobile phase. This implies that **3** undergoes two chloride dissociations to form $[RuCl_2(H_2O)_2(Im)_2]^+$, while **4** undergoes indazole displacements to form $[RuCl_4(H_2O)_2]^-$ in an aqueous environment. HPCE agreed with the HPLC-MS results, detecting a positive and a negative hydrolytic product from **3** and **4**, respectively.

Further HPCE studies were conducted on the equimolar reactions of each of **3** and **4** with nucleoside monophosphates at 37 °C.[40] Both complexes preferably formed adducts with GMP and AMP, and no adduct was observed in the case of CMP and TMP. In a competitive study, GMP binding was greater than that of AMP, this agreeing with a previous study where binding to poly(dGdC) was greater than that of poly(dAdT).[41] The nucleotide binding in **3** was pH-dependent: binding at pH 6.0 was significantly greater than that at pH 7.4. This implies an advantage in the anticancer treatment where **3** can react more rigorously with tumor cells, which are more acidic than normal cells. The pH-

dependence of the nucleotide binding of **4** was not determined because the complex precipitated immediately at pH 7.4 in a phosphate buffer.

1.4 Ruthenium(III) Complexes Containing Sulfoxide and Imidazole Ligands: NAMI and NAMI-A

1.4.1 Synthesis, Structure, and Aqueous Chemistry

Alessio *et al.* reported the synthesis and structure of Na[*trans*-Ru(Im)(DMSO)Cl_4] (NAMI) (**5**), made by reacting Na[*trans*-Ru(DMSO)$_2Cl_4$] with excess imidazole in DMSO and acetone,[42,43] while (ImH)[*trans*-Ru(Im)(DMSO)Cl_4] (NAMI-A) (**6**) was later characterized by the same group.[44] The structures of **5** and **6** are shown in Figure 1.13. Complex **5** did not exhibit any dissociation of the imidazole or DMSO in water, where stepwise chloride dissociation formed aquo species analogous to those observed in the aqueous chemistry of **3** (see Figure 1.10).[42] In cyclic voltammetry studies, the $Ru^{III/II}$ reduction potential of **5** was more positive than that of **3** by ~0.5 V; the π-acceptor effect of DMSO makes the Ru center more positive, and more susceptible to *in vivo* reduction and activation of Ru^{III} prodrugs.[42] Of note, Clarke *et al.* have presented an extensive review on the solution chemistry and anticancer research of **5** and **6**.[45]

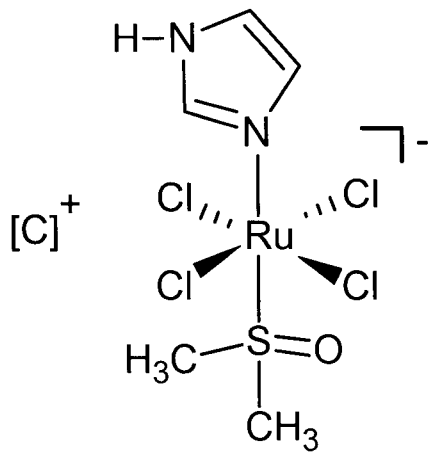

Figure 1.13 Structures of NAMI (**5**) (C = Na) and NAMI-A (**6**) (C = ImH).

References on page 25

1.4.2 Anticancer Bioassays of NAMI

Sava *et al.* demonstrated the anticancer activity of **5** in MCa mammary carcinoma in mice.[46] A key property of the Ru drug, very different to that of cisplatin, is that the former inhibited metastatic tumors more effectively than primary tumor growth. Evidently, **5** can distinguish between tumor cell populations, and selectively destroy tumors with a higher metastatic potential. Treatment with the Ru drug significantly prolonged the host survival time. Complex **5** may represent the first example of selective antimetastatic agents for postsurgical treatment following amputation of the primary tumor.[46]

Further studies indicated that **5** exhibits good *in vivo* antimetastatic activity but lacks *in vitro* cytotoxicity in MCa mammary carcinoma and TLX5 lymphoma models.[47] The mechanism of **5** in metastasis reduction is thought to be unrelated to direct tumor cytotoxicity. This implies that antimetastasis is not the result of DNA-binding, which is associated with the increase of cytotoxicity in cisplatin. The use of **5** as an antimetastatic agent would be advantageous because of fewer toxic side-effects.[48]

1.4.3 Binding Studies of DNA and Bovine Serum Albumin to NAMI

Messori *et al.* have investigated the interaction between **5** and calf thymus DNA.[49] Complex **5** prefers purine-base binding similar to cisplatin, but the degree of binding and the conformational alteration in DNA are significantly reduced. DNA damage was detected only at relatively high concentrations of **5**. No reduction of the Ru^{III} complex was observed upon DNA-binding. Further studies confirmed that the DNA-binding mode of **5** is different to that of cisplatin.[50] Complex **5** binds considerably faster than **3** or **4** due to the increased rate of chloride dissociation, and induces a greater conformational change.

The binding of **5** to bovine serum albumin was demonstrated by Messori *et al.*[51] One albumin molecule can bind up to five Ru moieties. The nonlabile axial ligands (DMSO and Im) are presumably retained upon binding, and the oxidation state remains Ru^{III}. The probable binding sites were thought to be the exposed histidine residues of albumin. Implication of the binding in relation to the anticancer activity of **5** is still not clear.

References on page 25

1.4.4 Anticancer Bioassays of NAMI-A

The antimetastatic activity of NAMI-A (**6**) was tested in comparison to that of NAMI (**5**) in Lewis lung carcinoma and MCa mammary carcinoma.[52] The application of **6** (replacing Na^+ with ImH^+) results in better chemical stability, synthetic reproducibility, and a slight improvement in antimetastatic properties. Treatment with **6** was observed to increase the thickness of the connective capsule surrounding the tumor mass, and could be a plausible mechanism in containing primary tumor and inhibiting its spreading. The postsurgical treatment of mice bearing MCa mammary carcinoma with **6** demonstrated a significant prolongation of the animal lifespan.[53] The anticancer mechanism of **6** is thought to be unrelated to direct tumor cytotoxicity, and such a mechanism may be responsible for the reduced host toxicity.[54]

The Triste group has reported on intravenous injection of **6** into mice in order to determine the Ru content of blood and different organs using atomic absorption spectroscopy.[55] After drug administration, **6** was rapidly cleared from the blood by the kidney. Only 10 % of the original dose was left in the blood after 5 min, at which time the kidney exhibited the highest Ru content. The rate of decomposition of **6** in mice was estimated to have a half-life of 18 h. A concentration of **6** was maintained at 10^{-4} M in the lungs up to 24 h, this providing an active concentration against lung metastases.

Sava *et al.* showed that the reduction of **6** by ascorbic acid, cysteine, or glutathione prior to administration gave a slightly more active antimetastatic species against MCa mammary carcinoma in mice.[56] The "activation by reduction" mechanism was not obvious in this case because both Ru^{III} and Ru^{II} species were active against metastases and indicated no host cytotoxicity. Nevertheless, reduction of **6** prior to administration can be a potential drug delivery route. Complex **6** is currently undergoing phase I clinical trials.[56]

1.5 Ruthenium Chemistry and Anticancer Research in the James Group

1.5.1 *Cis*-$RuCl_2(DMSO)_3(DMSO)$

References on page 25

Ru sulfoxide chemistry in the James group originated in the early 1970s. The synthesis of *cis*-$RuCl_2(DMSO)_3(DMSO)$ (**1**), which was later found to exhibit anticancer activity,[14] marked a historical starting point.[6] The structure of **1** was first solved at UBC.[8] The initial interest in work by McMillan *et al.* was to synthesize Ru sulfoxide complexes as olefin hydrogenation catalysts.[11] The studies of Ru chemistry in application to anticancer research were developed later in the 1980s.

1.5.2 *Cis*-$RuCl_2(TMSO)_4$

Bora and Singh first reported the synthesis of *cis*-$RuCl_2(TMSO)_4$ (**7**) in 1977 (TMSO = tetramethylenesulfoxide);[57] all the TMSO ligands were considered S-bonded based on the IR spectral data, but no structure was done. In 1989, Chan *et al.* synthesized the same complex and tentatively assigned a *trans*-configuration,[58] based on the X-ray structure of *trans*-$RuCl_2(DMSO)_4$ (**2**), which shows all S-bonded sulfoxides.[10] In 1990, the James and the Alessio groups independently published the X-ray structure of **7,** which was found to contain a *cis*-configuration and S-bonded TMSO ligands.[59,60] Contrasting the structure of **7** and **1** (which contains one O-bonded DMSO), an S-bonded TMSO appears to be sterically less demanding than an S-bonded DMSO.[59]

1.5.3 Ruthenium(II) Sulfoxide-Nitroimidazole Complexes as Radiosensitizers

Radiation therapy using ionizing radiation such as X-rays is a common method of cancer treatment. The presence of oxygen, which is converted to reactive superoxide species when irradiated, is essential for the effectiveness of the therapy.[61] The uncontrollable growth of cancer cells results in poorly oxygenated or hypoxic environments that are resistant to such therapy. Due to the electron-withdrawing property of the NO_2 group, nitroimidazoles were developed as radiosensitizers that compensate for the hypoxic effect in radiotherapy.[62]

Chan *et al.* synthesized a series of $RuCl_2(DMSO)_2(L)_2$ complexes by reacting **1** with two equivalents of nitroimidazole in alcohol (L = 2-nitroimidazole, misonidazole, 4-nitroimidazole, or metronidazole; see Figure 1.14).[63] As Ru sulfoxide complexes are capable of binding to DNA (see Section 1.2.3), Ru sulfoxide-nitroimidazole complexes were thought possibly useful as a radiation target on tumor DNA. At 200 μM,

References on page 25

$RuCl_2(DMSO)_2(4\text{-}NO_2Im)_2$ (**8**) (of uncertain geometric form) was the most effective radiosensitizer with a sensitizer enhancement ratio (SER) of 1.6 in hypoxic Chinese hamster ovary (CHO) cells;[63] SER is defined as the ratio of radiation doses required to kill a certain number of cells in the absence and presence of the drug. Ru nitroimidazole complexes were found to be better radiosensitizers and to exhibit lower toxicity in CHO cells than do the corresponding free nitroimidazoles.

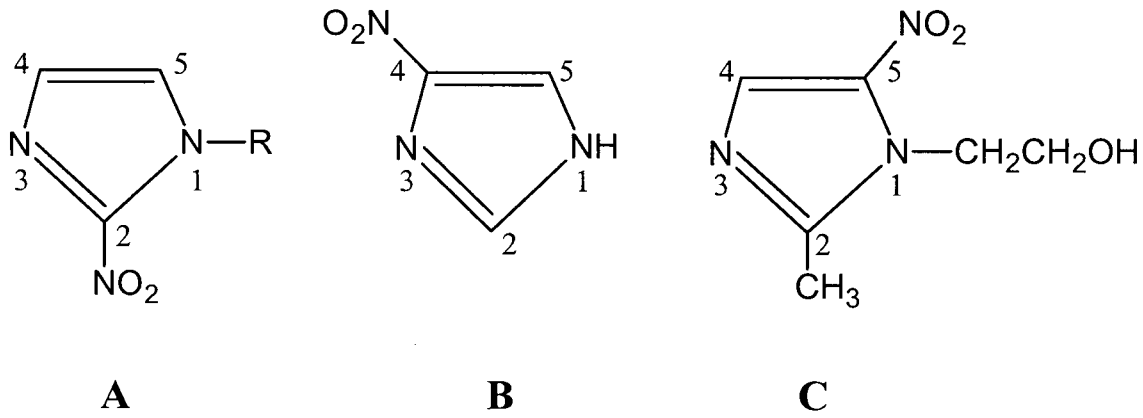

Figure 1.14 Structures of nitroimidazoles: (A) 2-nitroimidazole (R = H), misonidazole ($R = CH_2\text{-}CH(OH)\text{-}CH_2OCH_3$); (B) 4-nitroimidazole; (C) metronidazole.

Further studies showed that **8** induced *in vitro* chromosome damages in CHO cells.[64] The activity of **8** was greater than that of **1** and of 4-nitroimidazole, and was similar to that of misonidazole, but less than that of cisplatin. The biological "mechanism" of **8** probably involves Ru-DNA binding analogous to that of cisplatin, as well as the biochemical reduction of the coordinated nitroimidazoles.[64] Ru complexes with 4-substituted nitroimidazoles were synthesized to compare their radiosensitizing activities with that of **8,** but these complexes did not bind to DNA, and their SER values were found to be lower than that of **8**.[65]

The substitution of Br for Cl in the Ru complexes decreased the radiosensitizing ability, while similar SER values were obtained when DMSO was replaced with TMSO.[58] No X-ray structure was reported for any of the dichlorobis(sulfoxide)-bis(nitroimidazole)ruthenium(II) complexes, and their structures were tentatively

References on page 25

assigned as *cis*-, *cis*-, *cis*-geometry, with only S-bonded sulfoxides based on the IR data.[66] The assignment was probably correct because an analogous complex, *cis*-, *cis*-, *cis*-$RuCl_2(DMSO)_2(1,2\text{-dimethylimidazole})_2$, was later synthesized and spectroscopically well characterized by Iwamoto *et al.*[67]

1.5.4 Ruthenium(II) Bidentate Sulfoxide Complexes

Yapp *et al.* reported the syntheses and X-ray structures of *trans*-$RuCl_2(BMSE)_2$, *cis*-$RuCl_2(BESE)_2$, *trans*-$RuCl_2(BPSE)_2$, and *cis*-$RuCl_2(BMSP)_2$, that all contained only S-bonded sulfoxides (Figure 1.15).[68] The ligands were synthesized by the acid-catalyzed oxidations of the corresponding thioethers.[69] Preliminary *in vitro* assays indicated that all four complexes accumulated in the CHO cells without hypoxic selectivity.[68] The *trans*-Ru complexes accumulated and bound to DNA to a greater degree than the *cis*-complexes, but no toxicity was observed toward the CHO cells.

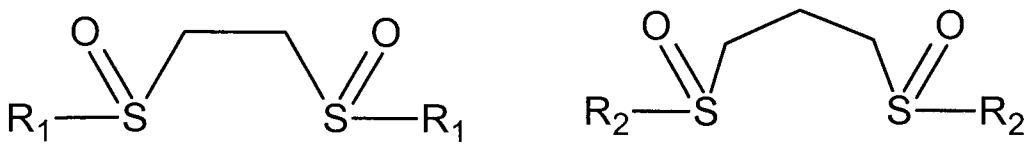

A **B**

Figure 1.15 Structures of bidentate sulfoxides: (A) BMSE = 1,2-bis(methylsulfinyl)ethane (R_1 = Me), BESE = 1,2-bis(ethylsulfinyl)ethane (R_1 = Et), BPSE = 1,2-bis(propylsulfinyl)ethane (R_1 = *n*-Pr), BBSE = 1,2-bis(butylsulfinyl)ethane (R_1 = *n*-Bu); (B) BMSP = 1,3-bis(methylsulfinyl)propane (R_2 = Me), BPSP = 1,3-bis(propylsulfinyl)propane (R_2 = *n*-Pr).

Cheu later synthesized a series of water-soluble, dinuclear Ru complexes: $[RuCl(H_2O)(L)]_2(\mu\text{-}Cl)_2$ (L = BESE, BPSE, or BBSE) and a mixed valence Ru^{II}/Ru^{III} complex, $[RuCl(BPSP)]_2(\mu\text{-}Cl)_3$ (Figure 1.15).[70] *In vitro* assays indicated that the complexes accumulate in the CHO cells and bind to DNA, but show no toxicity.

References on page 25

$[RuCl(H_2O)(BESE)]_2(\mu\text{-}Cl)_2$ and $[RuCl(BPSP)]_2(\mu\text{-}Cl)_3$ bind to DNA to a greater degree than do **1** and **2.**

Recently, Huxham synthesized and structurally characterized other Ru complexes, including *cis*-$RuCl_2$(BESE)(DMSO)(DMSO) (**9**), $[RuCl_2(p\text{-cymene})]_2(\mu\text{-BESE})$ (**10**), and $[RuCl(p\text{-cymene})(BESE)](PF_6)$ (*p*-cymene = *p*-isopropyltoluene).[71] Complexes **9** and **10** indicated no toxicity toward the CHO cells, but **10** exhibited *in vitro* anticancer activity (IC_{50} = 345 - 360 μM) against human breast cancer cells (MDA-MB-435s) as based on the MTT assay (see Chapter 4);[71] IC_{50} is defined as the concentration of the drug that kills 50 % of the cells relative to the control. Of note, Sadler's group has reported on the anticancer activity of cationic Ru *p*-cymene species containing ancillary diamine ligands.[72]

1.5.5 Ruthenium Imidazole and β-Diketonato Complexes

Baird *et al.* reported the syntheses of $[Ru(L)_6](CF_3SO_3)_2$ by reacting L with $[Ru(DMF)_6](CF_3SO_3)_3$ (DMF = *N,N*-dimethylformamide; L = imidazole (Im), N-methylimidazole (N-MeIm), or 5-methylimidazole (5-MeIm)).[73] In the case of 2-methylimidazole (2-MeIm), $[Ru(CO)(DMF)(2\text{-MeIm})_4](CF_3SO_3)_2$ was isolated, with the CO being abstracted from DMF. The complexes, *cis*-$[Ru(acac)_2(MeCN)_2](CF_3SO_3)$ and *cis*-$Ru(hfac)_2(MeCN)_2$, were reported to be precursors for $[Ru(acac)_2(L)_2](CF_3SO_3)$ and $Ru(hfac)_2(L)_2$, respectively, where L represents a series of imidazoles and nitroimidazoles (acac = acetylacetonato; hfac = 1,1,1,5,5,5-hexafluoroacetylacetonato).[74,75]

None of the Ru-imidazole complexes was toxic towards SCCVII (mouse squamous cell carcinoma) cells, except *cis*-$[Ru(acac)_2(Im)_2](CF_3SO_3)$ and *cis*-$[Ru(acac)_2(N\text{-MeIm})_2](CF_3SO_3)$, which indicated hypoxic-selective toxicity.[75] However, these complexes were the least active in cell accumulation and DNA-binding, while the Ru-EF5 complexes, $RuCl_3(EF5)_2(EtOH)$, $[Ru(DMF)_2(EF5)_2(EtOH)_2](CF_3SO_3)_3$, and $[Ru(acac)_2(EF5)_2](CF_3SO_3)$, were the most active (Figure 1.16). The fluorinated derivatives were developed for use as hypoxic markers.[76] $RuCl_3(SR2508)_2(EtOH)$ also significantly bound to DNA, but accumulated in the cells to a lesser degree (Figure 1.16).[75]

References on page 25

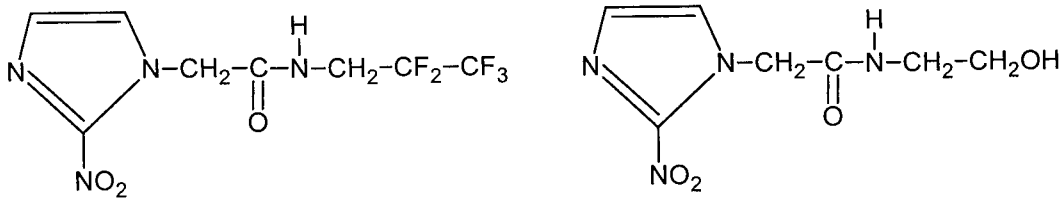

Figure 1.16 Structures of EF5 (left) and SR2508 (etanidazole).

1.6 Maltolato Complexes

1.6.1 Ruthenium Maltolato Complexes

Greaves and Griffith first synthesized $Ru(ma)_3$ in 1988 (ma = maltolato).[77] Maltol (3-hydroxy-2-methyl-4-pyranone, Figure 1.17), a non-toxic and water-soluble food additive, readily deprotonates at the hydroxy group (pK_a = 8.67) under basic conditions. Once deprotonated, it facilitates *O, O'*-chelation at the metal center. El-Hendawy and El-Shahawi have since reported the synthesis of $RuCl_2(PPh_3)_2(ma)$,[78] Capper *et al.* the syntheses and structures of Ru(mes)Cl(L) and $[Ru(mes)(CO)(L)](BF_4)$ (L = maltolato or ethylmaltolato; mes = 1,3,5-trimethylbenzene),[79] and Fryzuk *et al.* the syntheses of $Ru(ma)_2(PPh_3)_2$, $Ru(ma)_2(DMSO)_2$, and $Ru(ma)_2(COD)$, and structural characterization of the *cis*-isomers of the last two species (COD = 1,5-cyclooctadiene).[80]

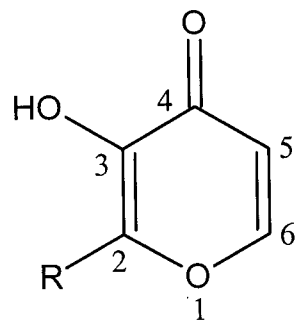

Figure 1.17 Structures of maltol (R = Me) and ethylmaltol (R = Et).

References on page 25

1.6.2 Other Maltolato Complexes

Morita *et al.* have synthesized first-row transition metal maltolato complexes: trivalent $M(ma)_3$ (M = Cr, Mn, or Fe) and divalent complexes of Co, Ni, Cu, and Zn,[81] while Ahmet *et al.* reported the structure of *mer*-$Fe(ma)_3$, which was proposed as a potential drug for iron-deficiency anaemia.[82] Within the lanthanide series, Dutt and Sarma have synthesized $M(ma)_3 \cdot H_2O$ (M = La, Pr, Nd, Sm, Gd, Dy, or Yb),[83] while Fregona *et al.* have reported the structure of $Pr(ma)_3(H_2O)_2$, an octa-coordinated species.[84]

The Orvig group has made many contributions to maltolato chemistry, including the syntheses of $Ga(ma)_3$ and $In(ma)_3$, and the structures of *mer*-$Al(ma)_3$ and (maltolato)diphenylboron.[85-88] Several Tc and Re maltolato complexes were studied, including the structures of *cis*-$ReOBr(ma)_2$, $[(n\text{-}Bu)_4N][ReOBr_3(ma)]$, and $[(n\text{-}Bu)_4N][TcOCl_3(ma)]$.[89] The syntheses of a series of vanadium maltolato complexes were reported, including the structure of $VO(ma)_2$, a potent insulin mimetic agent for the treatment of diabetes.[90]

Greaves and Griffith also synthesized *trans*-$OsO_2(ma)_2$, *trans*-$UO_2(ma)_2$, *cis*-$MoO_2(ma)_2$, $Rh(ma)_3$, and $[M(ma)(PPh_3)_2](BPh_4)$ (M = Pd or Pt),[77] and Lord *et al.* later determined the structure of *cis*-$MoO_2(ma)_2$.[91] Archer *et al.* have reported the syntheses and structures of *cis*-$[Re(ma)_2(NPh)(PPh_3)](BPh_4)$ and $[ReCl(ma)(N_2COPh)(PPh_3)_2]$;[92] Burgess and Parsons have prepared $Sn^{IV}(ma)_2Cl_2$,[93] and the same group later published the synthesis and structure of $Sn^{II}(ma)_2$.[94]

1.7 Thesis Overview

This thesis describes the synthesis of novel Ru^{II} complexes as potential anticancer agents. Our group has reported biological activities of Ru β-diketonato and imidazole complexes (Section 1.5.5). To further extend the project, Ru maltolato complexes, analogous to Ru β-diketonato *O, O'*-chelation systems, were synthesized and characterized. The advantages of maltol over β-diketone are that the former is a non-toxic food additive suitable for biological use, and its presence in a metal complex could increase the water-solubility of the species. Two main projects began the pursuit of this research in our group: one focused on Ru^{III} (conducted by D. Kennedy), while this thesis

References on page 25

work focused on Ru^{II}. The initial objective was to synthesize Ru^{II} mixed maltolato-nitroimidazole complexes, analogous to the Ru^{III} complexes, such as *trans*-$[Ru(ma)_2(metro)_2](CF_3SO_3)$, already synthesized by D. Kennedy (metro = metronidazole).[95] The comparison of their anticancer activities is potentially fruitful. However, the attempts at synthesis were unsuccessful, probably because the anionic maltolato ligands strongly favor the coordination of Ru^{III}. Ru^{II} maltolato complexes likely require the stabilization of good π-acceptors, such as coordinated S-bonded DMSO.

Because of the numerous reports on Ru sulfoxide complexes as promising anticancer drugs, the thesis work switched to the synthesis and characterization of Ru^{II} maltolato and ethylmaltolato complexes with ancillary monodentate and bidentate sulfoxide ligands (DMSO, TMSO, and BESE), in part, expansion of $Ru(ma)_2(DM\underline{S}O)_2$-type complexes first reported by Fryzuk's group.[80] This work also expands on the work by Chan *et al.* involving the synthesis of Ru^{II} bidentate sulfoxide-nitroimidazole complexes.[66] Chapter 2 describes the synthesis procedures for the Ru complexes and the collection of characterization data by different spectroscopic techniques, including NMR, UV-vis, IR, and MS; elemental analysis, conductivity, and CV data were also collected. X-ray structures were determined for *cis*-$Ru(ma)_2$(*S,R*-BESE), *trans*-$RuCl_2$(*R,R*-BESE)$(metro)_2$, and *trans*-$[Ru(ma)_2(metro)_2](CF_3SO_3)$. Chapter 3 interprets the results, and discusses structural information. Chapter 4 reports on the *in vitro* MTT assay, which screens a variety of Ru complexes for anticancer activities against human breast cancer cells (MDA435/LCC6). Chapter 5 provides a brief conclusion and the recommendations for future work.

References on page 25

1.8 References

(1) Griffiths, A. J. F.; Miller, J. H.; Suzuki, D. T.; Lewontin, R. C.; Gelbart, W. M. *An Introduction to Genetic Analysis, 6th Ed.;* W. H. Freeman and Company: New York, 1996, p.736.

(2) Rosenberg, B.; Van Camp, L.; Krigas, T. *Nature* **1965,** *205,* 698.

(3) Rosenberg, B.; Van Camp, L.; Trosko, J. E.; Mansour, V. H. *Nature* **1969,** *222,* 385.

(4) Wong, E.; Giandomenico, C. M. *Chem. Rev.* **1999,** 99, 2451.

(5) Guo, Z.; Sadler, P. J. *Angew. Chem. Int. Ed.* **1999,** *38,* 1512.

(6) James, B. R.; Ochiai, E.; Rempel, G. L. *Inorg. Nucl. Chem. Lett.* **1971,** *7,* 781.

(7) Evans, I. P.; Spencer, A.; Wilkinson, G. *J. Chem. Soc. Dalton Trans.* **1973,** 204.

(8) Mercer, A.; Trotter J. *J. Chem. Soc. Dalton Trans.* **1975,** 2480.

(9) Attia, W. M.; Calligaris, M. *Acta Cryst.* **1987,** *C43,* 1426.

(10) Alessio, E.; Mestroni, G.; Nardin, G.; Attia, W. M.; Calligaris, M.; Sava, G.; Zorzet, S. *Inorg. Chem.* **1988,** *27,* 4099.

(11) (a) McMillan, R. S.; Mercer, A.; James, B. R.; Trotter, J. *J. Chem. Soc. Dalton Trans.* **1975,** 1006.

(b) James, B. R.; McMillan, R. S.; Reimer, K. J. *J. Mol. Catal.* **1975/76,** *1,* 439.

(c) James, B. R.; McMillan, R. S. *Can. J. Chem.* **1977,** *55,* 3927.

(d) Davies, A. R.; Einstein, F. W. B.; Farrell, N. P.; James, B. R.; McMillan, R. S. *Inorg. Chem.* **1978,** *17,* 1965.

(e) James, B. R.; McMillan, R. S.; Morris, R. H.; Wang, D. K. W. *Adv. Chem. Ser.* **1978,** *167,* 122.

(12) (a) Monti-Bragadin, C.; Tamaro, M.; Banfi, E. *Chem.-Biol. Interact.* **1975,** *11,* 469.

(b) Monti-Bragadin, C.; Ramani, L.; Samer, L.; Mestroni, G.; Zassinovich, G. *Antimicrob. Agents Chemother.* **1975,** *7,* 825.

(13) Jaswal, J. S.; Rettig, S. J.; James, B. R. *Can. J. Chem.* **1990,** *68,* 1808.

(14) (a) Sava, G.; Giraldi, T.; Mestroni, G.; Zassinovich, G. *Chem.-Biol. Interact.* **1983,** *45,* 1.

(b) Sava, G.; Zorzet, S.; Giraldi, T.; Mestroni, G.; Zassinovich, G. *Eur. J. Cancer Clin. Oncol.* **1984,** *20,* 841.

(15) (a) Pacor, S.; Luxich, E.; Ceschia, V.; Sava, G.; Alessio, E.; Mestroni, G. *Pharmacol. Res.* **1989,** *21 (Suppl. 1),* 127.

(b) Sava, G.; Pacor, S.; Zorzet, S.; Alessio, E.; Mestroni, G. *Pharmacol. Res.* **1989,** *21,* 617.

(16) Coluccia, M.; Sava, G.; Loseto, F.; Nassi, A.; Boccarelli, A.; Giordano, D.; Alessio, E.; Mestroni, G. *Eur. J. Cancer* **1993,** *29A,* 1873.

(17) Farrell, N.; De Oliveira, N. G. *Inorg. Chim. Acta* **1982,** *66,* L61.

(18) Cauci, S.; Alessio, E.; Mestroni, G.; Quadrifoglio, F. *Inorg. Chim. Acta* **1987,** *137,* 19.

(19) Alessio, E.; Xu, Y.; Cauci, S.; Mestroni, G.; Quadrifoglio, F.; Viglino, P.; Marzilli, L. G. *J. Am. Chem. Soc.* **1989,** *111,* 7068.

(20) Tian, Y.-N.; Yang, P.; Li, Q.-S.; Guo, M.-L.; Zhao, M.-G. *Polyhedron* **1997,** *16,* 1993.

(21) Cauci, S.; Viglino, P.; Esposito, G.; Quadrifoglio, F. *J. Inorg. Biochem.* **1991,** *43,* 739.

(22) Davey, J. M.; Moerman, K. L.; Ralph, S. F.; Kanitz, R.; Sheil, M. M. *Inorg. Chim. Acta* **1998,** *281,* 10.

(23) Esposito, G.; Cauci, S.; Fogolari, F.; Alessio, E.; Scocchi, M.; Quadrifoglio, F.; Viglino, P. *Biochem.* **1992,** *31,* 7094.

(24) Anagnostopoulou, A.; Moldrheim, E.; Katsaros, N.; Sletten, E. *J. Biol. Inorg. Chem.* **1999,** *4,* 199.

(25) Nováková, O.; Hofr, C.; Brabec, V. *Biochem. Pharmacol.* **2000,** *60,* 1761.

(26) Keppler, B. K.; Rupp, W.; Juhl, U. M.; Endres, H.; Niebl, R.; Balzer, W. *Inorg. Chem.* **1987,** *26,* 4366.

(27) Ni Dhubhghaill, O. M.; Hagen, W. R.; Keppler, B. K.; Lipponer, K.-G.; Sadler, P. J. *J. Chem. Soc. Dalton Trans.* **1994,** 3305.

(28) Chatlas, J.; van Eldik, R.; Keppler, B. K. *Inorg. Chim. Acta* **1995,** *233,* 59.

(29) (a) Anderson, C.; Beauchamp, A. L. *Can. J. Chem.* **1995,** *73,* 471.

(b) Anderson, C.; Beauchamp, A. L. *Inorg. Chem.* **1995,** *34,* 6065.

(c) Anderson, C.; Beauchamp, A. L. *Inorg. Chim. Acta* **1995,** *233,* 33.

(30) Grazon, F. T.; Berger, M. R.; Keppler, B. K.; Schmähl, D. *Cancer Chemother. Pharmacol.* **1987,** *19,* 347.

(31) Keppler, B. K.; Wehe, D.; Endres, H.; Rupp, W. *Inorg. Chem.* **1987,** *26,* 844.

(32) Keppler, B. K.; Lipponer, K.-G.; Stenzel, B.; Kratz, F. *New Tumor-Inhibiting Ruthenium Complexes, in Metal Complexes in Cancer Chemotherapy (ed. B. K. Keppler);* VCH: Weinheim, 1993, p.187.

(33) Peti, W.; Pieper, T.; Sommer, M.; Keppler, B. K.; Giester, G. *Eur. J. Inorg. Chem.* **1999,** 1551.

(34) Kratz, F.; Hartmann, M.; Keppler, B.; Messori, L. *J. Biol. Chem.* **1994,** *269,* 2581.

(35) Smith, C. A.; Sutherland-Smith, A. J.; Keppler, B. K.; Kratz, F.; Baker, E. N. *J. Biol. Inorg. Chem.* **1996,** *1,* 424.

(36) Trynda-Lemiesz, L.; Keppler, B. K.; Koztowski, H. *J. Inorg. Biochem.* **1999,** *73,* 123.

(37) Hartmann, M.; Lipponer, K.-G.; Keppler, B. K. *Inorg. Chim. Acta* **1998,** *267,* 137.

(38) Clarke, M. J.; Bitler, S.; Rennert, D.; Buchbinder, M.; Kelman, A. D. *J. Inorg. Biochem.* **1980,** *12,* 79.

(39) Küng, A.; Pieper, T.; Wissiack, R.; Rosenberg, E.; Keppler, B. K. *J. Biol. Inorg. Chem.* **2001,** *6,* 292.

(40) Küng, A.; Pieper, T.; Keppler, B. K. *J. Chromatogr. B* **2001,** *759,* 81.

(41) Hartmann, M.; Einhäuser, T. J.; Keppler, B. K. *Chem. Commun.* **1996,** 1741.

(42) Alessio, E.; Balducci, G.; Lutman, A.; Mestroni, G.; Calligaris, M.; Attia, W. M. *Inorg. Chim. Acta* **1993,** *203,* 205.

(43) Alessio, E.; Balducci, G.; Calligaris, M.; Costa, G.; Attia, W. M.; Mestroni, G. *Inorg. Chem.* **1991,** *30,* 609.

(44) Mestroni, G.; Alessio, E.; Sava, G. 1998, International Patent PCT C07F 15/00, A61K 31/28. WO 98/00431.

(45) Clarke, M. J.; Zhu, F.; Frasca, D. R. *Chem. Rev.* **1999,** *99,* 2511.

(46) Sava, G.; Pacor, S.; Coluccia, M.; Mariggio, M.; Cocchietto, M.; Alessio, E.; Mestroni, G. *Drug Invest.* **1994,** *8,* 150.

(47) Sava, G.; Pacor, S.; Bergamo, A.; Cocchietto, M.; Mestroni, G.; Alessio, E. *Chem.-Biol. Interact.* **1995,** *95,* 109.

(48) Capozzi, I.; Clerici, K.; Cocchietto, M.; Salerno, G.; Bergamo, A.; Sava, G. *Chem.-Biol. Interact.* **1998,** *113,* 51.

(49) (a) Messori, L.; Casini, A.; Vullo, D.; Haroutiunian, S. G.; Dalian, E. B.; Orioli, P. *Inorg. Chim. Acta* **2000,** *303,* 282.

(b) Gallori, E.; Vettori, C.; Alessio, E.; Vilchez, F. G.; Vilaplana, R.; Orioli, P.; Casini, A.; Messori, L. *Arch. Biochem. Biophys.* **2000,** *376,* 156.

(50) Malina J.; Nováková, O.; Keppler, B. K.; Alessio, E.; Brabec, V. *J. Biol. Inorg. Chem.* **2001,** *6,* 435.

(51) Messori, L.; Orioli, P.; Vullo, D.; Alessio, E.; Iengo, E. *Eur. J. Biochem.* **2000,** *267,* 1206.

(52) Sava, G.; Capozzi, I.; Clerici, K.; Gagliargi, G.; Alessio, E.; Mestroni, G. *Clin. Exp. Metastasis* **1998,** *16,* 371.

(53) Sava, G.; Gagliardi, R.; Bergamo, A.; Alessio, E.; Mestroni, G. *Anticancer Res.* **1999,** *19,* 969.

(54) (a) Bergamo, A.; Gagliardi, R.; Scarcia, V.; Furlani, A.; Alessio, E.; Mestroni, G.; Sava, G. *J. Pharmacol. Exp. Ther.* **1999,** *289,* 559.

(b) Bergamo, A.; Zorzet, S.; Gava. B.; Sorc, A.; Alessio, E.; Iengo, E.; Sava, G. *Anti-Cancer Drugs* **2000,** *11,* 665.

(55) (a) Cocchietto, M.; Salerno, G.; Alessio, E.; Mestroni, G.; Sava, G. *Anticancer Res.* **2000,** *20,* 197.

(b) Cocchietto, M.; Sava, G. *Pharmacol. Toxicol.* **2000,** *87,* 193.

(56) Sava, G.; Bergamo, A.; Zorzet, S.; Gava, B.; Casarsa, C.; Cocchietto, M.; Furlani, A.; Scarcia, V.; Serli, B.; Iengo, E.; Alessio, E.; Mestroni, G. *Eur. J. Cancer* **2002,** *38,* 427.

(57) (a) Bora, T.; Singh, M. M. *J. Inorg. Nucl. Chem.* **1977,** *39,* 2282.

(b) Bora, T.; Singh, M. M. *Transition Met. Chem.* **1978,** *3,* 27.

(58) Chan, P. K. L.; James, B. R.; Frost, D. C.; Chan, P. K. H.; Hu, H.-L.; Skov. K. A. *Can. J. Chem.* **1989,** *67,* 508.

(59) Yapp, D. T. T.; Jaswal, J.; Rettig, S. J.; James, B. R.; Skov, K. A. *Inorg. Chim. Acta* **1990,** *177,* 199.

(60) Alessio, E.; Milani, B.; Mestroni, G.; Calligaris, M.; Faleschini, P.; Attia, W. M. *Inorg. Chim. Acta* **1990,** *177,* 255.

(61) Thomlinson, R. H.; Gray, L. H. *Br. J. Cancer* **1955,** *9,* 539.

(62) (a) Adams, G. E.; Clarke, E. D.; Flockhart, I. R.; Jacobs, R. S.; Sehmi, D. S.; Stratford, I. J.; Wardman, P.; Watts, M. E. *Int. J. Radiat. Biol.* **1979,** *35,* 133.
(b) Adams, G. E. *Radiat. Res.* **1992,** *132,* 129.

(63) Chan, P. K. L.; Skov, K. A.; James, B. R.; Farrell, N. P. *Int. J. Radiat. Oncol. Biol. Phys.* **1986,** *12,* 1059.

(64) Chan, P. K. L.; Skov, K. A.; James, B. R.; Farrell, N. P. *Chem.-Biol. Interact.* **1986,** *59,* 247.

(65) Chan, P. K. L.; Skov, K. A.; James, B. R. *Int. J. Radiat. Biol.* **1987,** *52,* 49.

(66) Chan, P. K. L.; Chan, P. K. H.; Frost, D. C.; James, B. R.; Skov, K. A. *Can. J. Chem.* **1988,** *66,* 117.

(67) Iwamoto, M.; Alessio, E.; Marzilli, L. G. *Inorg. Chem.* **1996,** *35,* 2384.

(68) Yapp, D. T. T.; Rettig, S. J.; James, B. R.; Skov, K. A. *Inorg. Chem.* **1997,** *36,* 5635.

(69) Hull, C. M.; Bargar, T. W. *J. Org. Chem.* **1975,** *40,* 3152.

(70) Cheu, E. L. S. *Thioether and Sulfoxide Complexes of Ruthenium; Preliminary In Vitro Studies of Water-Soluble Species;* Ph. D. Dissertation, University of British Columbia: Vancouver, 2000.

(71) Huxham, L. A. *The Synthesis and Characterization of Ruthenium Disulfoxide Complexes and Their Preliminary In Vitro Examination as Potential Chemotherapeutic Agents;* M. Sc. Dissertation, University of British Columbia: Vancouver, 2001.

(72) (a) Morris, R. E.; Aird, R. E.; del Socorro Murdoch, P.; Chen, H.; Cummings, J.; Hughes, N. D.; Parsons, S.; Parkin, A.; Boyd, G.; Jodrell, D. I.; Sadler, P. J. *J. Med. Chem.* **2001,** *44,* 3616.
(b) Aird, R. E.; Cummings, J.; Ritchie, A. A.; Muir, M.; Morris, R. E.; Chen, H.; Sadler, P. J.; Jodrell, D. I. *Br. J. Cancer* **2002,** *86,* 1652.

(73) Baird, I. R.; Rettig, S. J.; James, B. R.; Skov, K. A. *Can. J. Chem.* **1998,** *76,* 1379.

(74) Baird, I. R.; Rettig, S. J.; James, B. R.; Skov, K. A. *Can. J. Chem.* **1999,** *77,* 1821.

(75) Baird, I. R. *Fluorinated Nitroimidazoles and Their Ruthenium Complexes: Potential Hypoxia-Imaging Agents;* Ph. D. Dissertation, University of British Columbia: Vancouver, 1999.

(76) (a) Baird, I. R.; Skov, K. A.; James, B. R.; Rettig, S. J.; Koch, C. J. *Synth. Commun.* **1998,** *28,* 3701.

(b) Koch, C. J.; Kachur, A. V.; Evans, S. M.; Shiue, C.-Y.; Baird, I. R.; Skov, K. A.; James, B. R.; Dolbier, Jr., W. R.; Li, A.-R. 1998, UPN-3388; Serial No. 09/123,300.

(77) Greaves, S. J.; Griffith, W. P. *Polyhedron* **1988,** *7,* 1973.

(78) El-Hendawy, A. M.; El-Shahawi, M. S. *Polyhedron* **1989,** *8,* 2813.

(79) Capper, G.; Carter, L. C.; Davies, D. L.; Fawcett, J.; Russell, D. R. *J. Chem. Soc. Dalton Trans.* **1996,** 1399.

(80) Fryzuk, M. D.; Jonker, M. J.; Rettig, S. J. *Chem. Commun.* **1997,** 377.

(81) (a) Morita, H.; Hayashi, Y.; Shimomura, S.; Kawaguchi, S. *Chem. Lett.* **1975,** 339.

(b) Morita, H.; Shimomura, S.; Kawaguchi, S. *Bull. Chem. Soc. Jpn.* **1976,** *49,* 2461.

(82) Ahmet, M. T.; Frampton, C. S.; Silver, J. *J. Chem. Soc. Dalton Trans.* **1988,** 1159.

(83) Dutt, N. K.; Sarma, U. U. M. *J. Inorg. Nucl. Chem.* **1975,** *37,* 1801.

(84) Fregona, D.; Faraglia, G.; Graziani, R.; Casellato, U.; Sitran, S. *Gazz. Chim. Ital.* **1994,** *124,* 153.

(85) Finnegan, M. M.; Lutz, T. G.; Nelson, W. O.; Smith, A.; Orvig, C. *Inorg. Chem.* **1987,** *26,* 2171.

(86) Matsuba, C. A.; Nelson, W. O.; Rettig, S. J.; Orvig, C. *Inorg. Chem.* **1988,** *27,* 3935.

(87) Finnegan, M. M.; Rettig, S. J.; Orvig, C. *J. Am. Chem. Soc.* **1986,** *108,* 5033.

(88) Orvig, C.; Rettig, S. J.; Trotter, J. *Can. J. Chem.* **1987,** *65,* 590.

(89) Luo, H.; Rettig, S. J.; Orvig, C. *Inorg. Chem.* **1993,** *32,* 4491.

(90) Caravan, P.; Gelmini, L.; Glover, N.; Herring, F. G.; Li, H.; McNeill, J. H.; Rettig, S. J.; Setyawati, I. A.; Shuter, E.; Sun, Y.; Tracey, A. S.; Yuen, V. G.; Orvig, C. *J. Am. Chem. Soc.* **1995,** *117,* 12759.

(91) Lord, S. J.; Epstein, N. A.; Paddock, R. L.; Vogels, C. M.; Hennigar, T. L.; Zaworotko, M. J.; Taylor, N. J.; Driedzic, W. R.; Broderick, T. L.; Westcott, S. A. *Can. J. Chem.* **1999,** *77,* 1249.

(92) Archer, C. M.; Dilworth, J. R.; Jobanputra, P.; Harman, M. E.; Hursthouse, M. B.; Karaulov, A. *Polyhedron* **1991,** *10,* 1539.

(93) Burgess, J.; Parsons, S. A. *Polyhedron* **1993,** *12,* 1959.

(94) Ahmed, S. I.; Burgess, J.; Fawcett, J.; Parsons, S. A.; Russell, D. R.; Laurie, S. H. *Polyhedron* **2000,** *19,* 129.

(95) Kennedy, D.; James, B. R. *Unpublished Results,* 2000.

CHAPTER 2

General Experimental Procedures and Syntheses of the Ruthenium Complexes

2.1 Solvents, Gases, and Reagents

Reagent grade solvents were purchased from Fisher Scientific and dried under N_2 before use. The drying agents were Mg/I_2 for MeOH and EtOH; CaH_2 for Et_2O, CH_2Cl_2, benzene, and hexanes; K_2CO_3 for acetone; and Na/benzophenone for tetrahydrofuran (THF). Prepurified N_2 and H_2 were purchased from Praxair, and were used as received. Deuterated solvents, $CDCl_3$, D_2O, CD_3OD, C_6D_6, and acetone-d_6, were purchased from Cambridge Isotope Laboratories and used without purification.

$RuCl_3 \cdot 3H_2O$ was supplied by Colonial Metals. Maltol and ethylmaltol (Cultor Food Science and Pfizer Food Science, respectively) were generously donated by Mr. D. E. Green (Prof. Orvig's group at UBC). Potassium *tert*-butoxide was purchased from Acros Organics. Metronidazole, 4-nitroimidazole, trifluoromethanesulfonic acid (CF_3SO_3H), 1,2-dibromoethane, ethanethiol, tetrabutylammonium hexafluorophosphate ([*n*-Bu_4N](PF_6)), ferrocene ($FeCp_2$), bis(pentamethylcyclopentadienyl)iron(II) ($FeCp^*_2$), and tetramethylenesulfoxide (TMSO) were all purchased from Aldrich, and were used as received. Sodium acetate, conc. HCl, and dimethylsulfoxide (DMSO) were purchased from Fisher Scientific. Silica gel preparative thin layer chromatography (TLC) plates with fluorescent indicator (20 x 20 cm^2, Uniplate from Analtech) were purchased from Aldrich.

2.2 Physical Techniques and Instrumentation

^1H nuclear magnetic resonance (NMR) and ^1H 2D COSY spectra were recorded on Brucker AV300 (300 MHz for ^1H) or AV400 (400 MHz for ^1H) instruments; s = singlet, d = doublet, t = triplet, q = quartet, v = very, br = broad, and m = multiplet. Chemical shifts were calibrated using the residual protonated solvent peaks: δ 7.24

References on page 47

($CDCl_3$), 4.65 (D_2O), 4.78 (CD_3OD), 7.15 (C_6D_6), and 2.04 (acetone-d_6). Elemental analyses (C, H, N) were performed by Mr. P. Borda of this department on a Carlo Erba Instruments EA 1108 CHN-O analyzer, or by Mr. M. K. Yang of the SFU Chemistry Department.

The mass spectral data of Kratos Concept IIHQ liquid secondary ion mass spectrometry (LSIMS) using thioglycerol or 3-nitrobenzylalcohol (3-NBA) matrix, Brucker Esquire electrospray (ES ion trap), and Micromass LCT electrospray time of flight (ES TOF) mass spectrometry were collected by the staff of the UBC mass spectrometry laboratory under the supervision of Dr. G. Eigendorf. UV-vis electronic absorption spectra were recorded on a Hewlett Packard 8452A diode array spectrometer. UV-vis spectral data are presented as λ_{max} (±2 nm) (ε_{max} x 10^{-3} (M^{-1} cm^{-1})). Infrared spectra were recorded either as a Nujol mull between KBr plates or as a solid KBr pellet using an ATI Mattson Genesis or a Bomem-Michelson MB-100 FT-IR spectrometer. Selected IR stretching frequencies are reported in wavenumbers (±4 cm^{-1}) and functional groups are assigned.[1]

Conductivity measurements were carried out on a model RCM151B Serfass conductance bridge (A. H. Thomas Co. Ltd.) connected to a 3403 cell from the Yellow Springs Instrument Company. The cell was calibrated using a standard 0.01000 M aqueous KCl solution with a molar conductance (Λ_M) equal to 141.3 Ω^{-1} cm^2 mol^{-1} at 25 °C and a cell constant of 1.016 cm^{-1}.[2,3]

Cyclic voltammetry was measured in CH_2Cl_2 or THF containing 0.1 M [*n*-Bu_4N](PF_6) as supporting electrolyte. The voltammogram was recorded using a Pine Bipotentiostat (Model AFCBP1) and the software PineChem v2.00. The scan-rate was 200 mV/s using a Pt working electrode, a Pt wire counter electrode, and a silver wire reference electrode. $FeCp_2$ (0.46 V in CH_2Cl_2, 0.56 V in THF vs. SCE) or $FeCp^*_2$ (-0.13 V in CH_2Cl_2 vs. SCE) was added as an internal standard for calibration.[4] X-ray crystal structures were determined by Dr. B. O. Patrick of this department on a Rigaku/ADSC CCD area detector with graphite monochromated MoKα radiation.

2.3 Syntheses of Sulfur Compounds

References on page 47

2.3.1 Preparation of 3,6-Dithiaoctane (BETE) [MW = 150.307 g/mol]

This compound was synthesized according to a modified procedure of Morgan and Ledbury.[5] Inside a fume hood, ethanethiol (15.5 mL, 210 mmol) was added dropwise at room temperature (r.t.) to a white suspension of NaOH (8.40 g, 210 mmol) in 100 mL MeOH, and the mixture was refluxed for 1 h at 70 °C. The yellow suspension was cooled to 0 °C when 1,2-dibromoethane (9 mL, 105 mmol) was added dropwise with constant stirring to give a white precipitate. The mixture was then refluxed for 1 h at 70 °C, cooled to r.t., and transferred to a 500 mL separatory funnel. H_2O (100 mL) and Et_2O (40 mL) were added, and the top ether layer was collected in a Schlenk tube. The aqueous layer was extracted with Et_2O (2 x 40 mL), and the organic residues were combined. The Et_2O was removed under vacuum, and the oily product was dried over $MgSO_4$ and filtered to yield a yellow liquid.

Yield: 7.91 g (8.4 mL, 50 %). ^{1}H NMR ($CDCl_3$): δ 1.24 (t, 6H, C*H*$_3$, $^3J_{HH}$ = 7.4 Hz); 2.55 (q, 4H, C*H*$_2$CH$_3$, $^3J_{HH}$ = 7.4 Hz); 2.71 (s, 4H, C*H*$_2$SCH$_2$CH$_3$). The NMR data agree with those reported by Huxham.[6]

2.3.2 Preparation of 1,2-Bis(ethylsulfinyl)ethane (BESE) [MW = 182.306 g/mol]

This compound was synthesized according to the procedure of Hull and Bargar.[7] A solution of BETE (5 mL, 33 mmol), DMSO (5.5 mL, 78 mmol), and conc. HCl (0.2 mL) was refluxed for 16 h at 85 °C. The solution was cooled to 0 °C, and 20 mL acetone was then added. Sonication yielded a white crystalline precipitate that was isolated by filtration. The filtrate was heated for an additional 2 h at 85 °C to reduce its volume. The mixture was cooled to 0 °C to precipitate more crude product that was filtered, washed with acetone (50 mL), and re-crystallized twice from EtOH (2 x 20 mL). The white solid BESE was dried in vacuo at 78 °C for 16 h.

Yield: 1.69 g (30 %). ^{1}H NMR ($CDCl_3$): δ 1.35 (t, 6H, C*H*$_3$, $^3J_{HH}$ = 7.5 Hz); 2.81 (q, 4H, C*H*$_2$CH$_3$, $^3J_{HH}$ = 7.5 Hz); 3.08 (m, 4H, C*H*$_2$S(O)CH$_2$CH$_3$). Anal. Calcd for $C_6H_{14}O_2S_2$: C, 39.53; H, 7.74. Found: C, 39.44; H, 7.84. IR (Nujol): $\nu_{S=O}$ 1016, 1044. The NMR and IR data agree with those reported in the literature.[7,8]

2.4 Syntheses of Maltolate Salts

References on page 47

(See Figure 1.17 for the numbering scheme of maltol and ethylmaltol.)

2.4.1 Preparation of Potassium Maltolate (Kma) [MW = 164.200 g/mol]

This compound was synthesized according to a modified procedure of Fryzuk *et al.*[9] A suspension of maltol (1.00 g, 7.93 mmol) and potassium *tert*-butoxide (0.890 g, 7.93 mmol) was stirred in Et_2O (300 mL) at r.t. for 30 min. The cream yellow precipitate was filtered off and stirred in 200 mL CH_2Cl_2 at r.t. for 30 min. The solid was filtered, washed with Et_2O (3 x 20 mL), and dried in vacuo at r.t. for 16 h. The product was very hygroscopic, and was stored under vacuum.

Yield: 1.246 g (96 %). ^{1}H NMR (CD_3OD): δ 2.26 (s, 3H, C*H*$_3$); 6.17 (d, 1H, *H*$_5$, $^3J_{HH}$ = 5.3 Hz); 7.64 (d, 1H, *H*$_6$, $^3J_{HH}$ = 5.3 Hz). Anal. Calcd for $C_6H_5O_3K \cdot H_2O$: C, 39.55; H, 3.87. Found: C, 39.68; H, 3.55. UV-vis (H_2O): 222 (9.87), 276 (3.79), 320 (3.36). IR (KBr): $\nu_{C=O} + \nu_{C=C}$ 1519, 1575; $\nu_{C=O}$ 1621.

2.4.2 Preparation of Potassium Ethylmaltolate (Ketma) [MW = 178.226 g/mol]

This compound was synthesized following the procedure in Section 2.4.1, except ethylmaltol (1.00 g, 7.14 mmol) and potassium *tert*-butoxide (0.801 g, 7.14 mmol) were used.

Yield: 1.213 g (95 %). ^{1}H NMR (CD_3OD): δ 1.11 (t, 3H, C*H*$_3$, $^3J_{HH}$ = 7.5 Hz); 2.70 (q, 2H, C*H*$_2$, $^3J_{HH}$ = 7.5 Hz); 6.16 (d, 1H, *H*$_5$, $^3J_{HH}$ = 5.2 Hz); 7.67 (d, 1H, *H*$_6$, $^3J_{HH}$ = 5.2 Hz). Anal. Calcd for $C_7H_7O_3K \cdot H_2O$: C, 42.84; H, 4.62. Found: C, 42.31; H, 4.37 (very hygroscopic). UV-vis (H_2O): 222 (9.40), 276 (4.33), 320 (3.22). IR (KBr): $\nu_{C=O} + \nu_{C=C}$ 1505, 1575; $\nu_{C=O}$ 1620.

2.5 Spectroscopic Data of Maltols and Nitroimidazoles

(See Figures 1.14 and 1.17 for the numbering schemes of nitroimidazole and maltol compounds, respectively.)

Maltol [MW = 126.110 g/mol]: ^{1}H NMR ($CDCl_3$): δ 2.34 (s, 3H, C*H*$_3$); 6.39 (d, 1H, *H*$_5$, $^3J_{HH}$ = 5.5 Hz); 6.45 (br s, 1H, O*H*); 7.68 (d, 1H, *H*$_6$, $^3J_{HH}$ = 5.5 Hz). Anal. Calcd for $C_6H_6O_3$: C, 57.14; H, 4.80. Found: C, 57.36; H, 4.81. UV-vis (H_2O): 214 (11.5), 274

References on page 47

(9.45). IR (KBr): $\nu_{C=O}$ + $\nu_{C=C}$ 1561, 1618; $\nu_{C=O}$ 1655; ν_{OH} 3259. The NMR and IR data agree with those reported in the literature.[10]

Ethylmaltol [MW = 140.136 g/mol]: ^{1}H NMR ($CDCl_3$): δ 1.22 (t, 3H, C*H*$_3$, $^3J_{HH}$ = 7.6 Hz); 2.73 (q, 2H, C*H*$_2$, $^3J_{HH}$ = 7.6 Hz); 6.40 (d, 1H, *H*$_5$, $^3J_{HH}$ = 5.5 Hz); 6.68 (br s, 1H, O*H*); 7.71 (d, 1H, *H*$_6$, $^3J_{HH}$ = 5.5 Hz). Anal. Calcd for $C_7H_8O_3$: C, 59.99; H, 5.75. Found: C, 59.93; H, 5.90. UV-vis (H_2O): 214 (10.4), 276 (9.04). IR (KBr): $\nu_{C=O}$ + $\nu_{C=C}$ 1557, 1612; $\nu_{C=O}$ 1647; ν_{OH} 3085.

Metronidazole (metro) [MW = 171.154 g/mol]: ^{1}H NMR (acetone-*d*$_6$): δ 2.50 (s, 3H, C*H*$_3$); 3.88 (q, 2H, CH_2CH_2OH, $^3J_{HH}$ = 5.4 Hz); 4.22 (t, 1H, O*H*, $^3J_{HH}$ = 5.4 Hz); 4.49 (t, 2H, CH_2CH_2OH, $^3J_{HH}$ = 5.4 Hz); 7.87 (s, 1H, *H*$_4$). Anal. Calcd for $C_6H_9N_3O_3$: C, 42.10; H, 5.30; N, 24.55. Found: C, 42.30; H, 5.33; N, 24.43. UV-vis (H_2O): 232 (2.44), 320 (6.85). IR (KBr): $\nu_{N=O\ sym.}$ 1369; $\nu_{N=O\ asym.}$ 1474; ν_{OH} 3222. CV (CH_2Cl_2): $E_{½}$ (NO_2/ NO_2^-) = -1.22 V vs. SCE. The NMR and IR data agree with those reported by Chan,[11] and the CV data agree with those reported by Baird.[12]

4-Nitroimidazole (4-NO_2Im) [MW = 113.074 g/mol]: ^{1}H NMR (acetone-*d*$_6$): δ 7.77 (s, 1H, *H*$_5$); 8.13 (s, 1H, *H*$_2$). Anal. Calcd for $C_3H_3N_3O_2$: C, 31.87; H, 2.67; N, 37.16. Found: C, 32.02; H, 2.62; N, 36.89. UV-vis (H_2O): 224 (3.47), 298 (5.35). IR (KBr): $\nu_{N=O\ sym.}$ 1381; $\nu_{N=O\ asym.}$ 1495. CV (THF): $E_{½}$ (NO_2/NO_2^-) = -1.17 V vs. SCE. The NMR and IR data agree with those reported by Chan.[11]

2.6 Syntheses of Ruthenium(II) Precursors

2.6.1 Preparation of *Cis*-$RuCl_2(DMSO)_3(DMSO)$ [MW = 484.510 g/mol]

This compound was synthesized according to the procedure of Evans *et al.*[13] A dark brown-red solution of $RuCl_3 \cdot 3H_2O$ (500 mg, 1.91 mmol) in DMSO (5 mL, 70.5 mmol) was refluxed at 180 °C for 10 min. The resulting brown-yellow solution was cooled to r.t., and acetone (30 mL) was added. The mixture was sonicated to yield a bright yellow precipitate that was filtered off, washed with acetone (20 mL), and dried in vacuo at 78 °C for 16 h.

References on page 47

Yield: 550 mg (57 %). ^{1}H NMR ($CDCl_3$): δ 2.71 (s, 6H, $CH_3S(\underline{O})$); 3.31, 3.41, 3.48, 3.51 (s, 18H, $CH_3\underline{S}(O)$). Anal. Calcd for $C_8H_{24}O_4Cl_2S_4Ru$: C, 19.83; H, 4.99. Found: C, 20.00; H, 4.99. LR-MS (+LSIMS, thioglycerol): 485 (M^+), 449 (M^+ - Cl), 371 (M^+ - Cl - DMSO), 293 (M^+ - Cl - 2 DMSO). UV-vis (H_2O): 230 (12.1), 316 (0.30), 356 (0.45). IR (Nujol): $\nu_{S=O}$ 918 (O-bonded); 1095, 1122 (S-bonded). Λ_M (H_2O) = 35 (10 min), 75 (3 h), 115 (10 h) Ω^{-1} cm^2 mol^{-1} (1:1 electrolyte). CV (CH_2Cl_2): $E_{½}$ ($Ru^{III/II}$) = 1.11 V vs. SCE. The NMR and IR data agree with those reported by Chan,[11] and the UV-vis and conductivity data agree with those in the literature.[14]

2.6.2 Preparation of *Cis*-$RuCl_2(TM\underline{S}O)_4$ [MW = 588.660 g/mol]

This compound was synthesized according to the procedure of Yapp *et al.*[15] H_2 gas (1 atm) was bubbled through a mixture of $RuCl_3 \cdot 3H_2O$ (300 mg, 1.15 mmol) in 10 mL MeOH, and the mixture was refluxed at 70 °C for 3 h to generate a Ru "blue" solution.[16] TMSO (1.0 mL, 11.1 mmol) was then added, and the resulting green solution was refluxed for 5 h by which time a yellow-green precipitate had deposited. This was filtered off hot, washed with acetone (2 x 10 mL), and dried in vacuo at 78 °C for 16 h.

Yield: 509 mg (75 %). ^{1}H NMR ($CDCl_3$): δ 2.25 (m, 16H, $CH_2CH_2S(O)$); 3.42, 4.00 (m, 8H each, $CH_2CH_2S(O)$). Anal. Calcd for $C_{16}H_{32}O_4Cl_2S_4Ru$: C, 32.65; H, 5.48. Found: C, 32.53; H, 5.40. LR-MS (+LSIMS, thioglycerol): 590 (M^+), 553 (M^+ - Cl), 486 (M^+ - TMSO), 449 (M^+ - Cl - TMSO). UV-vis (H_2O): 238 (13.4), 362 (0.52). IR (Nujol): $\nu_{S=O}$ 1056, 1110 (S-bonded). Λ_M (H_2O) = 20 (5 min), 45 (3 h), 105 (10 h) Ω^{-1} cm^2 mol^{-1} (1:1 electrolyte). CV (CH_2Cl_2): $E_{½}$ ($Ru^{III/II}$) = 1.03 V vs. SCE. The NMR, UV-vis, and IR data agree with those reported in the literature.[15]

2.6.3 Preparation of $[RuCl(H_2O)(BESE)]_2(\mu\text{-}Cl)_2$ [MW = 744.590 g/mol]

This compound was synthesized according to the procedure of Cheu.[17] In a Schlenk tube, a mixture of $RuCl_3 \cdot 3H_2O$ (250 mg, 0.956 mmol) and conc. HCl (0.5 mL) in EtOH (25 mL) was refluxed at 85 °C for 8 h. BESE (175 mg, 0.960 mmol) was then added, and the mixture was refluxed for 16 h in the formation of a yellow precipitate. The volume was reduced to 10 mL under vacuum, and the product was filtered off, washed

References on page 47

with EtOH (10 mL), and dried in vacuo at r.t. for 1 h. The product was then dried in vacuo at 78 °C for 16 h.

Yield: 210 mg (59 %). ^{1}H NMR (D_2O): δ 1.48 (m, 12H, CH_3); 3.20 - 4.00 (br m, 16H, $CH_2S(O)CH_2CH_3$). Anal. Calcd for $C_{12}H_{32}O_6Cl_4S_4Ru_2$: C, 19.36; H, 4.33. Found: C, 19.49; H, 4.54. LR-MS (+ES TOF, H_2O): 709 (M^+ - Cl), 674 (M^+ - 2 Cl). UV-vis (H_2O): 230 (38.8), 342 (2.60). IR (Nujol): $\nu_{S=O}$ 1065, 1116 (S-bonded). Λ_M (H_2O) = 410 Ω^{-1} cm^2 mol^{-1} (3:1 electrolyte). CV (CH_2Cl_2): $E_{½}$ ($Ru^{III/II}$) = 0.92 V vs. SCE. The NMR, UV-vis, IR, and conductivity data agree with those reported by Cheu,[17] and the MS data agree with those reported by Huxham.[6]

2.7 Syntheses of Ruthenium(II) Maltolato Complexes Containing Ancillary Monodentate Sulfoxide Ligands

2.7.1 Preparation of Ru(ma)$_2$(DMSO)$_2$ [MW = 507.543 g/mol]

This compound was synthesized by a modified procedure of Fryzuk *et al.*[9] In a Schlenk tube, a suspension of *cis*-$RuCl_2(DMSO)_3(DMSO)$ (100 mg, 0.206 mmol) and Kma (85 mg, 0.518 mmol) in EtOH (20 mL) was refluxed at 80 °C for 16 h, resulting in a dark red solution. The solvent was removed under vacuum, and the residue was extracted with benzene (2 x 20 mL). The solution was then filtered through Celite, and the filtrate was reduced to 10 mL under vacuum. Hexanes (60 mL) was added to yield a yellow precipitate that was filtered off under N_2 and dried in vacuo at r.t. for 16 h. The product was very hygroscopic, and was stored under N_2.

Yield: 55 mg (53 %). ^{1}H NMR (C_6D_6): δ 2.07, 2.13, 2.14, 2.18 (s, 6H, CH_3-maltolato); 2.77, 2.86, 2.87, 2.94, 2.98, 3.07, 3.13, 3.19, 3.21, 3.28, 3.30, 3.34 (s, 12H, $CH_3S(O)$); 6.03 - 6.15 (multiple d, 2H, H_5-maltolato, $^3J_{HH}$ = 5.1 Hz); 6.47 - 6.59 (multiple d, 2H, H_6-maltolato, $^3J_{HH}$ = 5.1 Hz). Anal. Calcd for $C_{16}H_{22}O_8S_2Ru$: C, 37.86; H, 4.37. Found: C, 38.00; H, 4.55. LR-MS (+LSIMS, thioglycerol): 509 (M^+), 430 (M^+ - DMSO), 368 (M^+ - DMSO - C_2H_6S), 352 (M^+ - 2 DMSO). UV-vis (H_2O): 212 (32.0), 270 (10.7), 356 (6.03). IR (KBr): $\nu_{S=O}$ 1094 (S-bonded); $\nu_{C=O}$ + $\nu_{C=C}$ 1547; $\nu_{C=O}$ 1595. Λ_M (H_2O) = 8

References on page 47

Ω^{-1} cm^2 mol^{-1} (non-conducting). CV (CH_2Cl_2): $E_{½}$ ($Ru^{III/II}$) = 0.52 V vs. SCE. The NMR and IR data agree with those reported by Jonker.[18]

2.7.2 Preparation of Ru(etma)$_2$(DMSO)$_2$ [MW = 535.596 g/mol]

This new compound was synthesized following the procedure in Section 2.7.1, except Ketma (92 mg, 0.516 mmol) was used.

Yield: 50 mg (45 %). ^{1}H NMR (C_6D_6): δ 0.94 - 1.10 (br m, 6H, C*H*$_3$-ethylmaltolato); 2.49 - 2.85 (br m, 4H, C*H*$_2$-ethylmaltolato); 2.79, 2.88, 2.95, 2.99, 3.07, 3.09, 3.13, 3.18, 3.20, 3.28, 3.30, 3.36 (s, 12H, C*H*$_3$S(O)); 6.02 - 6.16 (multiple d, 2H, *H*$_5$-ethylmaltolato, $^3J_{HH}$ = 5.1 Hz); 6.51 - 6.64 (multiple d, 2H, *H*$_6$-ethylmaltolato, $^3J_{HH}$ = 5.1 Hz). Anal. Calcd for $C_{18}H_{26}O_8S_2Ru$: C, 40.36; H, 4.89. Found: C, 40.38; H, 4.88. LR-MS (+LSIMS, thioglycerol): 537 (M^+), 459 (M^+ - DMSO), 396 (M^+ - DMSO - C_2H_6S), 380 (M^+ - 2 DMSO). UV-vis (H_2O): 212 (29.5), 272 (10.1), 356 (5.82). IR (KBr): $\nu_{S=O}$ 1097 (S-bonded); $\nu_{C=O}$ + $\nu_{C=C}$ 1546; $\nu_{C=O}$ 1592. Λ_M (H_2O) = 15 Ω^{-1} cm^2 mol^{-1} (essentially non-conducting). CV (CH_2Cl_2): $E_{½}$ ($Ru^{III/II}$) = 0.51 V vs. SCE.

2.7.3 Preparation of Ru(ma)$_2$(TMSO)$_2$ [MW = 559.617 g/mol]

This new compound was synthesized following the procedure in Section 2.7.1, except *cis*-$RuCl_2$(TMSO)$_4$ (100 mg, 0.170 mmol) and Kma (70 mg, 0.426 mmol) were used in 50 mL EtOH.

Yield: 50 mg (53 %). ^{1}H NMR (C_6D_6): δ 1.50 - 2.50 (br m, 8H, C*H*$_2$CH$_2$S(O)); 2.07, 2.18, 2.20, 2.24 (s, 6H, C*H*$_3$-maltolato); 3.00 - 4.60 (br m, 8H, CH$_2$C*H*$_2$S(O)); 6.05 - 6.25 (multiple d, 2H, *H*$_5$-maltolato, $^3J_{HH}$ = 5.1 Hz); 6.45 - 6.65 (multiple d, 2H, *H*$_6$-maltolato, $^3J_{HH}$ = 5.1 Hz). Anal. Calcd for $C_{20}H_{26}O_8S_2Ru \cdot H_2O$: C, 41.59; H, 4.89. Found: C, 41.49; H, 4.71. LR-MS (+LSIMS, thioglycerol): 561 (M^+), 456 (M^+ - TMSO), 368 (M^+ - TMSO - C_4H_8S), 352 (M^+ - 2 TMSO). UV-vis (H_2O): 210 (31.0), 270 (9.60), 354 (5.44). IR (KBr): $\nu_{S=O}$ 1056, 1117 (S-bonded); $\nu_{C=O}$ + $\nu_{C=C}$ 1549; $\nu_{C=O}$ 1594. Λ_M (H_2O) = 30 Ω^{-1} cm^2 mol^{-1}. CV (CH_2Cl_2): $E_{½}$ ($Ru^{III/II}$) = 0.52 V vs. SCE.

2.7.4 Preparation of Ru(etma)$_2$(TMSO)$_2$ [MW = 587.670 g/mol]

References on page 47

This new compound was synthesized following the procedure in Section 2.7.1, except *cis*-$RuCl_2(TM\underline{S}O)_4$ (100 mg, 0.170 mmol) and Ketma (76 mg, 0.426 mmol) were used in 50 mL EtOH.

Yield: 50 mg (50 %). ^{1}H NMR (C_6D_6): δ 0.70 - 1.30 (br m, 6H, C*H*$_3$-ethylmaltolato); 1.40 - 2.10 (br m, 8H, C*H*$_2$CH$_2$S(O)); 2.40 - 2.90 (br m, 4H, C*H*$_2$-ethylmaltolato); 3.00 - 4.50 (br m, 8H, CH$_2$C*H*$_2$S(O)); 6.00 - 6.25 (multiple d, 2H, *H*$_5$-ethylmaltolato, $^3J_{HH}$ = 5.1 Hz); 6.45 - 6.70 (multiple d, 2H, *H*$_6$-ethylmaltolato, $^3J_{HH}$ = 5.1 Hz). Anal. Calcd for $C_{22}H_{30}O_8S_2Ru$: C, 44.96; H, 5.15. Found: C, 44.78; H, 5.08. LR-MS (+LSIMS, thioglycerol): 589 (M^+), 484 (M^+ - TMSO), 396 (M^+ - TMSO - C_4H_8S), 380 (M^+ - 2 TMSO). UV-vis (H_2O): 214 (31.0), 272 (10.6), 358 (5.95). IR (KBr): $\nu_{S=O}$ 1055, 1116 (S-bonded); $\nu_{C=O}$ + $\nu_{C=C}$ 1546; $\nu_{C=O}$ 1592. Λ_M (H_2O) = 20 Ω^{-1} cm^2 mol^{-1}. CV (CH_2Cl_2): $E_{½}$ ($Ru^{III/II}$) = 0.52 V vs. SCE.

2.8 Syntheses of New Ruthenium(II) Maltolato Complexes Containing An Ancillary Bidentate Sulfoxide Ligand

2.8.1 Preparation of *Cis*-Ru(ma)$_2$(BESE) [MW = 533.580 g/mol]

In a Schlenk tube, a suspension of [RuCl(H_2O)(BESE)]$_2$(μ-Cl)$_2$ (100 mg, 0.134 mmol) and Kma (110 mg, 0.670 mmol) in EtOH (20 mL) was refluxed at 80 °C for 16 h, this resulting in a dark red solution. The solvent was removed under vacuum, and the residue was then extracted with benzene (3 x 20 mL); the mixture was then filtered through Celite. The volume was reduced to 10 mL under vacuum, and hexanes (60 mL) was added to yield a yellow precipitate that was filtered off under N_2, dried in vacuo at r.t. for 1 h, and then dried in vacuo at 78 °C for 16 h. The product was very hygroscopic, and was stored under N_2. Crystals suitable for X-ray diffraction analysis were grown from an acetone solution of the complex layered with hexanes. The structure shows *trans*-carbonyl oxygens of the maltolato ligands and an S-bonded *S,R*-BESE.

Yield: 57 mg (40 %). ^{1}H NMR of a mixture of isomers (D_2O): δ 1.15 - 1.50 (br m, 6H, C*H*$_3$-BESE); 2.23, 2.26, 2.34, 2.37 (s, 6H, C*H*$_3$-maltolato); 2.60 - 3.90 (br m, 8H, C*H*$_2$S(O)C*H*$_2$CH$_3$); 6.47 - 6.71 (multiple d, 2H, *H*$_5$-maltolato, $^3J_{HH}$ = 5.0 Hz); 7.82 - 7.95

References on page 47

(multiple d, 2H, H_6-maltolato, $^3J_{HH}$ = 5.0 Hz). The ^{1}H 2D COSY spectrum shown in Figure 3.5B (p.56) provides for more detailed assignments. ^{1}H NMR of the crystals (D_2O): δ 1.20 - 1.50 (m, 6H, CH_3-BESE); 2.35, 2.39 (s, 6H, CH_3-maltolato); 2.60 - 3.90 (m, 8H, CH_2S(O)CH_2CH$_3$); 6.53, 6.55 (d, 2H, H_5-maltolato, $^3J_{HH}$ = 5.1 Hz); 7.84, 7.88 (d, 2H, H_6-maltolato, $^3J_{HH}$ = 5.1 Hz). Anal. Calcd for $C_{18}H_{24}O_8S_2Ru$: C, 40.52; H, 4.53. Found: C, 40.39; H, 4.53. LR-MS (+LSIMS, thioglycerol): 535 (M^+), 368 (M^+ - $C_6H_{14}S_2O$), 352 (M^+ - BESE). UV-vis (H_2O): 208 (34.7), 266 (13.9), 354 (6.94). IR (KBr): $\nu_{S=O}$ 1079, 1113 (S-bonded); $\nu_{C=O}$ + $\nu_{C=C}$ 1549, 1560; $\nu_{C=O}$ 1595. Λ_M (H_2O) = 4 Ω^{-1} cm^2 mol^{-1} (non-conducting). CV (CH_2Cl_2): $E_{½}$ ($Ru^{III/II}$) = 0.55 V vs. SCE.

2.8.2 Preparation of *Cis*-Ru(etma)$_2$(BESE) [MW = 561.633 g/mol]

This new compound was synthesized following the procedure in Section 2.8.1, except Ketma (120 mg, 0.516 mmol) was used.

Yield: 50 mg (33 %). ^{1}H NMR (D_2O): δ 1.06 (m, 6H, CH_3-ethylmaltolato); 1.15 - 1.50 (br m, 6H, CH_3-BESE); 2.55 - 3.95 (br m, 12H, CH$_3$CH_2-ethylmaltolato and CH_2S(O)CH_2CH$_3$); 6.50 - 6.70 (multiple d, 2H, H_5-ethylmaltolato, $^3J_{HH}$ = 5.1 Hz); 7.83 - 7.97 (multiple d, 2H, H_6-ethylmaltolato, $^3J_{HH}$ = 5.1 Hz). The ^{1}H 2D COSY spectrum shown in Figure 3.6B (p.57) provides for more detailed assignments. Anal. Calcd for $C_{20}H_{28}O_8S_2Ru$: C, 42.77; H, 5.03. Found: C, 43.03; H, 5.00. LR-MS (+LSIMS, thioglycerol): 562 (M^+), 396 (M^+ - $C_6H_{14}S_2O$), 380 (M^+ - BESE). UV-vis (H_2O): 210 (32.1), 268 (13.1), 358 (6.71). IR (KBr): $\nu_{S=O}$ 1079, 1114 (S-bonded); $\nu_{C=O}$ + $\nu_{C=C}$ 1545, 1559; $\nu_{C=O}$ 1593. Λ_M (H_2O) = 9 Ω^{-1} cm^2 mol^{-1} (non-conducting). CV (CH_2Cl_2): $E_{½}$ ($Ru^{III/II}$) = 0.55 V vs. SCE.

2.9 Syntheses of New Ruthenium(II) Bidentate Sulfoxide-Nitroimidazole Complexes

2.9.1 Preparation of RuCl$_2$(BESE)(metro)$_2$ [MW = 696.589 g/mol]

In a Schlenk tube, a suspension of [RuCl(H_2O)(BESE)]$_2$(μ-Cl)$_2$ (150 mg, 0.201 mmol) and metronidazole (207 mg, 1.21 mmol) in MeOH (60 mL) was refluxed at 75 °C

References on page 47

for 16 h, this resulting in formation of a yellow mixture. The volume was reduced to 5 mL under vacuum, and the content was loaded onto a silica gel preparative TLC plate. The solvent was allowed to evaporate. The plate was eluted in a glass chamber using CH_2Cl_2:MeOH (90:10). The second major band from the top was removed, extracted with MeOH (3 x 20 mL), and the mixture was then filtered through Celite. The filtrate was reduced to 5 mL under vacuum, and Et_2O (60 mL) was added to precipitate a yellow product that was filtered off and dried in vacuo at r.t. for 1 h. The product was then dried in vacuo at 78 °C for 16 h. Some crystals appeared later, deposited from the filtrate (MeOH/Et_2O), and they were suitable for X-ray diffraction analysis. The structure shows a *trans*-arrangement of the chloride ligands and an S-bonded *R,R*-BESE.

Yield 72 mg (26 %). ^{1}H NMR (D_2O, 5 min): δ 1.00 - 1.60 (br m, 6H, C*H*$_3$-BESE); 2.34, 2.47, 2.60, 2.79 (s, 6H, C*H*$_3$-metro); 3.15 - 4.00 (br m, 12H, C*H*$_2$S(O)C*H*$_2$CH$_3$ and metro-CH$_2$C*H*$_2$OH); 4.30 - 4.80 (br m, 4H, metro-C*H*$_2$CH$_2$OH); 8.09, 8.14, 8.30, 8.49 (s, 2H, metro-*H*$_4$). The ^{1}H 2D COSY spectrum shown in Figure 3.10B (p.64) provides for more detailed assignments. Anal. Calcd for $C_{18}H_{32}N_6O_8Cl_2S_2Ru{\cdot}2H_2O$: C, 29.51; H, 4.95; N, 11.47. Found: C, 29.87; H, 4.70; N, 10.69. LR-MS (+ES Ion Trap, MeOH): 661 (M^+ - Cl), 491 (M^+ - Cl - metro), 456 (M^+ - 2 Cl - metro). UV-vis (H_2O): 310 (13.9). IR (KBr): $\nu_{S=O}$ 1079, 1114 (S-bonded); $\nu_{N=O\ sym.}$ 1364; $\nu_{N=O\ asym.}$ 1480; ν_{OH} 3422. Λ_M (H_2O) = 180 (5 min), 200 (30 min), 210 (3 h), 220 (24 h) Ω^{-1} cm^2 mol^{-1} (2:1 electrolyte). CV (CH_2Cl_2): $E_{½}$ (NO_2/NO_2^-) = -1.16, $E_{½}$ ($Ru^{III/II}$) = 1.18 V vs. SCE.

2.9.2 Attempted Preparation of $RuCl_2$(BESE)(4-NO_2Im)$_2$ [MW = 580.431 g/mol]

In a Schlenk tube, a suspension of [RuCl(H_2O)(BESE)]$_2$(μ-Cl)$_2$ (50 mg, 0.0672 mmol) and 4-nitroimidazole (46 mg, 0.407 mmol) in H_2O (20 mL) was refluxed at 100 °C for 16 h, this resulting in a dark brown suspension. The brown precipitate was filtered off, washed with MeOH (10 mL), and dried in vacuo at 78 °C for 16 h.

Yield: 33 mg (42 %). LR-MS (+ES TOF, 0.1 % formic acid in MeOH): 545 (M^+ - Cl), 467 (M^+ - 4-NO_2Im), 432 (M^+ - Cl - 4-NO_2Im). IR (KBr): $\nu_{S=O}$ 1085 (S-bonded); $\nu_{N=O\ sym.}$ 1380; $\nu_{N=O\ asym.}$ 1523. The MS data thus showed peaks likely corresponding to the title complex, but the elemental analysis was unsatisfactory (Anal. Calcd for $C_{12}H_{20}N_6O_6Cl_2S_2Ru$: C, 24.83; H, 3.47; N, 14.48. Found: C, 23.15; H, 3.77; N, 9.25).

References on page 47

Because of the insolubility of the product in common solvents, purification by chromatography was not attempted.

2.10 Syntheses of Ruthenium(II) Nitroimidazole Complexes

2.10.1 Preparation of $RuCl_2(metro)_4$ [MW = 856.591 g/mol]

This compound was synthesized according to the procedure of Baird.[12] H_2 gas (1 atm) was bubbled through a mixture of $RuCl_3 \cdot 3H_2O$ (100 mg, 0.382 mmol) in MeOH (10 mL), and the mixture was refluxed at 70 °C for 3 h to generate a Ru "blue" solution.[16] Metronidazole (262 mg, 1.53 mmol) was then added, and the blue-green mixture was refluxed for 16 h by which time a black-purple precipitate had deposited on the flask wall. The product was filtered off, washed with MeOH (2 x 10 mL), and dried in vacuo at 78 °C for 16 h.

Yield: 120 mg (37 %). ^{1}H NMR (acetone-d_6): δ 2.62 (br s, 12H, CH_3); 3.71 (br m, 8H, CH_2CH_2OH); 4.23 (br m, 4H, O*H*); 4.48 (br m, 8H, CH_2CH_2OH); 7.00 (v br s, 4H, H_4). Anal. Calcd for $C_{24}H_{36}N_{12}O_{12}Cl_2Ru$: C, 33.65; H, 4.24; N, 19.62. Found: C, 33.37; H, 4.36; N, 19.52. LR-MS (+LSIMS, 3-NBA): 858 (M^+), 822 (M^+ - Cl), 686 (M^+ - metro), 650 (M^+ - Cl - metro), 514 (M^+ - 2 metro). UV-vis (acetone): 548 (4.96). IR (KBr): $\nu_{N=O\ sym.}$ 1352; $\nu_{N=O\ asym.}$ 1475; ν_{OH} 3398. Λ_M (acetone) = 4 Ω^{-1} cm^2 mol^{-1} (non-conducting). CV (THF): $E_{½}$ (NO_2/NO_2^-) = -1.07, $E_{½}$ ($Ru^{III/II}$) = 0.19 V vs. SCE. The NMR, UV-vis, and IR data agree with those reported by Baird.[12]

2.10.2 Preparation of $RuCl_2(4\text{-}NO_2Im)_4$ [MW = 624.275 g/mol]

This new compound was synthesized following the procedure in Section 2.10.1, except 4-nitroimidazole (173 mg, 1.53 mmol) was used. A black precipitate was isolated.

Yield: 140 mg (59 %). Anal. Cald for $C_{12}H_{12}N_{12}O_8Cl_2Ru$: C, 23.09; H, 1.94; N, 26.92. Found: C, 23.27; H, 2.24; N, 26.95. LR-MS data were not obtained because of insolubility of the complex in the common matrices. IR (KBr): $\nu_{N=O\ sym.}$ 1381; $\nu_{N=O\ asym.}$ 1496. The complex is insoluble in common solvents, and thus ^{1}H NMR, UV-vis, conductivity, and CV data were not obtained.

References on page 47

2.11 Syntheses of Ruthenium(III) Maltolato and Mixed Maltolato-Metronidazole Complexes

2.11.1 Preparation of *Mer*-Ru(ma)$_3$ [MW = 476.376 g/mol]

This compound was synthesized according to a modified procedure of Greaves and Griffith.[10] A suspension of $RuCl_3 \cdot 3H_2O$ (200 mg, 0.765 mmol), sodium acetate (627 mg, 7.64 mmol), and maltol (482 mg, 3.82 mmol) in H_2O (20 mL) was refluxed at 110 °C for 4 h, this resulting in the formation of a dark red precipitate. The condenser was removed, and the mixture was heated for 1 h at 125 °C to reduce the volume to about 10 mL. The resulting suspension was cooled to r.t., and the precipitate was filtered off and added to CH_2Cl_2 (30 mL). The suspension was filtered through Celite, and the filtrate was then reduced to 10 mL under vacuum. Hexanes (60 mL) was added to yield a deep red precipitate that was collected, dried in vacuo at r.t. for 1 h, and then in vacuo at 78 °C for 16 h. The product was hygroscopic and stored under N_2.

Yield: 172 mg (47 %). Anal. Calcd for $C_{18}H_{15}O_9Ru$: C, 45.38; H, 3.17. Found: C, 45.00; H, 3.25. LR-MS (+LSIMS, thioglycerol): 477 (M^+), 352 (M^+ - maltolato). UV-vis (H_2O): 216 (45.1), 284 (14.0), 380 (10.4). IR (KBr): $\nu_{C=O} + \nu_{C=C}$ 1551, 1561; $\nu_{C=O}$ 1600. Λ_M (H_2O) = 26 Ω^{-1} cm^2 mol^{-1}. CV (CH_2Cl_2): $E_{½}$ ($Ru^{III/II}$) = -1.27, $E_{½}$ ($Ru^{IV/III}$) = 0.49 V vs. SCE. The IR and CV data agree with those reported in the literature.[10] The X-ray structure, showing a *mer*-configuration, was determined by Kennedy *et al.*[19]

2.11.2 Preparation of *Mer*-Ru(etma)$_3$ [MW = 518.456 g/mol]

This compound was synthesized following the procedure in Section 2.11.1, except ethylmaltol (536 mg, 3.82 mmol) was used. Crystals were grown from a CH_2Cl_2 solution of the complex layered with Et_2O. The X-ray diffraction data indicated the presence of twinned crystals.

Yield: 160 mg (40 %). Anal. Calcd for $C_{21}H_{21}O_9Ru$: C, 48.65; H, 4.08. Found: C, 48.48; H, 4.03. LR-MS (+LSIMS, thioglycerol): 519 (M^+), 380 (M^+ - ethylmaltolato). UV-vis (H_2O): 216 (44.8), 284 (14.5), 382 (10.5). IR (KBr): $\nu_{C=O} + \nu_{C=C}$ 1550; $\nu_{C=O}$ 1596.

References on page 47

Λ_M (H_2O) = 40 Ω^{-1} cm^2 mol^{-1}. CV (CH_2Cl_2): $E_{½}$ ($Ru^{III/II}$) = -1.29, $E_{½}$ ($Ru^{IV/III}$) = 0.48 V vs. SCE.

2.11.3 Preparation of *Trans*-[Ru(ma)$_2$(metro)$_2$](CF$_3$SO$_3$) [MW = 842.652 g/mol]

This compound was synthesized according to the procedure of Kennedy and James.[20] In a Schlenk tube, a solution of *mer*-Ru(ma)$_3$ (100 mg, 0.210 mmol) in EtOH (10 mL) was stirred at 60 °C. CF_3SO_3H (20 μL, 0.226 mmol) was added dropwise using a syringe, and the mixture was heated for 30 min at 80 °C. Metronidazole (144 mg, 0.841 mmol) was then added to the dark red mixture, which was refluxed for 16 h at 80 °C, this resulting in a dark blue-green suspension. The solvent was removed under vacuum, and CH_2Cl_2 (20 mL) was added to form a suspension that was filtered through a glass frit. The isolated precipitate was washed with CH_2Cl_2 (2 x 20 mL) and then dissolved in acetone (20 mL). The mixture was filtered through a layer of Celite, and hexanes (60 mL) was added to precipitate a blue-black product that was filtered off and dried in vacuo at 78 °C for 16 h. Crystals suitable for X-ray diffraction were grown from an acetone solution of the complex layered with hexanes. The structure shows a centrosymmetric *trans*-configuration.

Yield: 60 mg (34 %). Anal. Calcd for $C_{25}H_{28}N_6O_{15}F_3SRu$: C, 35.63; H, 3.35; N, 9.97. Found: C, 35.95; H, 3.40; N, 9.79. LR-MS (+LSIMS, thioglycerol): 694 (M^+ - CF_3SO_3), 523 (M^+ - CF_3SO_3 - metro), 352 (M^+ - CF_3SO_3 - 2 metro). UV-vis (acetone): 392 (7.01), 480 (2.02), 592 (2.28). IR (KBr): $\nu_{N=O\ sym.}$ 1367; $\nu_{N=O\ asym.}$ 1468; $\nu_{C=O}$ + $\nu_{C=C}$ 1551, 1560; $\nu_{C=O}$ 1604; ν_{OH} 3449. Λ_M (acetone) = 120 Ω^{-1} cm^2 mol^{-1} (1:1 electrolyte). CV (THF): $E_{½}$ (NO_2/NO_2^-) = -1.25, $E_{½}$ ($Ru^{III/II}$) = -0.53 V vs. SCE.

2.11.4 Preparation of *Trans*-[Ru(etma)$_2$(metro)$_2$](CF$_3$SO$_3$) [MW = 870.705 g/mol]

This compound was synthesized following the procedure in Section 2.11.3, except *mer*-Ru(etma)$_3$ (100 mg, 0.193 mmol), CF_3SO_3H (20 μL, 0.226 mmol), and metronidazole (132 mg, 0.771 mmol) were used.[20]

Yield: 65 mg (39 %). Anal. Calcd for $C_{27}H_{32}N_6O_{15}F_3SRu \cdot H_2O$: C, 36.49; H, 3.86; N, 9.46. Found: C, 36.52; H, 3.72; N, 9.55. LR-MS (+LSIMS, thioglycerol): 722 (M^+ - CF_3SO_3), 380 (M^+ - CF_3SO_3 - 2 metro). UV-vis (acetone): 394 (7.67), 482 (2.22), 592

References on page 47

(2.56). IR (KBr): $\nu_{N=O\ sym.}$ 1368; $\nu_{N=O\ asym.}$ 1472; $\nu_{C=O} + \nu_{C=C}$ 1549, 1560; $\nu_{C=O}$ 1600; ν_{OH} 3439. Λ_M (acetone) = 117 Ω^{-1} cm^2 mol^{-1} (1:1 electrolyte). CV (THF): $E_{½}$ (NO_2/NO_2^-) = -1.27, $E_{½}$ ($Ru^{III/II}$) = -0.52 V vs. SCE. The X-ray structure, showing a centrosymmetric *trans*-configuration, was determined by Kennedy *et al.*[19]

The ^{1}H NMR spectra of the paramagnetic Ru^{III} complexes described in Sections 2.11.1 to 2.11.4 are currently being investigated by D. Kennedy.

References on page 47

2.12 References

(1) Pavia, D. L.; Lampman, G. M.; Kriz, G. S. *Introduction to Spectroscopy, 2nd Ed.;* Harcourt Brace & Company: Orlando, 1996.

(2) Geary, W. J. *Coord. Chem. Rev.* **1971,** *7,* 81.

(3) Huheey, J. E. *Inorganic Chemistry: Principles of Structure and Reactivity, 3rd Ed.;* Harper Collins Publishers, Inc.: New York, 1983, p.362.

(4) Connelly, N. G.; Geiger, W. E. *Chem. Rev.* **1996,** *96,* 877.

(5) Morgan, G. T.; Ledbury W. *J. Chem. Soc.* **1922,** *121,* 2882.

(6) Huxham, L. A. *The Synthesis and Characterization of Ruthenium Disulfoxide Complexes and Their Preliminary In Vitro Examination as Potential Chemotherapeutic Agents;* M. Sc. Dissertation, University of British Columbia: Vancouver, 2001.

(7) Hull, C. M.; Bargar, T. W. *J. Org. Chem.* **1975,** *40,* 3152.

(8) Yapp, D. T. T.; Rettig, S. J.; James, B. R.; Skov, K. A. *Inorg. Chem.* **1997,** *36,* 5635.

(9) Fryzuk, M. D.; Jonker, M. J.; Rettig, S. J. *Chem. Commun.* **1997,** 377.

(10) Greaves, S. J.; Griffith, W. P. *Polyhedron* **1988,** *7,* 1973.

(11) Chan, P. K. L. *Ruthenium Nitroimidazole Complexes as Radiosensitizers;* Ph. D. Dissertation, University of British Columbia: Vancouver, 1988.

(12) Baird, I. R. *Fluorinated Nitroimidazoles and Their Ruthenium Complexes: Potential Hypoxia-Imaging Agents;* Ph. D. Dissertation, University of British Columbia: Vancouver, 1999.

(13) Evans, I. P.; Spencer, A.; Wilkinson, G. *J. Chem. Soc. Dalton Trans.* **1973,** 204.

(14) Alessio, E.; Mestroni, G.; Nardin, G.; Attia, W. M.; Calligaris, M.; Sava, G.; Zorzet, S. *Inorg. Chem.* **1988,** *27,* 4099.

(15) Yapp, D. T. T.; Jaswal, J.; Rettig, S. J.; James, B. R. *Inorg. Chim. Acta* **1990,** *177,* 199.

(16) Rose, D.; Wilkinson, G. *J. Chem. Soc. A* **1970,** 1791.

(17) Cheu, E. L. S. *Thioether and Sulfoxide Complexes of Ruthenium; Preliminary In Vitro Studies of Water-Soluble Species;* Ph. D. Dissertation, University of British Columbia: Vancouver, 2000.

(18) Jonker, M. J. *Synthesis, Characterization, and Reactivity of Ruthenium Maltolato Complexes;* M. Sc. Dissertation, University of British Columbia: Vancouver, 1993.

(19) Kennedy, D.; Patrick, B. O.; James, B. R. *Unpublished Results,* 2000.

(20) Kennedy, D.; James, B. R. *Unpublished Results,* 2000.

CHAPTER 3

Characterization of Ruthenium Maltolato, Sulfoxide, and Nitroimidazole Complexes

3.1 Ruthenium(II) Maltolato Complexes Containing Ancillary Monodentate Sulfoxide Ligands

3.1.1 The Ambidentate Nature of Sulfoxide Ligands

The structure of dimethylsulfoxide (DMSO) can be described using three resonance forms according to the valence bond model (Figure 3.1).[1] Studies have shown that sulfoxides are polarized, with a partial positive charge on the S, implying that a resonance contribution between **A** and **B** is predominant.[1] In the structure of *cis*-$RuCl_2(DMSO)_3(DMSO)$ (**1**), DMSO shows the capability of bonding through either the S- or O-atoms.[2] These bonding modes can be readily distinguished by IR spectroscopy. O-bonding withdraws electron density from the S-O bond and results in a lower IR stretching frequency ($\nu_{S=O}$) (versus that of non-coordinated sulfoxide), while S-bonding increases the electron donation from the O to S and strengthens the S-O bond, resulting in an increase of the IR frequency.

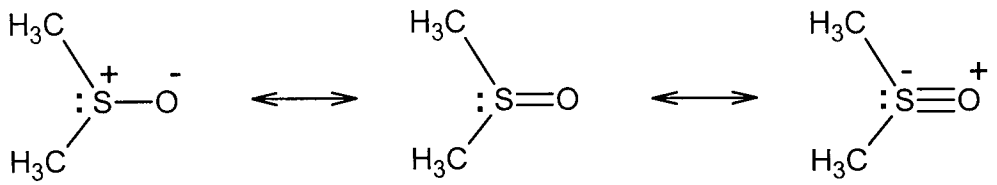

A **B** **C**

Figure 3.1 Resonance structures of DMSO. The lone pairs on the O are not shown (adapted from ref. 1).

References on page 81

^{1}H NMR spectroscopy can also be used to determine S- or O-bonding within sulfoxide ligands. S-bonding withdraws electron density from the C-S bond, and deshields the α-protons of, for example, DMSO.[3] The proton signals are observed ~1 ppm downfield from those of free DMSO. O-bonding results in a smaller withdraw of the electron density from the C-S bond, and the α-proton signals are less than 0.5 ppm downfield from those of free DMSO.[3]

The preference for S- or O-bonding has been proposed to follow the general trend of the hard-soft acid-base (HSAB) theory.[1] First-row transition metals (hard Lewis acids) prefer O-bonding, O being a hard Lewis base, but S-bonding to second- and third-row transition metals is not prevalent, where it mostly favors d^6 or d^8 metal complexes such as Ru^{II} and Pt^{II}; this suggests that a particular electronic structure is required in complexes with S-bonding.[1] π back-bonding from the metal to S is presumably necessary to stabilize the π-accepting property of S-bonded sulfoxides.[1]

Electronic and steric factors introduced by ancillary ligands can also influence S- or O-bonding. In the example of **1,** the presence of an O-bonded DMSO relieves the steric constraints from the neighboring S-bonded DMSO ligands,[2] while the analogue, *cis*-$RuCl_2(TM\underline{S}O)_4$ (**7**), contains no O-bonded TMSO, implying that an S-bonded DMSO is more sterically demanding than an S-bonded TMSO (TMSO = tetramethylenesulfoxide).[4,5]

The structure of *trans*-$RuCl_2(DM\underline{S}O)_4$ (**2**) shows that the S-bonded DMSO ligands are *trans* to one another.[6] The Ru-S bonds in **2** (average bond length = 2.352 Å) are weaker and longer than those of **1** (2.268 Å), which is the thermodynamically more stable product. This suggests that two, mutually *trans* S-bonded DMSO ligands is an electronically less favored situation because their π-accepting property competes for the electron density of the metal. This is manifested in the aqueous chemistry of **2** (see Figure 1.2, p.3), where two *cis*-DMSO ligands are immediately displaced by H_2O after the dissolution of the complex, because of the *trans*-effect of S-bonded DMSO.[6] In the case of **1**, only the O-bonded DMSO is displaced, while the other S-bonded DMSO ligands remain coordinated in water.

3.1.2 $Ru(ma)_2(DM\underline{S}O)_2$ and $Ru(etma)_2(DM\underline{S}O)_2$

References on page 81

The yellow solids, $Ru(ma)_2(DM\underline{S}O)_2$ (**11**) and $Ru(etma)_2(DM\underline{S}O)_2$ (**12**), were synthesized by reacting **1** with two equivalents of Kma or Ketma, respectively (ma = maltolato; etma = ethylmaltolato). The synthesis of **11** was first reported by Fryzuk *et al.*, with an X-ray structure showing a *cis*-isomer with S-bonded DMSO ligands (structure **C** in Figure 3.2).[7] The IR spectroscopic data obtained in this thesis work are consistent with S-bonded DMSO ligands ($\nu_{S=O}$ = 1094 cm^{-1}) and agree with the reported data.[7] Ru-S coordination increases $\nu_{S=O}$ compared to that of free DMSO ($\nu_{S=O}$ = 1055 cm^{-1}).[3] Five stereoisomers, three *cis* and two *trans,* are possible for **11** or **12,** due to the inequivalent maltolato oxygen donors (Figure 3.2).

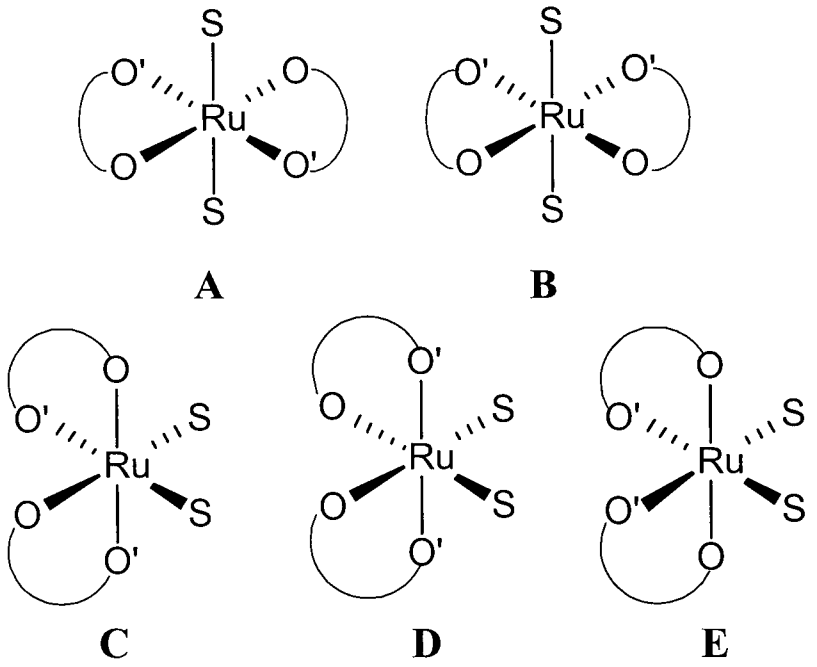

Figure 3.2 Five possible stereoisomers of $Ru(ma)_2(DM\underline{S}O)_2$ (**11**) or $Ru(etma)_2(DM\underline{S}O)_2$ (**12**). S represents S-bonded DMSO, and O—O′ represents the chemically inequivalent oxygen atoms of maltolato or ethylmaltolato ligands.

The ^1H NMR data of **11** in this work agree with those reported.[7] The spectrum (Figure 3.3A) shows four singlets centered around 2.1 ppm due to the methyl resonances of the maltolato ligands. Two sets of four doublets are assigned as the maltolato H_5- and H_6-protons centered around 6.1 and 6.5 ppm, respectively. These data are tentatively assigned to the presence of the three *cis*-isomers, the inequivalent maltolato ligands in **C**

References on page 81

(Figure 3.2) giving rise to two methyl singlets, while those in **D** and **E** are equivalent and give rise to one singlet each. The doublet sets are assigned similarly to the H_5- and H_6-protons in the structures of **C, D,** and **E.** Twelve singlets between 2.7 and 3.4 ppm are due to the methyl groups of S-bonded DMSO ligands; isomers **C, D,** and **E** each give a singlet for each methyl group of DMSO. Although the DMSO ligands in **D** and **E** are equivalent, the methyl groups are within a pyramidal sulfoxide moiety, and appear to be inequivalent in the ^{1}H NMR spectrum.

The presence of the *trans*-isomers (**A** and **B**) rather than the *cis*-isomers (**D** and **E**) is possible because ^{1}H NMR spectroscopy cannot distinguish the equivalent maltolato ligands of the *cis*- from those of the *trans*-isomers. However, the formation of the *cis*- over the *trans*-isomers is preferred because the DMSO ligands *trans* to each other are electronically less favored because of the "competing" π-accepting *trans*-DMSO ligands, while the *cis*-DMSO ligands are *trans* to electron-donating, anionic maltolato ligands. The *cis*-isomers (**C, D,** and **E**) are chiral at the Ru center; each isomer also exists as an enantiomer.

Complex **12** also possesses S-bonded DMSOs based on the IR spectroscopic data ($\nu_{S=O}$ = 1097 cm^{-1}). The ^{1}H NMR spectrum of **12** (Figure 3.3B) is similar to that of **11,** but is complicated by the ethylmaltolato CH_3CH_2 protons which give a triplet (CH_3) and a quartet (CH_2). Due to the proposed presence of three isomers, multiplets are observed from the overlapping peaks. The CH_2 multiplets also partially overlap with the DMSO methyl peaks. Both complexes are very soluble in water, immediately forming yellow solutions, which are non-conducting; their UV-vis spectra do not undergo significant changes over 24 h. As solids, **11** and **12** are very hygroscopic and exhibit a color change over time from yellow to orange-red when stored in air.

3.1.3 Ru(ma)$_2$(TMSO)$_2$ and Ru(etma)$_2$(TMSO)$_2$

Ru(ma)$_2$(TMSO)$_2$ (**13**) and Ru(etma)$_2$(TMSO)$_2$ (**14**) were synthesized by reacting *cis*-RuCl$_2$(TMSO)$_4$ (**7**) with two equivalents of Kma or Ketma, respectively. The synthesis of the TMSO complexes is analogous to that of **11** and **12**. The IR spectra show S-bonded TMSO ligands for **13** ($\nu_{S=O}$ = 1056 and 1117 cm^{-1}) and **14** ($\nu_{S=O}$ = 1055 and 1116 cm^{-1}), these values being higher than that of free TMSO (1023 cm^{-1}).[5]

References on page 81

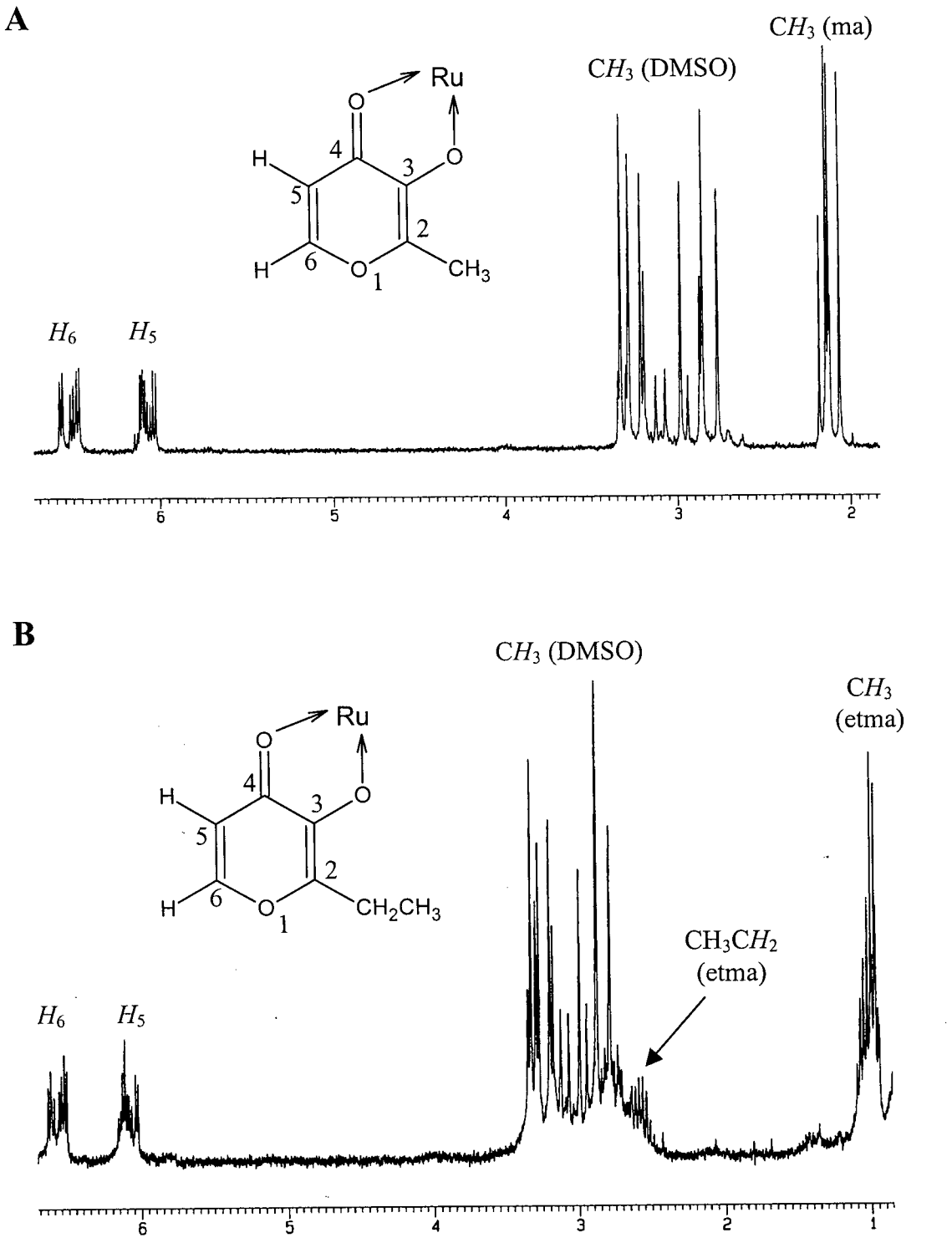

Figure 3.3 The ^{1}H NMR spectra (300 MHz, benzene-d_6) of Ru(ma)$_2$(DMSO)$_2$ (**11**) (A) and Ru(etma)$_2$(DMSO)$_2$ (**12**) (B).

References on page 81

The ^{1}H NMR spectrum of free TMSO shows three sets of multiplets at 1.65 and 2.01 (α-protons), and 2.44 ppm (β-protons) with an integration ratio of 1:1:2 in agreement with the literature.[4] The multiplets result from couplings between the α- and β-protons. In the ^{1}H NMR spectrum of **7,** the α-protons shift further downfield (3.42 and 4.00 ppm), while the β-protons shift slightly upfield (2.25 ppm). Similar trends are observed in the ^{1}H NMR spectra of **13** and **14,** but the spectra are complicated due to the presence of isomers. The signals of the α-protons of TMSO are observed as broad multiplets between 3.0 and 4.5 ppm, while those of the β-protons appear between 1.5 and 2.5 ppm. The four singlets for the methyl resonances of **13,** centered around 2.2 ppm, are similar to those in **11,** although these signals overlap with those of the TMSO β-protons. Based on the spectroscopic data, the structures of **13** and **14** are tentatively assigned as all *cis*-isomers similar to those of **11** and **12.** Complexes **13** and **14** are very soluble in water, and are slightly conducting (Λ_M = 20 and 30 Ω^{-1} cm^2 mol^{-1}, respectively), presumably due to partial dissociation of the maltolato and ethylmaltolato ligands, respectively.

3.2 Ruthenium(II) Maltolato Complexes Containing An Ancillary Bidentate Sulfoxide Ligand

3.2.1 [RuCl(H$_2$O)(BESE)]$_2$(μ-Cl)$_2$ as a Precursor

Cheu first prepared [RuCl(H$_2$O)(BESE)]$_2$(μ-Cl)$_2$ (**15**) by refluxing RuCl$_3$·3H$_2$O in EtOH and conc. HCl for 5 h, and then adding one equivalent BESE and refluxing for 6 h.[8] The addition of two equivalents of BESE yielded *cis*-RuCl$_2$(BESE)$_2$ (**16**). An X-ray analysis of the dimeric **15** showed the coordinated H$_2$O and one BESE per Ru. The structures of **15** and **16** revealed that all the BESE ligands are S-bonded.[8]

Complex **15** was found to be a convenient precursor for the synthesis of complexes containing one BESE ligand per Ru. Attempts to displace one BESE ligand from **16** with other ligands such as maltolate or imidazoles were unsuccessful, probably because of the chelate effect of bidentate S-bonded BESE. In contrast, monodentate sulfoxides of **1** and **7** can be substituted to form complexes of **11** and **13,** respectively. The reaction of **15** with one equivalent of BESE in H$_2$O unexpectedly yielded *trans*-

References on page 81

$RuCl_2(BESE)_2$, the thermodynamically less stable isomer of **16,**[8] while reaction between **15** and excess DMSO in H_2O has yielded *cis*-$RuCl_2$(BESE)(DMSO)(DMSO) (**9**), a mixed sulfoxide complex.[9]

3.2.2 *Cis*-Ru(ma)$_2$(BESE) and *Cis*-Ru(etma)$_2$(BESE)

Cis-Ru(ma)$_2$(BESE) (**17**) and *cis*-Ru(etma)$_2$(BESE) (**18**) were synthesized by reacting **15** with five equivalents of Kma or Ketma, respectively. Due to the bidentate nature of S-bonded BESE, only the *cis*-isomers are possible (Figure 3.4). All three *cis*-isomers are observed by ^{1}H NMR spectroscopy in D_2O for both **17** and **18** (Figures 3.5A and 3.6A). Four singlets centered around 2.3 ppm for the maltolato methyl resonance of **17** are observed similar to those of **11,** and four sets of doublets are observed for each maltolato H_5- and H_6-proton centered around 6.6 and 7.9 ppm, respectively. Ethylmaltolato CH_3 and CH_2 protons in **18** give overlapping triplets (1.1 ppm) and quartets (2.6 ppm), respectively. The *cis*-isomers are chiral at the Ru center; each also exists as an enantiomer. The above assignments are considered approximate, and are based on the BESE ligand being considered non-chiral, in the presence of only three geometric isomers (and their enantiomers). BESE exhibits two chiral sulfur centers, but re-crystallizations of BESE from EtOH isolates only the *meso* form.[10] The presence of chiral BESE (presumably in the *meso* form) in **17** and **18** generates inequivalent maltolato and ethylmaltolato ligands, respectively, in isomers **B** and **C** (Figure 3.4), giving rise to more overlapping signals in the ^{1}H NMR spectra.

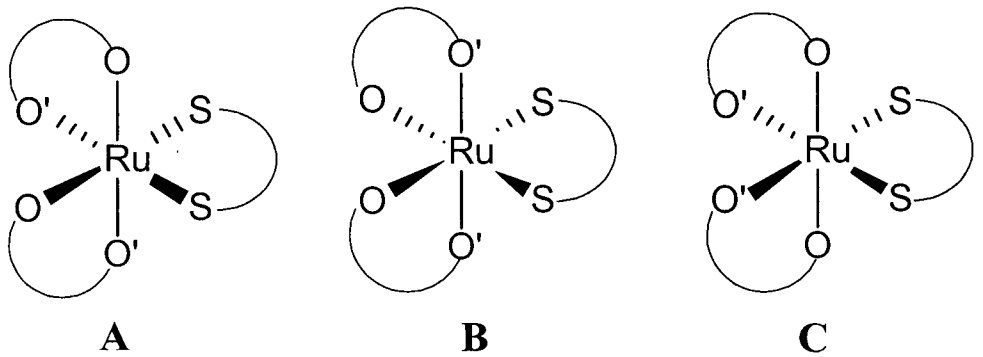

Figure 3.4 Three stereoisomers of *cis*-Ru(ma)$_2$(BESE) (**17**) or *cis*-Ru(etma)$_2$(BESE) (**18**). S—S represents S-bonded BESE, and O—O′ represents the chemically inequivalent oxygen atoms of maltolato or ethylmaltolato ligands.

References on page 81

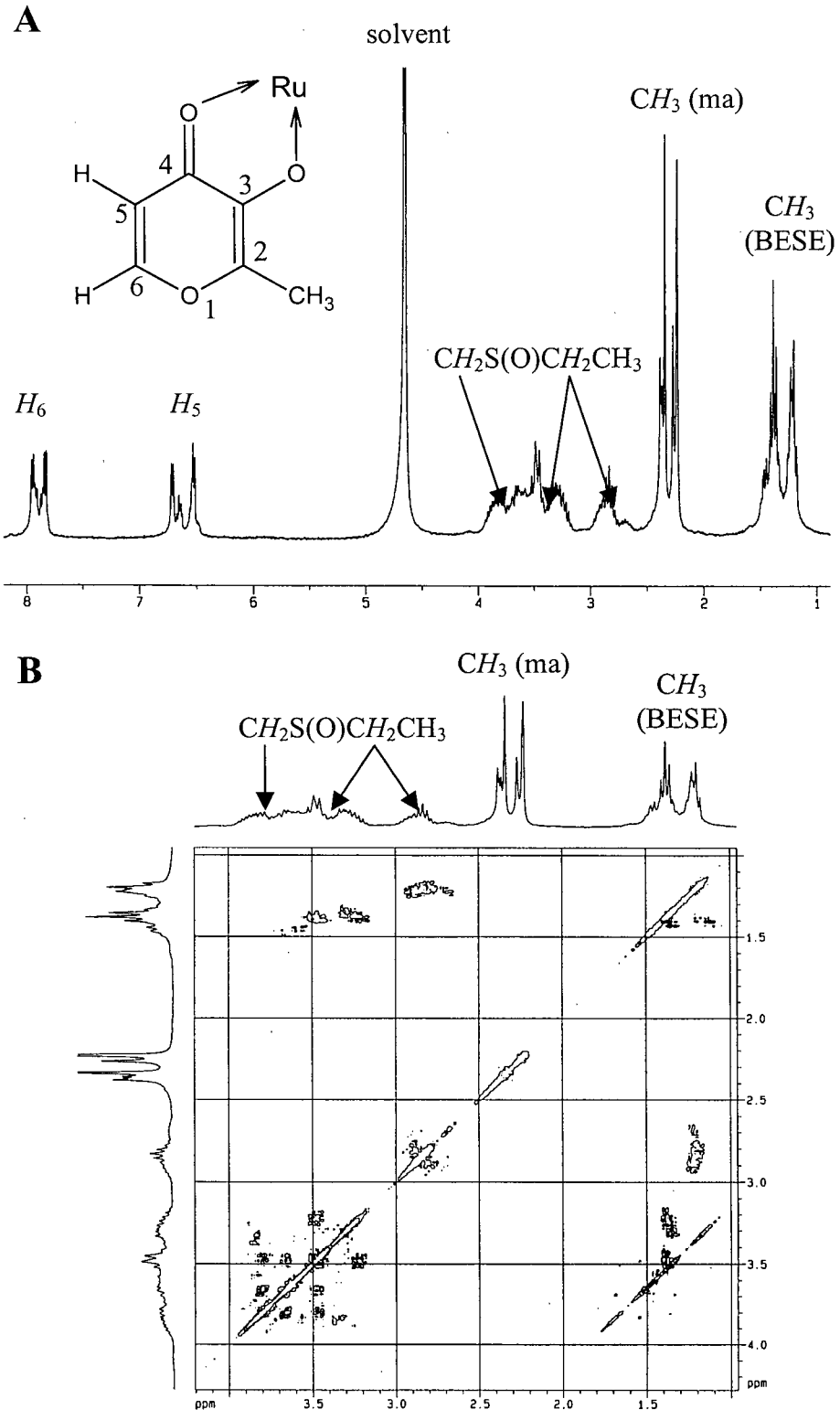

Figure 3.5 ^{1}H NMR (A) and ^{1}H 2D COSY (B) spectra (300 MHz, D_2O) of *cis*-Ru(ma)$_2$(BESE) (**17**).

References on page 81

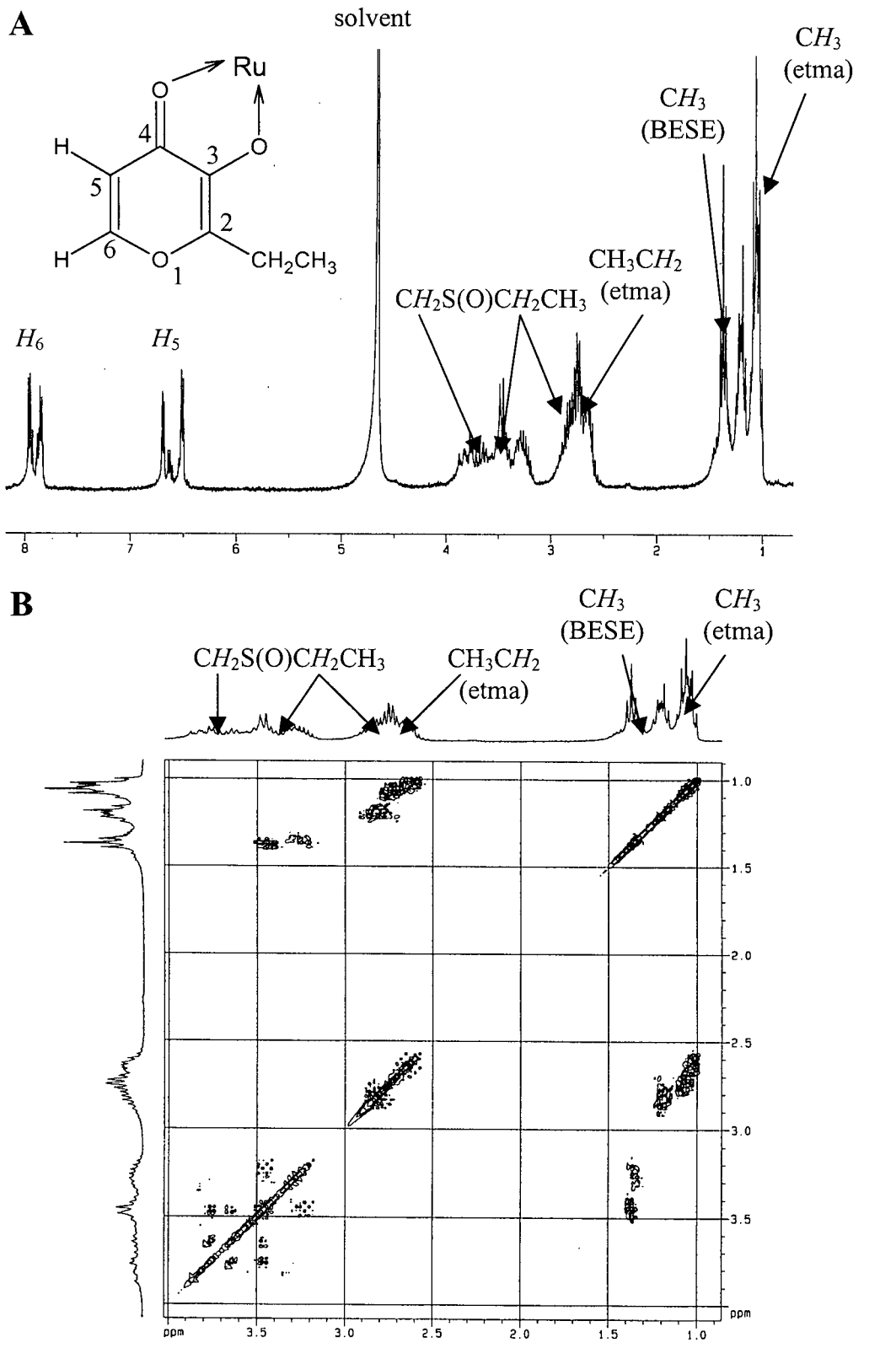

Figure 3.6 ^{1}H NMR (A) and ^{1}H 2D COSY (B) spectra (300 MHz, D_2O) of *cis*-Ru(etma)$_2$(BESE) (**18**).

References on page 81

The BESE methyl signals of **17** and **18** result in multiplets between 1.2 and 1.5 ppm, and the $CH_3CH_2S(O)CH_2$ protons appear as overlapping multiplets between 2.6 and 4.0 ppm. To better assign these ^{1}H NMR signals, ^{1}H 2D COSY NMR spectroscopy was used to further analyze the spectrum (Figures 3.5B and 3.6B). The couplings between multiplets can now be assigned from the crosspeaks of the COSY spectrum. The coupling between the BESE methyl and $CH_3CH_2S(O)$ protons is observed, and also between the $CH_3CH_2S(O)$ and $CH_3CH_2S(O)CH_2$ protons. For **17** and **18**, the $CH_3CH_2S(O)$ signal is located upfield from the $CH_3CH_2S(O)CH_2$ signal. The ethylmaltolato CH_3CH_2 signal of **18** is partially overlapped with the downfield $CH_3CH_2S(O)$ signal. The coupling between ethylmaltolato CH_3 and CH_2 protons is also observed. No coupling was observed for maltolato methyl protons in **17,** and H_5- and H_6-protons are expectedly coupled to each other (this region of the COSY spectrum is not shown).

Crystals of **17,** suitable for X-ray diffraction analysis, were grown from an acetone solution of the complex layered with hexanes. The X-ray structure (Figure 3.7) corresponds to isomer **B** (Figure 3.4) when designating O′ and O as carbonyl and hydroxyl oxygens of the maltolato ligands, respectively. Although isomer **B** does not consider the chirality of BESE and indicates equivalent maltolato ligands, the X-ray structure of **17** shows an *S,R*-BESE ligand (S1 = *S* and S2 = *R*), which gives rise to inequivalent maltolato ligands. This aspect is observed in the ^{1}H NMR spectrum of a solution of the crystal, *cis*-Ru(ma)$_2$(*S,R*-BESE) (Figure 3.8), where two maltolato methyl singlets with equal intensity are shown, as well as two sets of doublets for each of the H_5- and H_6-protons. The structure of *cis*-Ru(ma)$_2$(*S,R*-BESE) shows chirality at the Ru center, and its enantiomeric form therefore exists. The other diastereomers, *cis*-Ru(ma)$_2$(*R,R*-BESE) or *cis*-Ru(ma)$_2$(*S,S*-BESE), were not observed in the ^{1}H NMR spectrum. Of interest, time-dependent ^{1}H NMR spectroscopy showed that the single isomer in D_2O does not isomerize to other *cis*- or *trans*-isomers.

The X-ray structure of **17** is the first structurally characterized Ru complex containing both maltolato and a bidentate sulfoxide ligand. An analogous structure, *cis*-Ru(ma)$_2$(DMSO)$_2$ (**11**), has been reported,[7] and both structures show similar Ru-S bond distances between 2.18 and 2.21 Å, and Ru-O bond distances between 2.08 and 2.15 Å. Both structures indicate slightly distorted octahedral geometry, and the coordination of

References on page 81

the maltolato ligands gives rise to a five-membered ring with O-Ru-O′ angles between 80.3 and 81.2°. The structure of **17** shows *trans*-carbonyl oxygens of the maltolato ligands with an O′-Ru-O′ angle of 168.2°, while **11** shows that a maltolato carbonyl oxygen is *trans* to the other maltolato hydroxy oxygen with an O-Ru-O′ angle of 169.8°.

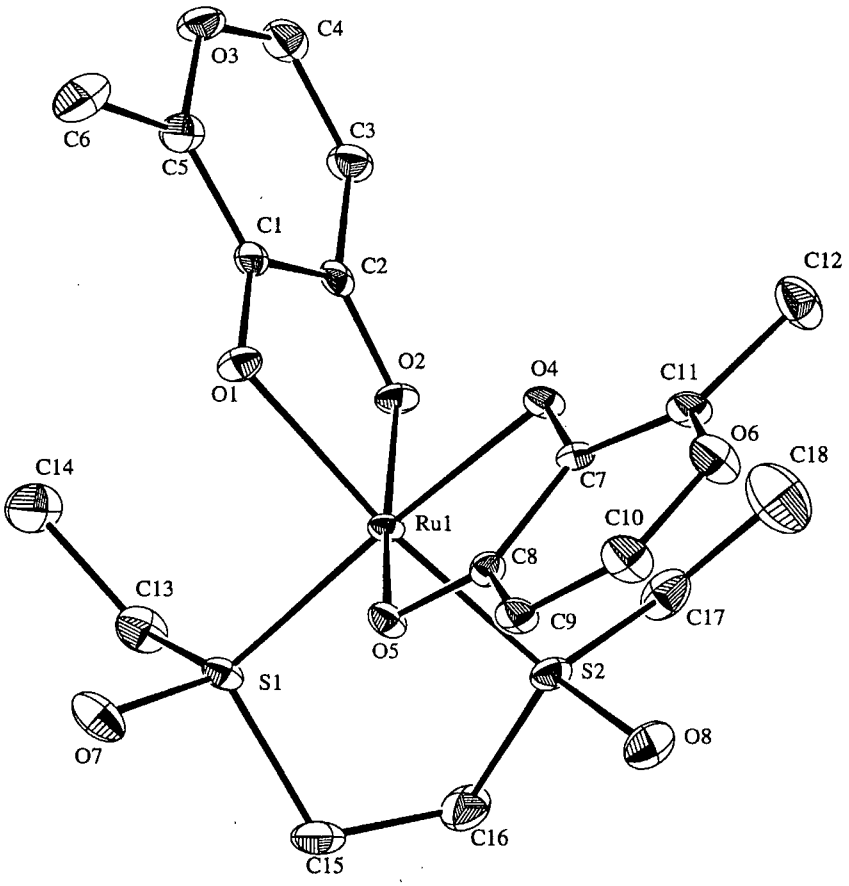

Figure 3.7 ORTEP diagram of *cis*-Ru(ma)$_2$(*S,R*-BESE) (**17**) with 50 % probability ellipsoids. The carbonyl oxygens of the maltolato ligands are *trans* to each other. Selected bond lengths and angles are shown in Table 3.1, and full experimental details and structural parameters are provided in Appendix 1.

References on page 81

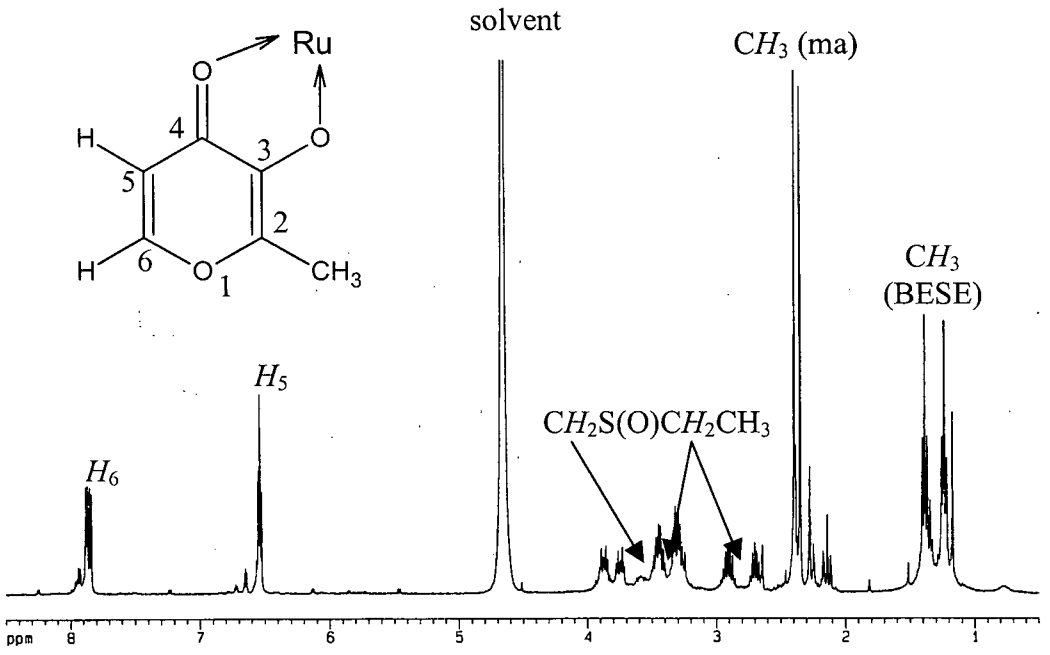

Figure 3.8 ^{1}H NMR spectrum (400 MHz, D_2O) of *cis*-Ru(ma)$_2$(*S,R*-BESE) (**17**).

Table 3.1 Selected bond lengths and angles of *cis*-Ru(ma)$_2$(*S,R*-BESE) (**17**) with estimated standard deviations in parentheses.

Bond	Length (Å)	Bond	Angle (°)
Ru(1)-O(1)	2.141(2)	S(1)-Ru(1)-O(4)	174.52(5)
Ru(1)-O(2)	2.082(2)	S(2)-Ru(1)-O(1)	172.93(6)
Ru(1)-O(4)	2.098(2)	O(2)-Ru(1)-O(5)	168.24(7)
Ru(1)-O(5)	2.085(2)	O(1)-Ru(1)-O(2)	80.37(7)
Ru(1)-S(1)	2.2054(7)	O(4)-Ru(1)-O(5)	81.17(7)
Ru(1)-S(2)	2.1807(7)	S(1)-Ru(1)-S(2)	88.27(3)
S(1)-O(7)	1.487(2)	Ru(1)-O(1)-C(1)	107.9(2)
S(2)-O(8)	1.476(2)	Ru(1)-O(2)-C(2)	111.1(2)
O(1)-C(1)	1.318(3)	O(7)-S(1)-C(15)	105.9(1)
O(2)-C(2)	1.281(2)	C(13)-S(1)-C(15)	100.9(1)

References on page 81

The IR spectra show S-bonded BESE ligands for **17** ($\nu_{S=O}$ = 1079 and 1113 cm^{-1}) and **18** ($\nu_{S=O}$ = 1079 and 1114 cm^{-1}), these values being higher than that of free BESE (1015 cm^{-1}).[10] The $\nu_{S=O}$ data for the Ru^{II} maltolato-sulfoxide complexes and the corresponding free ligands are shown in Table 3.2. All sulfoxide ligands are S-bonded, and presumably in a *cis*-configuration to stabilize electron density donated by *trans* anionic oxygen ligands. The maltolato $\nu_{C=O}$ and $\nu_{C=C}$, located between 1545 and 1595 cm^{-1}, are less than those of free maltol (between 1550 and 1650 cm^{-1}).[11] The Ru-O coordination withdraws electron density from the C-O bond and results in a decrease in the IR stretching frequency. This is similar to the case of an O-bonded sulfoxide that exhibits a lower $\nu_{S=O}$ than that of the free sulfoxide.

Table 3.2 Selected IR data of ruthenium(II) maltolato-sulfoxide complexes and the corresponding free ligands.

Complex[a]	$\nu_{S=O}$[b]	$\nu_{C=O} + \nu_{C=C}$[c]	$\nu_{C=O}$[c]	Ref.
$Ru(ma)_2(DMSO)_2$ (**11**)	1094	1547	1595	*d*
$Ru(etma)_2(DMSO)_2$ (**12**)	1097	1546	1592	*d*
$Ru(ma)_2(TMSO)_2$ (**13**)	1056, 1117	1549	1594	*d*
$Ru(etma)_2(TMSO)_2$ (**14**)	1055, 1116	1546	1592	*d*
cis-$Ru(ma)_2$(BESE) (**17**)	1079, 1113	1549, 1560	1595	*d*
cis-$Ru(etma)_2$(BESE) (**18**)	1079, 1114	1545, 1559	1593	*d*
DMSO	1055	-	-	3
TMSO	1023	-	-	5
BESE	1015	-	-	10
maltol	-	1550, 1610	1650	11
ethylmaltol	-	1557, 1612	1647	*d*

[a] All coordinated sulfoxides are S-bonded. [b] IR stretching frequency (cm^{-1}) of free or coordinated sulfoxides. [c] IR stretching frequency (cm^{-1}) of free or coordinated maltol(ato) or ethylmaltol(ato). [d] This work.

References on page 81

The presence of maltolato ligands increases the solubility of Ru sulfoxide complexes in water. For example, **17** is much more water-soluble than are *cis*- and *trans*-$RuCl_2(BESE)_2$, and the latter is in fact insoluble.[8] This increased water-solubility is a potential advantage for medicinal use, with the added benefit that maltol can be easily approved for therapeutic use because of its non-toxicity. The coordination of maltolate to a Ru complex does not always generate water-solubility as $Ru(ma)_2(PPh_3)_2$ and $Ru(ma)_2(COD)$ are insoluble in water.[7]

3.3 Ruthenium(II) Bidentate Sulfoxide-Nitroimidazole Complexes

3.3.1 $RuCl_2(BESE)(metro)_2$

$RuCl_2(BESE)(metro)_2$ (**19**) was synthesized by reacting $[RuCl(H_2O)(BESE)]_2(\mu\text{-}Cl)_2$ (**15**) with six equivalents of metronidazole (metro) in MeOH. The complex was purified by silica gel preparative thin layer chromatography (TLC) using CH_2Cl_2:MeOH (90:10) as the eluent. The yellow complex was extracted from the silica gel using MeOH, and was precipitated by addition of Et_2O.

Once dissolved in water, **19** dissociates both chlorides, based on the conductivity data (180 Ω^{-1} cm^2 mol^{-1} at 5 min, increasing to a steady value of 220 Ω^{-1} cm^2 mol^{-1} after 24 h) that show an approximate 2:1 electrolyte, water probably coordinating. Three stereoisomers of the supposed $[Ru(D_2O)_2(BESE)(metro)_2]^{2+}$ (Figure 3.9) are thought to be observed in the ^{1}H NMR spectrum in D_2O at the 5 min stage (Figure 3.10A). Four singlets for each of the methyl and H_4-protons of the metronidazole ligands are observed, centered around 2.6 and 8.3 ppm, respectively. The diaquo species, isomers **A** and **B** (Figure 3.9), contain equivalent metronidazole ligands, and therefore each gives rise to one methyl singlet, while the inequivalent metronidazole ligands in isomer **C** give rise to two methyl singlets, for a total of four singlets. Likewise, four singlets are seen for the H_4-protons. Of note, isomer **C** is chiral at the Ru center; it also exists as an enantiomer.

The other signals are complicated by proton couplings. The BESE methyl multiplets are located between 1.0 and 1.6 ppm, while the $CH_3CH_2S(O)CH_2$ signals overlap with those of the CH_2OH protons of metronidazole, giving rise to multiplets

References on page 81

between 3.2 and 4.0 ppm. The CH_2CH_2OH resonance of metronidazole, found between 4.3 and 4.8 ppm, partially overlaps with the residual solvent signal of D_2O.

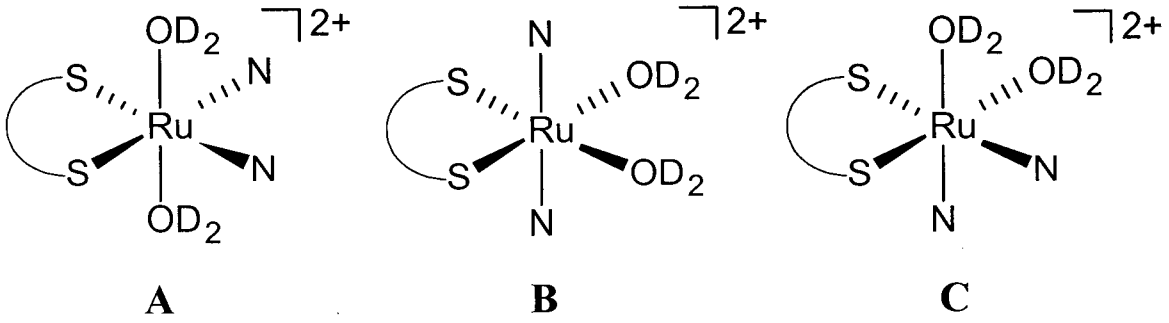

Figure 3.9 Three stereoisomers of $[Ru(D_2O)_2(BESE)(metro)_2]^{2+}$. S—S and N represent S-bonded BESE and metronidazole, respectively.

In an attempt to assign these multiplets, ^1H 2D COSY NMR spectroscopy was used to further analyze the spectrum (Figure 3.10B). The couplings between the BESE methyl protons and $CH_3CH_2S(O)$ protons are observed, and also between the $CH_3CH_2S(O)$ and $CH_3CH_2S(O)CH_2$ protons. The CH_2CH_2OH signals couple with the CH_2CH_2OH signals of metronidazole, and no crosspeak is observed for the metronidazole methyl or H_4-signal. The metronidazole CH_2CH_2OH multiplet is located downfield while overlapping with the $CH_3CH_2S(O)CH_2$ multiplet. The ^1H NMR spectrum shows no significant change over 24 h, indicating no dissociation of either BESE or metronidazole ligands in D_2O. The above ^1H NMR assignments are approximate, in that the chirality of the BESE ligand is not considered. The presence of chiral BESE will generate more signals, and further complicate the ^1H NMR spectrum.

Orange-red crystals of **19** were deposited overnight from the TLC filtrate ($MeOH/Et_2O$), and were suitable for analysis by X-ray crystallography. The X-ray structure (Figure 3.11) shows a *trans*-arrangement of the chloride ligands, and an S-bonded *R,R*-BESE, which suggests that the BESE, used for the synthesis of the precursor of **19,** contained both the *racemic* and *meso* forms. The X-ray structure exhibits C_2 symmetry, by which the metronidazole ligands are equivalent. Unfortunately, there were insufficient crystals to carry out a ^1H NMR analysis in a D_2O solution of the crystal.

References on page 81

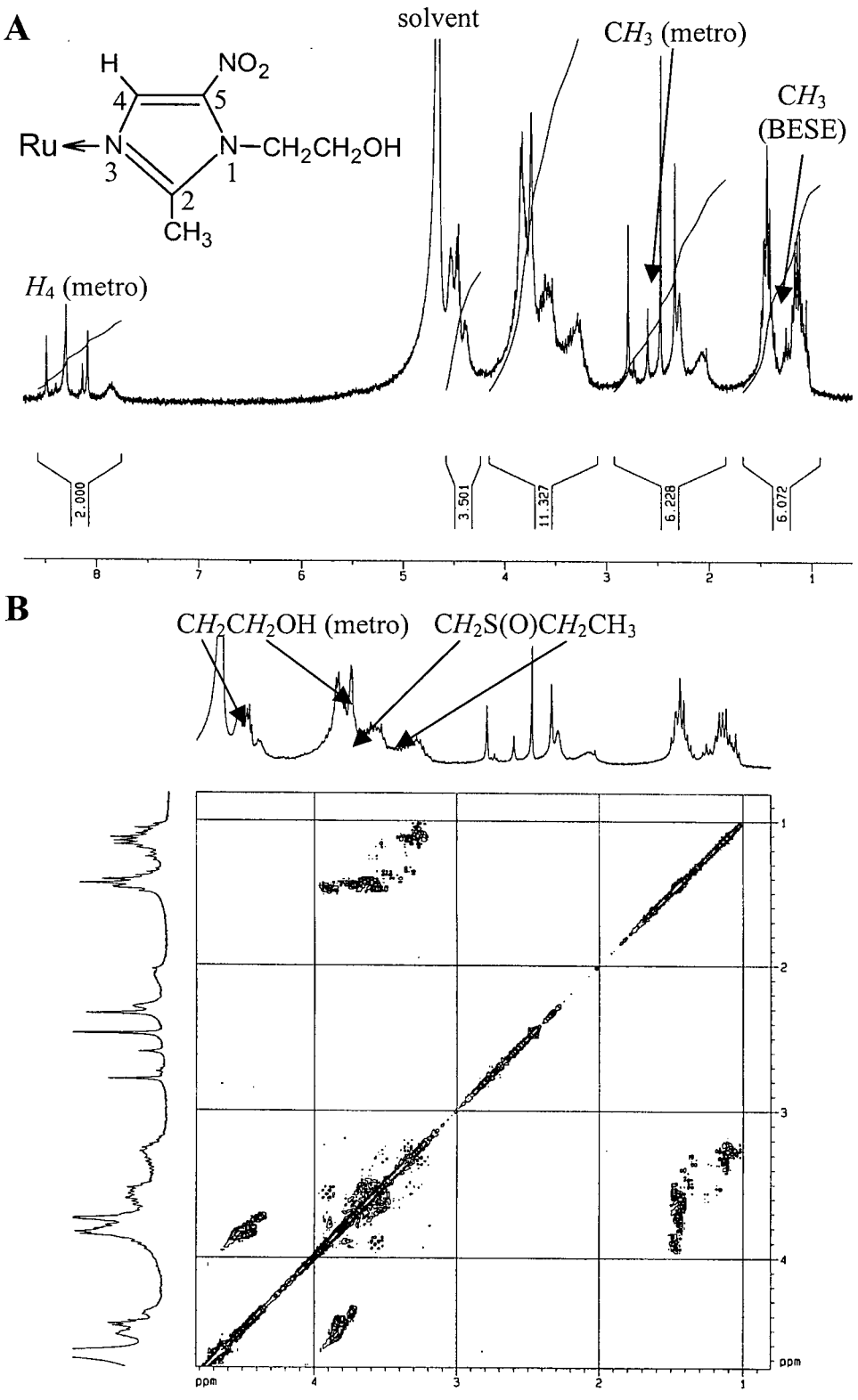

Figure 3.10 ^{1}H NMR (A) and ^{1}H 2D COSY (B) spectra (300 MHz) of $RuCl_2(BESE)(metro)_2$ (**19**) dissolved in D_2O.

References on page 81

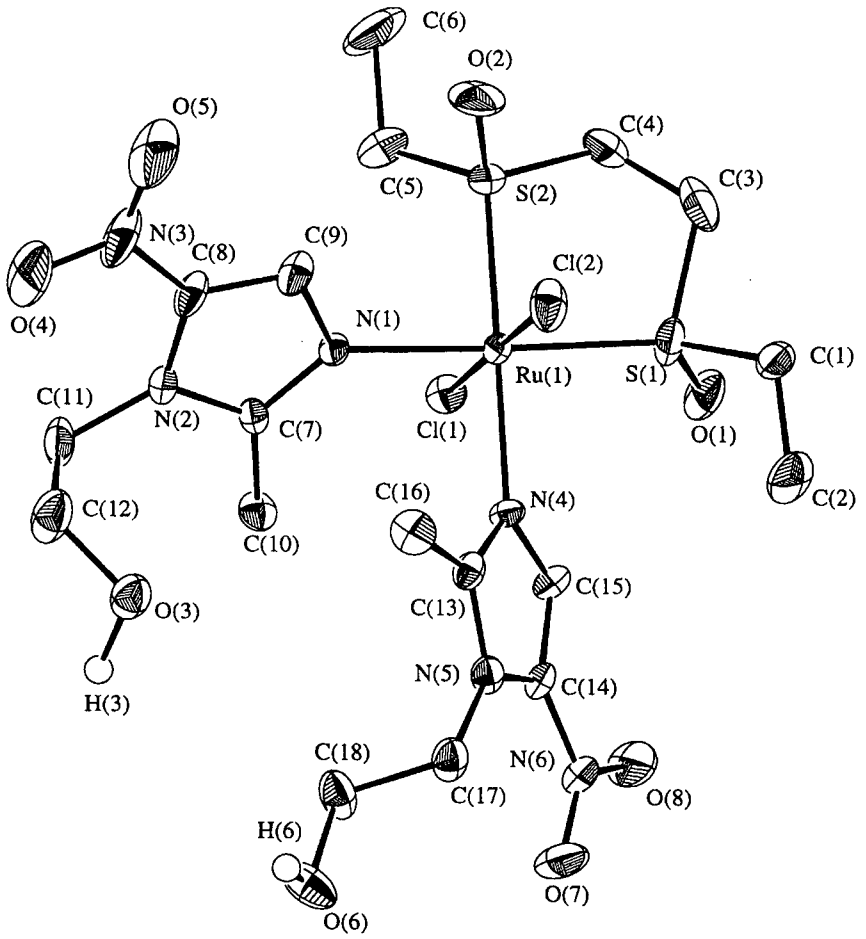

Figure 3.11 ORTEP diagram of *trans*-$RuCl_2$(*R,R*-BESE)$(metro)_2$ (**19**) with 50 % probability ellipsoids. Selected bond lengths and angles are shown in Table 3.3, and full experimental details and structural parameters are provided in Appendix 2.

The X-ray structure of **19** represents the first structurally characterized Ru complex containing both nitroimidazole and sulfoxide ligands. Comparisons of bond lengths and angles of **19** with those of other Ru^{II} BESE complexes are shown in Tables 3.4 and 3.5, respectively. The Ru-S bonds in **19** are significantly shorter than those found in *cis*- or *trans*-$RuCl_2(BESE)_2$.[8,10] This implies that a stronger Ru-S bond is perhaps due to the increased electron donation of metronidazole ligands *trans* to S, while the electron donation of Cl or S-bonded BESE *trans* to a Ru-S bond is less than that of metronidazole.

References on page 81

However, the Ru-S bonds in **19** are essentially the same as the BESE Ru-S bond which is *trans* to an O-bonded DMSO in *cis*-$RuCl_2$(BESE)(DMSO)(DMSO).[9] Bond angle comparison (Table 3.5) shows that **19** exhibits an octahedral geometry, similar to that of the other Ru^{II} BESE complexes, with little distortion.

Table 3.3 Selected bond lengths and angles of *trans*-$RuCl_2$(*R,R*-BESE)(metro)$_2$ (**19**) with estimated standard deviations in parentheses.

Bond	Length (Å)	Bond	Angle (°)
Ru(1)-N(1)	2.139(3)	N(1)-Ru(1)-S(1)	177.93(9)
Ru(1)-N(4)	2.143(3)	N(4)-Ru(1)-S(2)	179.03(8)
Ru(1)-S(1)	2.2267(11)	Cl(2)-Ru(1)-Cl(1)	179.41(4)
Ru(1)-S(2)	2.2174(11)	S(2)-Ru(1)-S(1)	87.23(4)
Ru(1)-Cl(1)	2.4148(10)	N(1)-Ru(1)-N(4)	89.26(12)
Ru(1)-Cl(2)	2.4006(11)	N(1)-Ru(1)-S(2)	90.86(9)
S(1)-O(1)	1.477(3)	N(1)-Ru(1)-Cl(1)	90.69(8)
S(2)-O(2)	1.495(3)	S(1)-Ru(1)-Cl(1)	90.11(4)
O(4)-N(3)	1.238(5)	O(1)-S(1)-C(1)	108.4(3)
O(5)-N(3)	1.214(5)	C(3)-S(1)-C(1)	92.6(3)

Table 3.4 Selected bond lengths of ruthenium(II) BESE complexes.

Complex[a]	Ru-Cl (Å)	Ru-S[b] (Å)	S-O[b] (Å)	S-C[b] (Å)
19	2.4006, 2.4148	2.2174, 2.2267	1.477, 1.495	1.789-1.819
A	2.428, 2.434	2.250,[c] 2,214[d]	1.471, 1.474	1.792-1.809
B	2.4018	2.3212, 2.3288	1.479, 1.480	1.797-1.809
C	2.4217, 2.4486	2.2636,[c] 2.2697[c] 2.299,[e] 2.302[e]	1.470-1.479	1.796-1.814

[a] **A** = *cis*-$RuCl_2$(BESE)(DMSO)(DMSO) (ref. 9), **B** = *trans*-$RuCl_2$(BESE)$_2$ (ref. 8), **C** = *cis*-$RuCl_2$(BESE)$_2$ (refs. 10, 12). [b] Bond length of coordinated BESE. [c] *Trans* to Cl. [d] *Trans* to O-bonded DMSO. [e] *Trans* to S-bonded BESE.

References on page 81

Table 3.5 Selected bond angles of ruthenium(II) BESE complexes.

Complex[a]	Ru *cis* angle (°)	Ru *trans* angle (°)	C-S-O[b] (°)	C-S-C[b] (°)
19	87.23-92.66	177.93-179.41	105.2-108.4	92.6, 102.5
A	86.41-93.38	175.93-179.10	106.4-108.3	99.9, 100.9
B	85.42-94.58	180.00	106.6-108.1	99.1, 101.3
C	87.19-92.08	176.92-178.54	106.3-109.3	102.2-102.7

[a] **A** = *cis*-$RuCl_2$(BESE)(DMSO)(DMSO) (ref. 9), **B** = *trans*-$RuCl_2(BESE)_2$ (ref. 8), **C** = *cis*-$RuCl_2(BESE)_2$ (refs. 10, 12). [b] Bond angle of coordinated BESE.

The IR spectroscopic data for **19** are consistent with S-bonded BESE, with $\nu_{S=O}$ at 1079 and 1114 cm^{-1} (Table 3.6), which are significantly greater than that observed for free BESE (1015 cm^{-1}).[10] The IR data of **19** also show the symmetric and asymmetric $\nu_{N=O}$ of the coordinated metronidazole at 1364 and 1480 cm^{-1}, respectively, similar to those of free metronidazole (1369 and 1474 cm^{-1}). Coordination of metronidazole to Ru does not significantly affect the vibrational frequency of the NO_2 group.

Table 3.6 Selected IR spectroscopic data of ruthenium(II) sulfoxide complexes and the corresponding free sulfoxides.

Complex[a]	$\nu_{S=O}$[b]	Ref.
$RuCl_2(BESE)(metro)_2$	1079, 1114	*c*
$RuCl_2(DMSO)_2(metro)_2$	1094, 1162	13
cis-$RuCl_2$(BESE)(DMSO)(DMSO)	1029, 1101, 1135 (S-bonded)	9
	926 (O-bonded)	
cis-$RuCl_2(BESE)_2$	1128	10
trans-$RuCl_2(BESE)_2$	1093, 1119	8
BESE	1015	10
DMSO	1055	3

[a] All coordinated sulfoxides are S-bonded, except in *cis*-$RuCl_2$(BESE)(DMSO)(DMSO). [b] IR stretching frequency (cm^{-1}) of free or coordinated sulfoxides. [c] This work.

References on page 81

3.3.2 Attempted Synthesis of $RuCl_2(BESE)(4\text{-}NO_2Im)_2$

The synthesis of $RuCl_2(BESE)(4\text{-}NO_2Im)_2$ (**20**) was attempted by reacting $[RuCl(H_2O)(BESE)]_2(\mu\text{-}Cl)_2$ (**15**) with six equivalents of 4-nitroimidazole (4-NO_2Im) in H_2O. A brown solid precipitated from the solution and was isolated. The IR data show the presence of coordinated 4-nitroimidazole at 1380 ($\nu_{N=O\ sym.}$) and 1523 cm^{-1} ($\nu_{N=O\ asym.}$), and S-bonded BESE ($\nu_{S=O}$ = 1085 cm^{-1}). The electrospray mass spectrum of the solid contains a parent peak of the title complex, but satisfactory elemental analyses were not obtained. Further purification of the complex by chromatography was impractical because of the insolubility of this material in common solvents. The motivation for synthesizing **20** was that its analogue, $RuCl_2(DMSO)_2(4\text{-}NO_2Im)_2$ (**8**), has been shown to be a potent radiosensitizer,[14] and it would have been of interest to compare the radiosensitizing activity of **20** with that of the DMSO derivative. Unfortunately, the replacement of DMSO ligands by BESE greatly reduces the solubility of the Ru complex, and limits its use in biological conditions.

3.4 Ruthenium(II) Nitroimidazole Complexes

3.4.1 $RuCl_2(metro)_4$ and $RuCl_2(4\text{-}NO_2Im)_4$

$RuCl_2(metro)_4$ (**21**) was synthesized following the procedure of Baird.[15] A Ru "blue" solution was generated by H_2 reduction of $RuCl_3{\cdot}3H_2O$ in refluxing MeOH.[16] Four equivalents of metronidazole were then added, and a black-purple solid was precipitated and isolated after refluxing for an additional 16 h (Scheme 3.1). $RuCl_2(4\text{-}NO_2Im)_4$ (**22**) was synthesized as a black precipitate using a similar procedure. Complex **22** is insoluble in common solvents, and was characterized by elemental analysis and IR spectroscopy, although whether the chlorides are *cis* or *trans* is uncertain.

Scheme 3.1

$$RuCl_3{\cdot}3H_2O \xrightarrow[MeOH]{H_2,\ 3\ h} \text{"Ru blue"} \xrightarrow[H_2,\ MeOH]{+\ 4\ metro,\ 16\ h} RuCl_2(metro)_4$$

References on page 81

Nitroimidazoles are generally less soluble than imidazoles, and this is also true for the corresponding Ru complexes. The increased solubility of **21** is likely due to the CH_2CH_2OH group at the N_1-position of metronidazole. Complex **21** dissolves in acetone to give a non-conducting solution, whose ^1H NMR spectrum in acetone-d_6 shows a broad singlet for both the methyl and H_4-protons, and three sets of broad multiplets for the CH_2CH_2OH protons with a 2:2:1 integration ratio. The IR data for **21** show the symmetric and asymmetric $\nu_{N=O}$ of the coordinated metronidazole at 1352 and 1475 cm^{-1}, respectively. Similar IR bands are observed for **22** at 1381 ($\nu_{N=O\ sym.}$) and 1496 cm^{-1} ($\nu_{N=O\ asym.}$) of the coordinated 4-nitroimidazole. Unfortunately, **21** is not soluble in water, and was therefore not tested for its anticancer activity against human breast cancer cells.

3.5 Ruthenium(III) Maltolato and Mixed Maltolato-Metronidazole Complexes

3.5.1 *Mer*-Ru(ma)$_3$ and *Mer*-Ru(etma)$_3$

The synthesis of *mer*-Ru(ma)$_3$ (**23**) was first reported by Greaves and Griffith, by refluxing aqueous $RuCl_3 \cdot 3H_2O$ with excess maltol and sodium acetate, and the red product was precipitated and filtered off in air.[11] Re-precipitation from CH_2Cl_2/hexanes yielded an analytically pure product. Sodium acetate is required to deprotonate the hydroxy group of maltol in order to facilitate *O, O'*-metal chelation. *Mer*-Ru(etma)$_3$ (**24**) was synthesized in this thesis work using an analogous procedure.

The X-ray structure of **23,** determined by Kennedy *et al.,* clearly illustrates a *mer*-configuration, but the data are not publishable due to distortion in the crystal lattice.[17] Crystals of **24** were grown from a CH_2Cl_2 solution of the complex layered with Et_2O in this thesis work, but X-ray diffraction analysis is complicated by the presence of twinned crystals. The structure of **24** is therefore poorly refined, but shows a *mer*-configuration identical to that of **23.** Complexes **23** and **24** are chiral at the Ru center; each also exists as an enantiomer. The paramagnetic ^1H NMR spectra of **23** and **24** are currently being investigated by D. Kennedy.

References on page 81

The IR spectroscopic data for **23** agree with those in the literature.[11] Overlapping maltolato $\nu_{C=O}$ and $\nu_{C=C}$ bands occur between 1551 and 1600 cm^{-1}. Similar IR bands are observed for **24,** with overlapping $\nu_{C=O}$ and $\nu_{C=C}$ between 1550 and 1596 cm^{-1}. Both **23** and **24** are soluble in water, and the solutions are slightly conducting (Λ_M = 26 and 40 Ω^{-1} cm^2 mol^{-1}, respectively), probably due to partial dissociation of the maltolato and ethylmaltolato ligands. The UV-vis spectra of the aqueous solutions exhibit no significant changes over 24 h. These Ru^{III} complexes were tested *in vitro* for their anticancer activity against human breast cancer cells for comparison with the activity of Ru^{II} maltolato-sulfoxide complexes (see Chapter 4).

3.5.2 *Trans*-[Ru(ma)$_2$(metro)$_2$](CF$_3$SO$_3$) and *Trans*-[Ru(etma)$_2$(metro)$_2$](CF$_3$SO$_3$)

Trans-[Ru(ma)$_2$(metro)$_2$](CF$_3$SO$_3$) (**25**) was synthesized according to the procedure of Kennedy and James by treating **23** with one equivalent of CF_3SO_3H in EtOH, followed by the addition of four equivalents of metronidazole and refluxing for 16 h.[18] The blue-black product was isolated by re-precipitation from acetone/hexanes. *Trans*-[Ru(etma)$_2$(metro)$_2$](CF$_3$SO$_3$) (**26**) was synthesized analogously, and its X-ray structure was determined by Kennedy *et al.*[17] Crystals of **25** were grown from an acetone solution of the complex layered with hexanes, and X-ray diffraction analysis shows a centrosymmetric *trans*-configuration (Figure 3.12).

The X-ray structures of **25** and **26** show the same stereoisomer **A** (Figure 3.13). In terms of the synthesis, the addition of CF_3SO_3H to a EtOH solution of **23** results in the dissociation of one maltolato ligand, followed by EtOH coordination ([Ru(ma)$_2$(EtOH)$_2$](CF$_3$SO$_3$) has been isolated by D. Kennedy),[18] the other two maltolato ligands presumably initially remaining in a *cis*-configuration. The structures of **25** and **26** imply that isomerization then takes place, facilitating the subsequent *trans*-addition of metronidazole (Figure 3.14). The formation of a centrosymmetric *trans*-isomer is apparently favored over the formation of other isomers. The paramagnetic ^1H NMR spectra of **25** and **26** are currently being investigated by D. Kennedy.

The structure of **25** shows an octahedral geometry, and the coordination of maltolato ligands gives rise to a five-membered ring with O-Ru-O′ angles of 81.5°. The metronidazole O*H* moiety forms hydrogen bonds with the triflate oxygen atoms. The Ru-

References on page 81

O bonds of **25** (2.01 to 2.06 Å) are slightly shorter than those of *cis*-Ru(ma)$_2$(*S,R*-BESE) (**17**) (2.08 to 2.14 Å) because of the stronger bonding of the maltolato ligands to Ru^{III}.

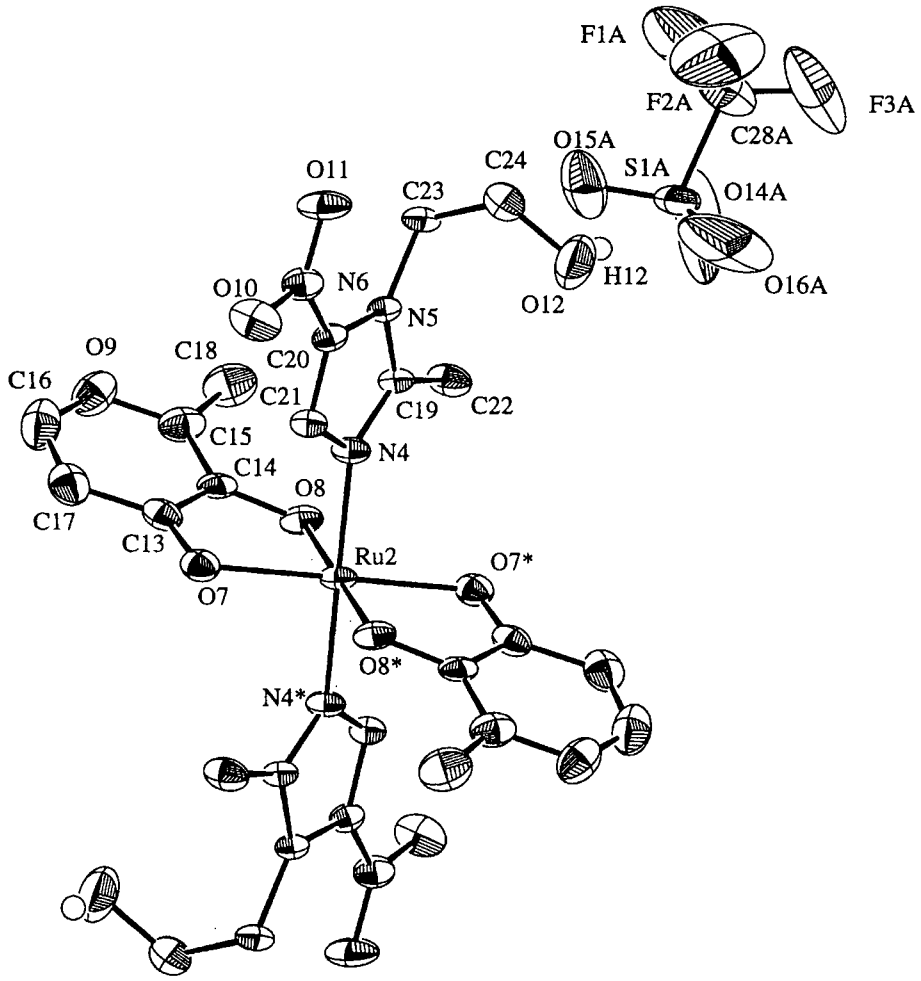

Figure 3.12 ORTEP diagram of *trans*-[Ru(ma)$_2$(metro)$_2$](CF$_3$SO$_3$) (**25**) with 50 % probability ellipsoids. Selected bond lengths and angles are shown in Table 3.7, and full experimental details and structural parameters are provided in Appendix 3.

References on page 81

Table 3.7 Selected bond lengths and angles of *trans*-[Ru(ma)$_2$(metro)$_2$](CF$_3$SO$_3$) (**25**) with estimated standard deviations in parentheses.

Bond	Length (Å)	Bond	Angle (°)
Ru(2)-O(7)	2.060(3)	O(7)*-Ru(2)-O(7)	180.0
Ru(2)-O(8)	2.007(3)	O(8)*-Ru(2)-O(8)	180.0
Ru(2)-N(4)	2.075(3)	N(4)-Ru(2)-N(4)*	179.999(1)
O(10)-N(6)	1.225(5)	O(7)-Ru(2)-N(4)	86.82(13)
O(11)-N(6)	1.231(4)	O(8)-Ru(2)-N(4)	88.07(12)
N(6)-C(20)	1.414(5)	O(8)-Ru(2)-O(7)	81.48(12)
H(12)···O(15A)[a]	2.3611	C(13)-O(7)-Ru(2)	110.6(3)
H(12)···O(16A)[a]	2.2755	C(14)-O(8)-Ru(2)	109.3(2)

[a] Hydrogen-bonding.

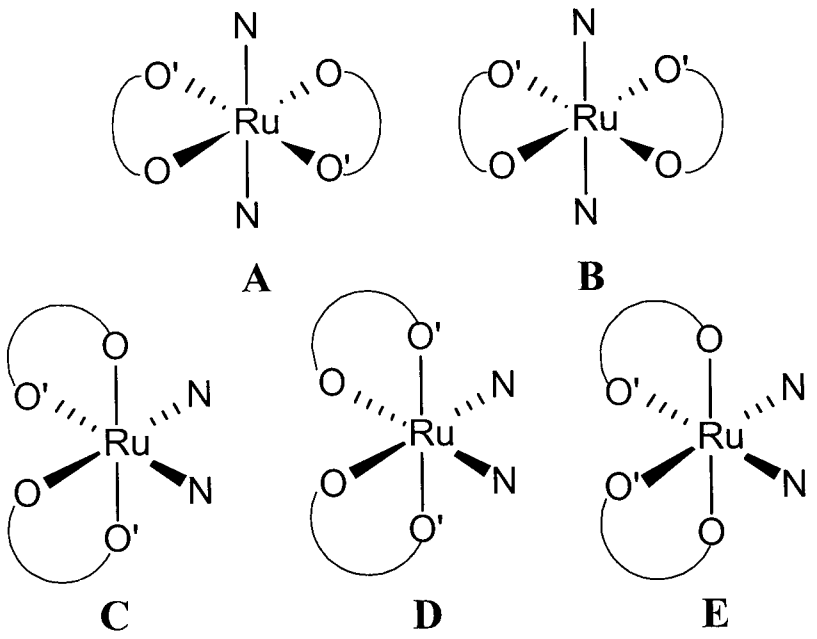

Figure 3.13 The structures of *trans*-[Ru(ma)$_2$(metro)$_2$](CF$_3$SO$_3$) (**25**) and *trans*-[Ru(etma)$_2$(metro)$_2$](CF$_3$SO$_3$) (**26**) correspond to isomer **A,** although a total of five geometric isomers is possible. N represents metronidazole, and O—O′ represents the chemically inequivalent oxygen atoms of maltolato or ethylmaltolato ligands.

References on page 81

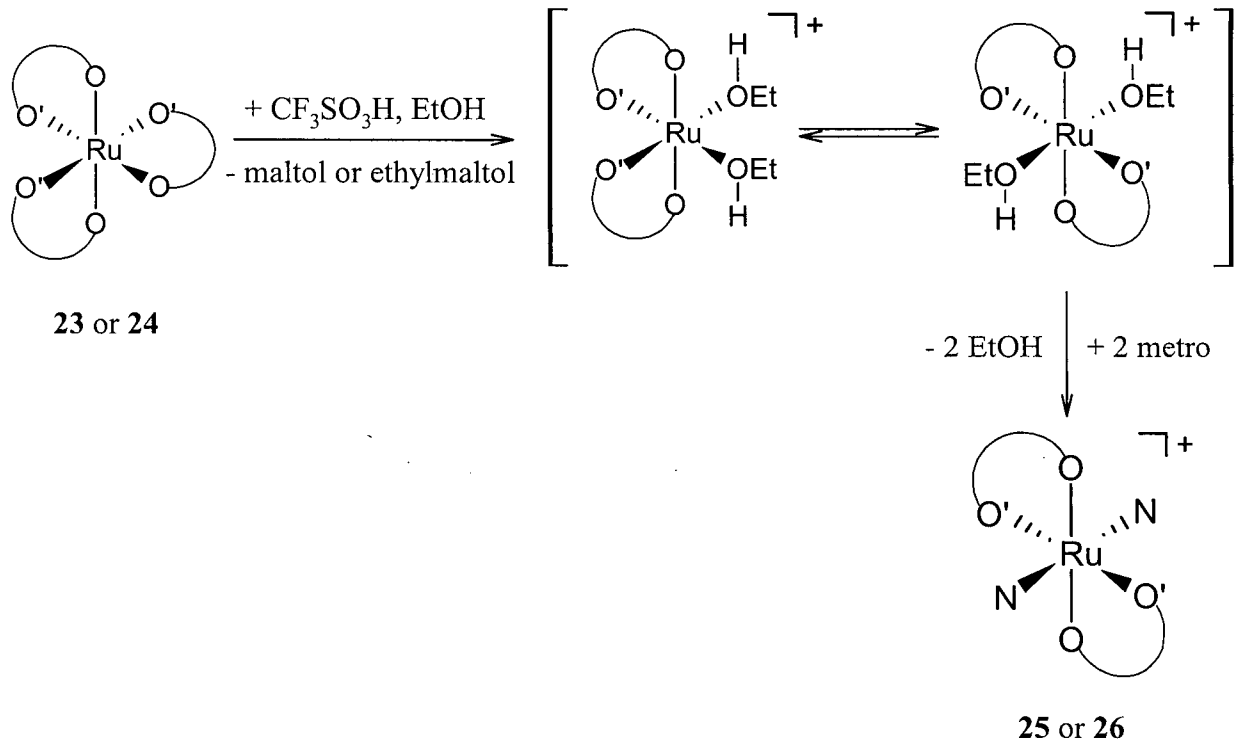

23 or **24**

25 or **26**

Figure 3.14 Speculation on the synthesis of *trans*-$[Ru(ma)_2(metro)_2](CF_3SO_3)$ (**25**) and *trans*-$[Ru(etma)_2(metro)_2](CF_3SO_3)$ (**26**) from *mer*-$Ru(ma)_3$ (**23**) and *mer*-$Ru(etma)_3$ (**24**), respectively. N represents metronidazole, and O—O′ represents the chemically inequivalent oxygen atoms of the maltolato or ethylmaltolato ligands (the $CF_3SO_3^-$ counter-ion is not shown for the cationic Ru species).

Selected IR spectroscopic data of some Ru complexes and the corresponding free ligands are shown in Table 3.8. The data for **25** show overlapping bands assigned to maltolato $\nu_{C=O}$ and $\nu_{C=C}$ between 1551 and 1604 cm^{-1}. Similarly, the ethylmaltolato IR bands ($\nu_{C=O}$ and $\nu_{C=C}$) of **26** are located between 1549 and 1600 cm^{-1}. The IR spectroscopic data of **25** also indicate the symmetric and asymmetric $\nu_{N=O}$ of the coordinated metronidazole at 1367 and 1468 cm^{-1}, respectively, while those of **26** appear at 1368 and 1472 cm^{-1}. Both **25** and **26** are conducting in acetone solution, indicating a 1:1 electrolyte, which is consistent with the solid-state ionic structure.

References on page 81

Table 3.8 Selected IR spectroscopic data of ruthenium complexes and the corresponding free ligands.

Complex	$\nu_{N=O}$ sym.[a]	$\nu_{N=O}$ asym.[a]	$\nu_{C=O} + \nu_{C=C}$[b]	$\nu_{C=O}$[b]	Ref.
$RuCl_2(metro)_4$ (**21**)	1345	1472	-	-	15
$RuCl_2(4\text{-}NO_2Im)_4$ (**22**)	1381	1496	-	-	*c*
mer-$Ru(ma)_3$ (**23**)	-	-	1565	1600	11
mer-$Ru(etma)_3$ (**24**)	-	-	1550	1596	*c*
trans-$[Ru(ma)_2(metro)_2]^+$ (**25**)	1367	1468	1551,1560	1604	*c*
trans-$[Ru(etma)_2(metro)_2]^+$ (**26**)	1368	1472	1549, 1560	1600	*c*
metronidazole	1369	1474	-	-	*c*
4-nitroimidazole	1381	1495	-	-	*c*
maltol	-	-	1550, 1610	1650	11
ethylmaltol	-	-	1557, 1612	1647	*c*

[a] IR stretching frequency (cm^{-1}) of free or coordinated nitroimidazoles. [b] IR stretching frequency (cm^{-1}) of free or coordinated maltol(ato) or ethylmaltol(ato). [c] This work.

3.6 Attempted Synthesis of $Ru^{II}(ma)_2(metro)_2$

The initial objective of this project was to synthesize Ru^{II} maltolato and imidazole complexes analogous to the Ru^{III} complexes previously synthesized by D. Kennedy of this group. Comparisons of the anticancer activity of Ru^{II} and Ru^{III} complexes are potentially fruitful. The first complex attempted was $Ru(ma)_2(metro)_2$, the Ru^{II} analogue of **25.** The reaction between $RuCl_2(metro)_4$ (**21**) and two equivalents of Kma was attempted, as was the substitution of DMSO in $Ru(ma)_2(DMSO)_2$ (**11**) by metronidazole. These reactions provided no signs of the desired product, as judged by ^1H NMR spectroscopy: the former reaction indicated no maltolato coordination, while the latter indicated no DMSO substitution. The synthesis of $Ru(ma)_2(CH_3CN)_2$, a possible precursor to $Ru(ma)_2(metro)_2$, was also attempted from the reaction between *trans*-$RuCl_2(CH_3CN)_4$ and two equivalents of Kma, but it was also unsuccessful.

References on page 81

Examination of a series of Ru β-diketonato complexes, synthesized by I. Baird in our group,[15] provides some insight into the synthetic problem. The β-diketonate ligands, acetylacetonate (acac) and 1,1,1,5,5,5-hexafluoroacetylacetonate (hfac), are similar to maltolate and are capable of *O, O'*-chelation to Ru (Figure 3.15). The general trend shows that the acac ligands lead to the formation of Ru^{III} complexes such as $[Ru(acac)_2(L)_2](CF_3SO_3)$, while the hfac ligands generate Ru^{II} complexes such as $Ru(hfac)_2(L)_2$ (L = imidazoles or nitroimdazoles). This implies that the electron-donating acac ligand favors stabilization of Ru^{III}, while the more electron-deficient hfac ligand favors Ru^{II}. Complex **25** is structurally analogous to $[Ru(acac)_2(metro)_2](CF_3SO_3)$, suggesting that maltolate behaves similar to acac and favors Ru^{III} coordination. This offers some rationale for why attempts to prepare $Ru^{II}(ma)_2(metro)_2$ have to date been unsuccessful.

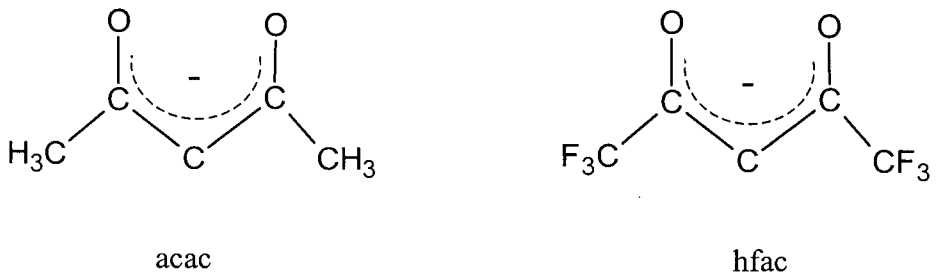

acac hfac

Figure 3.15 Structures of the β-diketonate ligands, acetylacetonate (acac) and 1,1,1,5,5,5-hexafluoroacetylacetonate (hfac).

Ru^{III} exhibits a d^5 low-spin electronic configuration, while Ru^{II} is typically d^6 low-spin. Ru^{III} favors the coordination of anionic maltolate, while Ru^{II}, with a fully occupied t_{2g} state, requires the presence of a good π-acceptor to stabilize maltolato complexes such as $Ru(ma)_2(L)_2$ (L = DMSO, PPh_3, or L_2 = COD).[7]

3.7 Electrochemical Studies of the Ruthenium Complexes

The Ru complexes were studied using cyclic voltammetry (CV) to determine the half-wave reduction potential ($E_{1/2}$) of the $Ru^{III/II}$ couple and the NO_2/NO_2^- couple of the

References on page 81

coordinated metronidazole. Cyclic voltammograms were measured using a Pt working electrode, a Pt wire counter electrode, and a silver wire reference electrode in 0.1 M [*n*-Bu_4N](PF_6) CH_2Cl_2 or THF solutions, depending on the solubility of a given complex. $FeCp_2$ or $FeCp^*_2$ was used as an internal standard to calibrate $E_{1/2}$ values to a standard calomel electrode (SCE).[19] The appropriate internal standard was chosen to avoid overlapping waves between $Ru^{III/II}$ and $Fe^{III/II}$ potentials.

3.7.1 The Reduction Potential of Ruthenium(III/II)

The $Ru^{III/II}$ half-wave reduction potentials of the maltolato, sulfoxide, and metronidazole complexes, described in this thesis, are shown in Table 3.9. The $Ru^{III/II}$ reduction potentials of the maltolato-sulfoxide complexes occur between 0.51 and 0.55 V vs. SCE. Figure 3.16A shows a typical cyclic voltammogram for these complexes. The maltolato and ethylmaltolato complexes show essentially identical data. The BESE complexes exhibit a slightly more positive potential than the DMSO and TMSO complexes, and all the potentials are very similar, strongly indicating that the DMSO and TMSO complexes exist as the *cis*-isomers as in the BESE complexes, because it is well established within Ru systems that *cis*-isomers have reduction potentials ~0.2 V higher than those of the corresponding *trans*-isomers.[20]

The $Ru^{III/II}$ potentials of **23** (-1.27 V, Figure 3.16B) and **24** (-1.29 V) are more negative than those of **25** (-0.53 V) and **26** (-0.52 V), showing that the replacement of an anionic maltolato ligand by two neutral metronidazole ligands gives a more positive potential. As expected, the stronger electron-donating, anionic ligands favor the Ru^{III} oxidation state, and therefore cause a more negative reduction potential. In contrast, π-accepting ligands such as S-bonded sulfoxides lead to more positive potentials and stabilize the Ru^{II} state. The $Ru^{III/II}$ reduction potentials of the Ru^{II} dichloro sulfoxide complexes occur between 0.92 and 1.18 V, while that of $RuCl_2(metro)_4$ (**21**) is at 0.19 V. The sulfoxide ligands generally give rise to a more positive reduction potential than do metronidazole ligands.

References on page 81

Table 3.9 Selected CV data for ruthenium(III/II) half-wave reduction potentials vs. SCE.

Complex[a]	Fe(III/II) $E_{1/2}$ (V) vs. Pt	Ru(III/II) $E_{1/2}$ (V) vs. Pt	Ru(III/II) $E_{1/2}$ (V) vs. SCE
$Ru^{II}(ma)_2(DMSO)_2$ (**11**)	0.06	0.71	0.52
$Ru^{II}(etma)_2(DMSO)_2$ (**12**)	0.02	0.66	0.51
$Ru^{II}(ma)_2(TMSO)_2$ (**13**)	0.06	0.71	0.52
$Ru^{II}(etma)_2(TMSO)_2$ (**14**)	0.06	0.71	0.52
cis-$Ru^{II}(ma)_2$(BESE) (**17**)	0.08	0.76	0.55
cis-$Ru^{II}(etma)_2$(BESE) (**18**)	0.08	0.76	0.55
mer-$Ru^{III}(ma)_3$ (**23**)	-0.01	-1.15	-1.27
mer-$Ru^{III}(etma)_3$ (**24**)	0.03	-1.13	-1.29
trans-$[Ru^{III}(ma)_2(metro)_2](CF_3SO_3)$ (**25**)[b]	0.07	-1.02	-0.53
trans-$[Ru^{III}(etma)_2(metro)_2](CF_3SO_3)$ (**26**)[b]	0.39	-0.69	-0.52
cis-$Ru^{II}Cl_2(DMSO)_3(DMSO)$ (**1**)	0.05	1.29	1.11
cis-$Ru^{II}Cl_2(TMSO)_4$ (**7**)	-0.02	1.14	1.03
$[Ru^{II}Cl(H_2O)(BESE)]_2(\mu\text{-}Cl)_2$ (**15**)	0.02	1.07	0.92
$Ru^{II}Cl_2$(BESE)$(metro)_2$ (**19**)	0.03	1.34	1.18
$Ru^{II}Cl_2(metro)_4$ (**21**)[b]	0.48	0.11	0.19

[a] Measured in CH_2Cl_2 with an $FeCp^*_2$ internal standard (-0.13 V vs. SCE), unless stated otherwise. [b] Measured in THF with an $FeCp_2$ internal standard (0.56 V vs. SCE).

The $Ru^{III/II}$ $E_{1/2}$ values of **25** and **26** are similar to those of $[Ru(acac)_2(L)_2](CF_3SO_3)$, which occur between -0.42 and -0.55 V (L = Im, N-MeIm, 2-MeIm, or 5-MeIm);[15] this establishes more quantitatively the analogy between the acac- and maltolato-type ligands. The $Ru^{III/II}$ (-1.29 V) and $Ru^{IV/III}$ (0.49 V) potentials of **23** (Figure 3.16B) are similar to those reported by Greaves and Griffith (-1.31 and 0.43 V, respectively).[11] The potential of $RuCl_2(4\text{-}NO_2Im)_4$ (**22**) could not be determined because of the insolubility of the complex in common solvents.

References on page 81

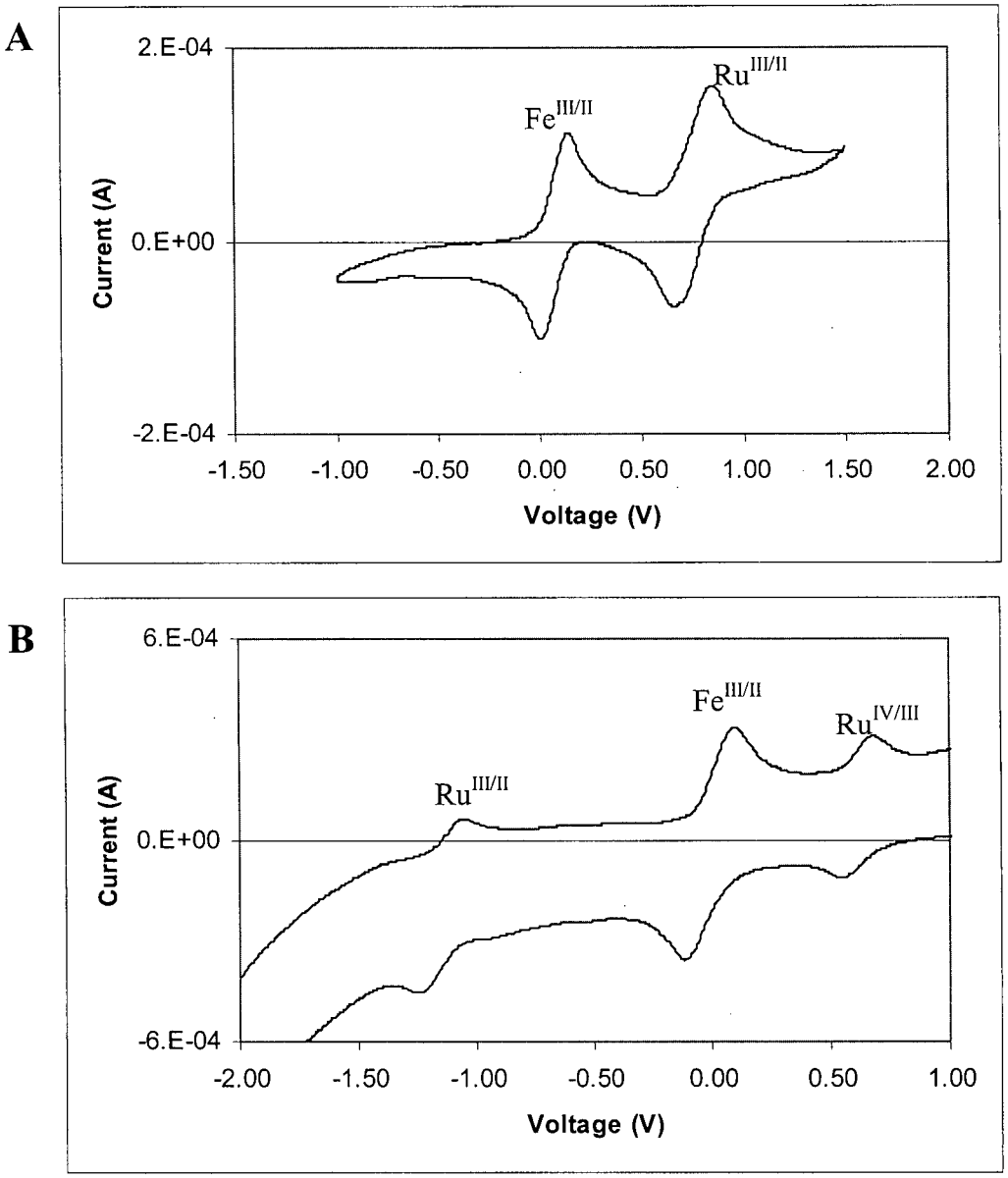

Figure 3.16 Cyclic voltammograms of *cis*-Ru(ma)$_2$(BESE) (**17**) (A) and *mer*-Ru(ma)$_3$ (**23**) (B), in 0.1 M [*n*-Bu$_4$N](PF$_6$) CH_2Cl_2 solutions with FeCp*$_2$ internal standard.

3.7.2 The Reduction Potential of NO_2/NO_2^- in the Metronidazole Complexes

The half-wave reduction potentials of the NO_2/NO_2^- couple in the Ru metronidazole complexes were determined, and the results are shown in Table 3.10. The NO_2/NO_2^- potentials of $RuCl_2$(BESE)(metro)$_2$ (**19**) (-1.16 V, Figure 3.17A) and

References on page 81

$RuCl_2(metro)_4$ (**21**) (-1.07 V, Figure 3.17B) are more positive than those of **25** (-1.25 V) and **26** (-1.27 V). These potentials for the Ru^{II} complexes are also more positive than that of free metronidazole (-1.22 V), while the Ru^{III} complexes have slightly more negative values. This provides evidence that the NO_2 group of a Ru^{II} metronidazole complex can be more susceptible to reduction than that of a Ru^{III} complex; this surprising conclusion cannot be applicable generally because the system here has different ancillary ligands (chloride and/or sulfoxide vs. maltolate). The NO_2/NO_2^- reduction potential of free metronidazole was measured in CH_2Cl_2 to be -1.22 V, more negative than that measured by I. Baird in MeCN (-1.09 V).[15] Clearly, different solvents can influence significantly the electrochemical potential of the metal or a ligand functional group.

Table 3.10 Selected CV data for NO_2/NO_2^- half-wave reduction potentials vs. SCE.

Complex[a]	Fe(III/II) $E_{1/2}$ (V) vs. Pt	NO_2/NO_2^- $E_{1/2}$ (V) vs. Pt	NO_2/NO_2^- $E_{1/2}$ (V) vs. SCE
$Ru^{II}Cl_2(BESE)(metro)_2$ (**19**)[b]	0.03	-1.00	-1.16
$Ru^{II}Cl_2(metro)_4$ (**21**)	0.48	-1.15	-1.07
trans-$[Ru^{III}(ma)_2(metro)_2](CF_3SO_3)$ (**25**)	0.07	-1.74	-1.25
trans-$[Ru^{III}(etma)_2(metro)_2](CF_3SO_3)$ (**26**)	0.39	-1.44	-1.27
Metronidazole[c]	0.36	-1.33	-1.22

[a] Measured in THF with $FeCp_2$ as the internal standard (0.56 V in THF vs. SCE), unless stated otherwise. [b] Measured in CH_2Cl_2 with $FeCp^*_2$ as the internal standard (-0.13 V in CH_2Cl_2 vs. SCE). [c] Measured in CH_2Cl_2 with $FeCp_2$ as the internal standard (0.46 V in CH_2Cl_2 vs. SCE).

References on page 81

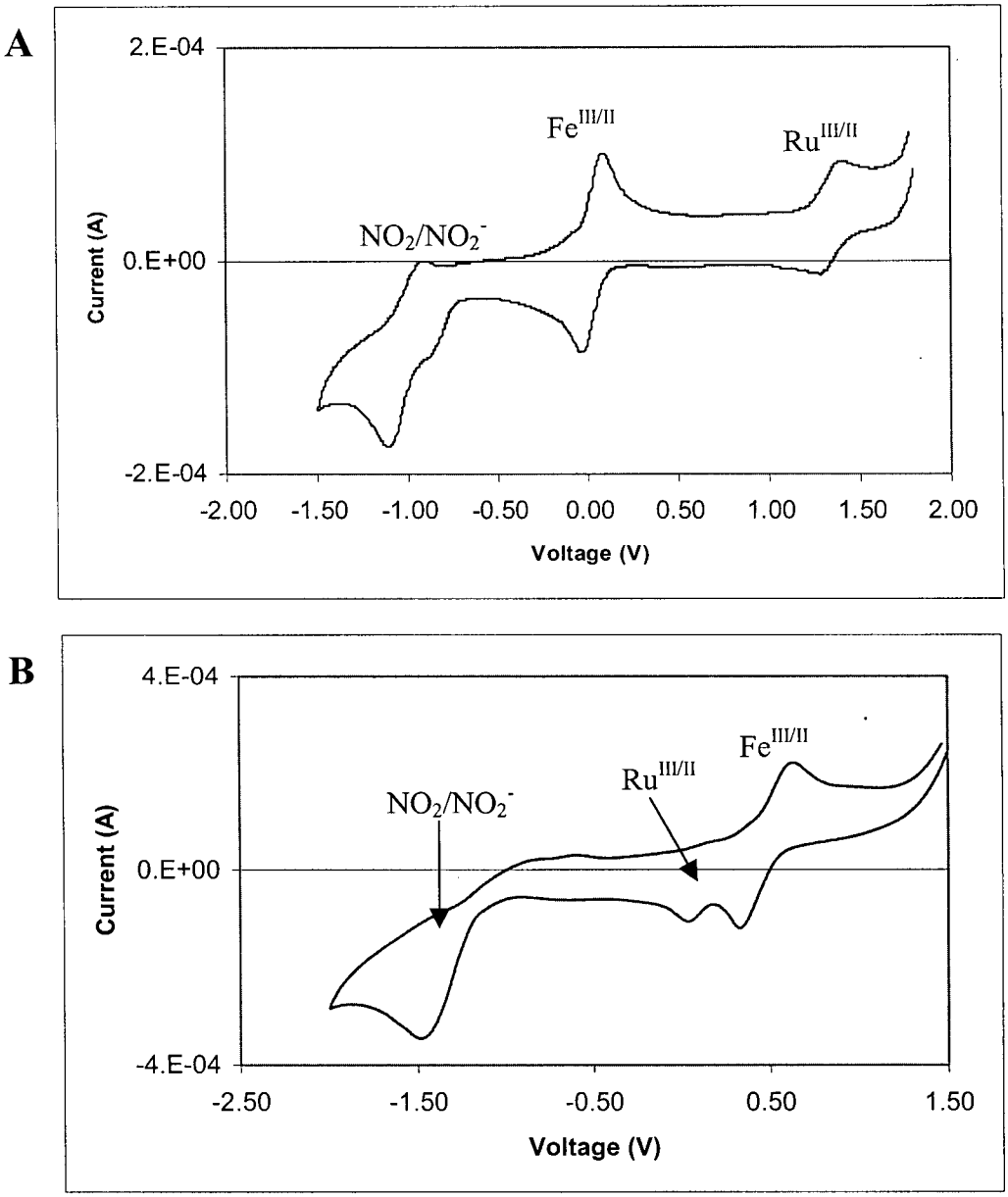

Figure 3.17 Cyclic voltammograms of $RuCl_2(BESE)(metro)_2$ (**19**) (A) and $RuCl_2(metro)_4$ (**21**) (B), with $FeCp^*_2$ (A) and $FeCp_2$ (B) internal standards in 0.1 M [*n*-Bu_4N](PF_6) CH_2Cl_2 and THF solutions, respectively.

References on page 81

3.8 References

(1) Calligaris, M.; Carugo, O. *Coord. Chem. Rev.* **1996,** *153,* 83.

(2) Mercer, A.; Trotter J. *J. Chem. Soc. Dalton Trans.* **1975,** 2480.

(3) Davies, J. A. *Adv. Inorg. Chem. Radiochem.* **1981,** *24,* 115.

(4) Yapp, D. T. T.; Jaswal, J.; Rettig, S. J.; James, B. R.; Skov, K. A. *Inorg. Chim. Acta* **1990,** *177,* 199.

(5) Alessio, E.; Milani, B.; Mestroni, G.; Calligaris, M.; Faleschini, P.; Attia, W. M. *Inorg. Chim. Acta* **1990,** *177,* 255.

(6) Alessio, E.; Mestroni, G.; Nardin, G.; Attia, W. M.; Calligaris, M.; Sava, G.; Zorzet, S. *Inorg. Chem.* **1988,** *27,* 4099.

(7) (a) Fryzuk, M. D.; Jonker, M. J.; Rettig, S. J. *Chem. Commun.* **1997,** 377.
(b) Jonker, M. J. *Synthesis, Characterization, and Reactivity of Ruthenium Maltolato Complexes;* M. Sc. Dissertation, University of British Columbia: Vancouver, 1993.

(8) Cheu, E. L. S. *Thioether and Sulfoxide Complexes of Ruthenium; Preliminary In Vitro Studies of Water-Soluble Species;* Ph. D. Dissertation, University of British Columbia: Vancouver, 2000.

(9) Huxham, L. A. *The Synthesis and Characterization of Ruthenium Disulfoxide Complexes and Their Preliminary In Vitro Examination as Potential Chemotherapeutic Agents;* M. Sc. Dissertation, University of British Columbia: Vancouver, 2001.

(10) Yapp, D. T. T.; Rettig, S. J.; James, B. R.; Skov, K. A. *Inorg. Chem.* **1997,** *36,* 5635.

(11) Greaves, S. J.; Griffith, W. P. *Polyhedron* **1988,** *7,* 1973.

(12) Yapp, D. T. T. The Synthesis and Characterization of New Sulfoxide Complexes of Ruthenium and their Potential as Anti-Cancer Agents; Ph. D. Dissertation, University of British Columbia: Vancouver, 1993.

(13) Chan, P. K. L. *Ruthenium Nitroimidazole Complexes as Radiosensitizers;* Ph. D. Dissertation, University of British Columbia: Vancouver, 1988.

(14) Chan, P. K. L.; Skov, K. A.; James, B. R.; Farrell, N. P. *Int. J. Radiat. Oncol. Biol. Phys.* **1986,** *12,* 1059.

(15) Baird, I. R. *Fluorinated Nitroimidazoles and Their Ruthenium Complexes: Potential Hypoxia-Imaging Agents;* Ph. D. Dissertation, University of British Columbia: Vancouver, 1999.

(16) Rose, D.; Wilkinson, G. *J. Chem. Soc. A* **1970,** 1791.

(17) Kennedy, D.; Patrick, B. O.; James, B. R. *Unpublished Results,* 2000.

(18) Kennedy, D.; James, B. R. *Unpublished Results,* 2000.

(19) Connelly, N. G.; Geiger, W. E. *Chem. Rev.* **1996,** *96,* 877.

(20) (a) Lever, A. B. P. *Inorg. Chem.* **1990,** *29,* 1271.

(b) Siebald, H. G. L.; Fabre, P.-L.; Dartiguenave, M.; Dartiguenave, Y.; Simard, M.; Beauchamp, A. L. *Polyhedron* **1996,** *15,* 4221.

(c) Queiroz, S. L.; Batista, A. A.; Oliva, G.; do P. Gambardella, M. T.; Santos, R. H. A.; MacFarlane, K. S.; Rettig, S. J.; James, B. R. *Inorg. Chim. Acta.* **1998,** *267,* 209.

CHAPTER 4

The *In Vitro* MTT Assay on Ruthenium Complexes

4.1 Introduction

The MTT assay is a colorimetric determination of cancer cell viability during *in vitro* treatment with a drug.[1] The assay, developed as an initial stage of drug screening, measures the amount of 3-(4,5-dimethylthiazol-2-yl)-2,5-diphenyltetrazolium bromide (MTT) reduction in the formation of formazan by mitochondrial dehydrogenase (Figure 4.1).[2] The assay assumes that the cell viability corresponds to the reductive activity, and is proportional to the production of purple formazan which is measured spectrophotometrically. The assay determines the IC_{50}, the drug concentration that kills 50 % of the cancer cells relative to the control. A low IC_{50} is desired and implies that the drug is effective at low concentrations.

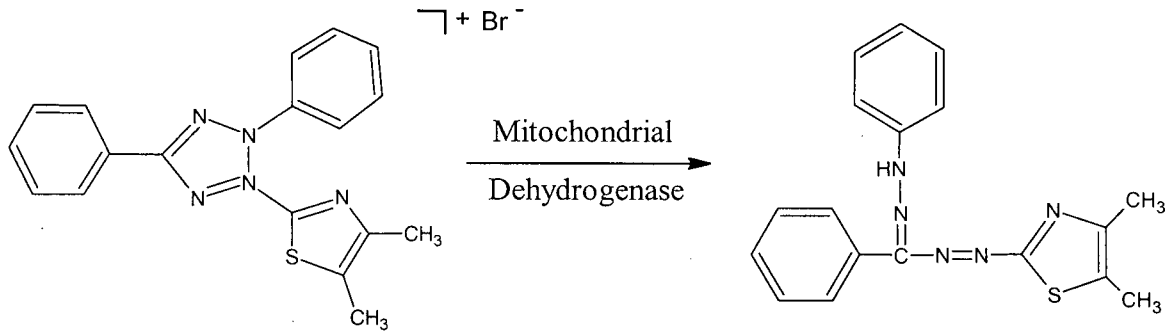

MTT (yellow) Formazan (purple)

Figure 4.1 Reduction of 3-(4,5-dimethylthiazol-2-yl)-2,5-diphenyltetrazolium bromide (MTT) to formazan by mitochondrial dehydrogenase.

The results of the MTT assay can be obtained within five days, and the assay is suitable for automation.[2] The results correlate well with those of other viability assays, such as the dye exclusion assay.[3] Disadvantages of the MTT assay include inconsistent

References on page 92

IC_{50} values in certain tumor lines, and the requirement of a good cellular metabolic rate on the tetrazolium salt.[2] Nevertheless, it is a good technique for initial screening, and provides a general assessment of the potency of a drug against certain tumor lines. This chapter presents the preliminary results of the potential therapeutic use of water-soluble Ru complexes against human breast cancer cells (MDA435/LCC6).[4]

4.2 Experimental

4.2.1 Reagents

All reagents were handled in a sterile fume hood. Dulbecco's modified Eagle's medium (DMEM) (with high glucose, L-glutamine, and pyridoxine hydrochloride), Dulbecco's phosphate-buffered saline solution (PBS), penicillin-streptomycin, trypsin-EDTA (0.25 % trypsin and 1 mM Na_4(EDTA)), and trypan blue stain (0.4 %) were purchased from Gibco. Fetal bovine serum (FBS) was generously donated by J. Hutcheon from Prof. K. A. Skov's laboratory (BC Cancer Research Center). MTT was purchased from Aldrich. The growth medium consisted of 500 mL DMEM, 5 mL penicillin-streptomycin, and 50 mL FBS. The medium, PBS, and MTT were stored at 4 °C, while penicillin-streptomycin, trypsin-EDTA, and FBS were stored frozen at -10 °C and thawed before use.

4.2.2 Cell Preparation

Human breast cancer cells (MDA435/LCC6) were donated by J. Hutcheon and plated onto a T-75 flask (Becton Dickinson and Company) in the growth medium.[4] The cells were trypsinized and passaged to a new flask bi-weekly. The growth medium was removed when the cells remained plated at the bottom of the flask. The inside of the flask was washed with PBS (10 mL); trypsin-EDTA (5 mL) was then added, and distributed over the cells for 3 min. The growth medium (15 mL) was then added to deactivate the trypsin, and the cells were mixed by filling and emptying of a pipette. The cell suspension (~1 mL) was transferred to a new flask containing the growth medium (20 mL), and incubated at 37 °C under an atmosphere of 95 % air/5 % CO_2 in a water-jacketed incubator (Forma Scientific).

References on page 92

A hemacytometer (Hausser Scientific, 0.100 mm deep) was used to determine the concentration of the remainder of the cells. A mixture of cells (50 μL) and trypan blue (50 μL) was prepared, and a portion of it was pipetted onto the hemacytometer. Trypan blue stains and excludes the dead cell, thus only the live ones are visible. The cells were counted under a microscope, and the concentration was determined as the average cell count x 10^4 x 2 (dilution factor) cells per mL, 10^4 being a calibration factor of the hemacytometer. The cell solutions were diluted with the growth medium to a concentration of 6 x 10^5 cells in 6 mL, and transferred to a 96-well plate (Becton Dickinson and Company). The cells (1 x 10^4) in 100 μL were plated into each well of columns C and 1 to 8 (Figure 4.2). The growth medium (200 μL) was added to column B, and served as a blank. To each of the outside wells was added deionized water (200 μL) to prevent evaporation of water from the inner wells. The plate was then incubated at 37 °C for 24 h.

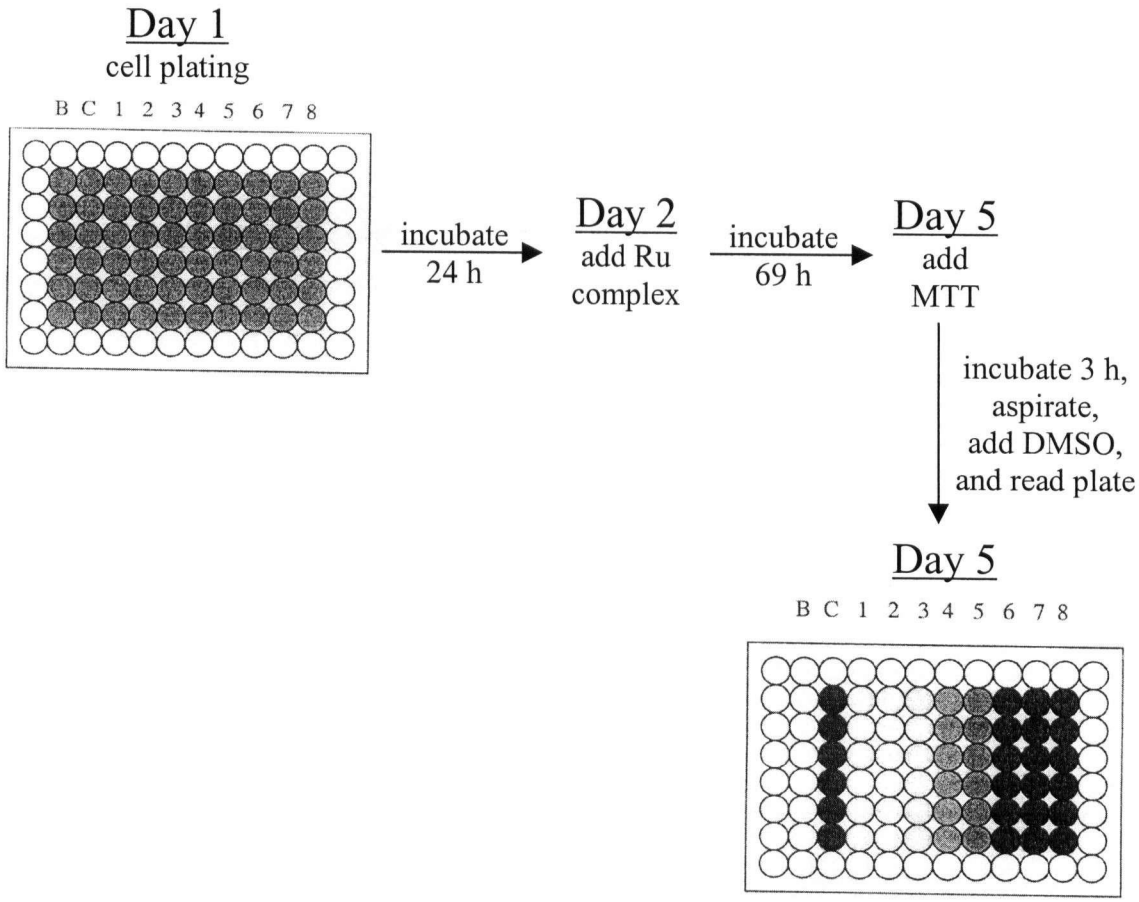

Figure 4.2 The schematic diagram of the MTT assay.

References on page 92

4.2.3 Preparation of Solutions of Ruthenium Complexes

A Ru complex (10 to 20 mg) was dissolved in PBS (5 mL), and the mixture was filtered through a 0.2 μm filter (Acrodisc from Pall Gelman Laboratory) to sterilize the solution. The solution was then serially diluted using the growth medium into fractions of the following final concentrations: 2, 1, 0.75, 0.5, 0.25, 0.1, 0.01, and 0.001 mM (see drug dilution sheet in Appendix 4). The Ru solutions (100 μL) were pipetted into each well in columns 1 to 8, which contained the highest to lowest concentrations, respectively. The growth medium (100 μL) was pipetted into each well in column C, and the plate was incubated at 37 °C for 69 h.

4.2.4 MTT Addition and Plate Reading

A modified procedure of Mosmann was used.[5] A solution of MTT (2.5 mg/mL), in a 1:1 mixture of PBS and the growth medium, was filtered through a 0.2 μm filter (Acrodisc), before being added (50 μL) to each well (columns B, C, and 1 to 8). The plate was incubated for 3 h, by which time a purple precipitate of formazan formed at the bottom of certain wells, especially those with zero or low concentration of the Ru complex. The contents of each well were carefully pipetted off to leave the formazan behind. DMSO (150 μL) was then added to each well to dissolve the formazan, and the plate was immediately analyzed by a plate reader (Spectra Max Plus from Molecular Devices) to determine the absorbance of each well at 570 nm. The percentage cell viability was calculated by dividing the average absorbance of the cells treated with a Ru complex by that of the control. Percent cell viability versus drug concentration (logarithmic scale in the x-axis) was plotted using Excel to determine the IC_{50}.

4.3 Results and Discussions

Ru^{II} maltolato-sulfoxide complexes indicate anticancer activity against human breast cancer cells. All sulfoxide ligands are S-bonded, and presumably have a *cis*-configuration (see Sections 3.1.2, 3.1.3, 3.2.2, and 3.7.1). The IC_{50} values of $Ru(ma)_2(DM\underline{S}O)_2$ (**11**) (650 μM) and $Ru(etma)_2(DM\underline{S}O)_2$ (**12**) (470 μM) (Figure 4.3) are lower than those of the corresponding TMSO and BESE complexes (Table 4.1). If the

References on page 92

mechanism of cell growth inhibition involves Ru-DNA binding, ligand displacement must occur to generate an open Ru coordination site for DNA. DMSO ligands should be more easily displaced than BESE, according to the chelate effect, and this would account for the higher activity of the DMSO species versus the BESE species. However, such a rationale does not correlate well with the lower performance of the TMSO complexes. This simple rationale would require that the TMSO ligands dissociate at the lowest rate.

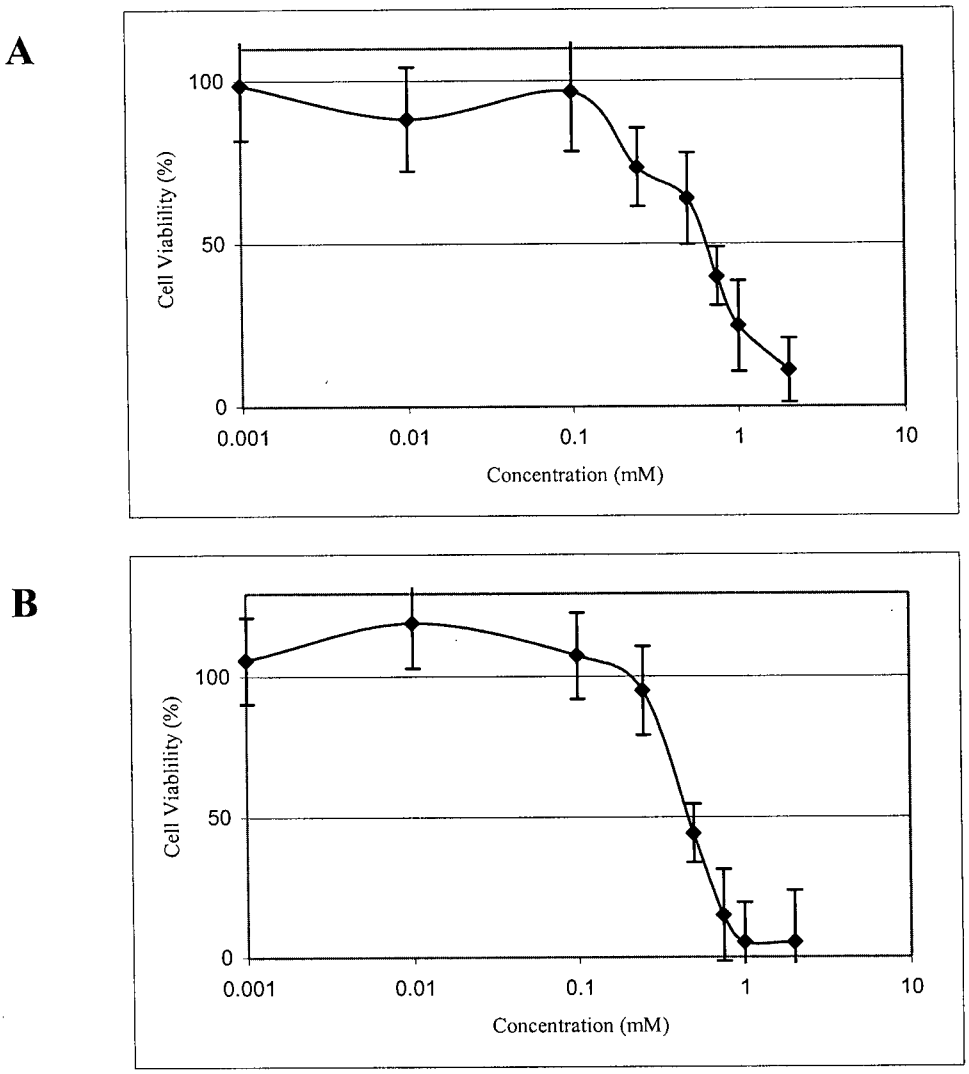

Figure 4.3 The MTT plots for $Ru(ma)_2(DMSO)_2$ (**11**) (A) and $Ru(etma)_2(DMSO)_2$ (**12**) (B), with IC_{50} values equal to 650 and 470 μM, respectively. The error bars indicate one standard deviation of the averaged cell percent viability.

References on page 92

Table 4.1 The IC_{50} values of the ruthenium complexes.

Complex[a]	IC_{50}[b] (μM)
$Ru(ma)_2(DMSO)_2$ (**11**)	650
$Ru(etma)_2(DMSO)_2$ (**12**)	470
$Ru(ma)_2(TMSO)_2$ (**13**)	1810
$Ru(etma)_2(TMSO)_2$ (**14**)	820
cis-$Ru(ma)_2$(BESE) (**17**)	1270
cis-$Ru(etma)_2$(BESE) (**18**)	880
mer-$Ru(ma)_3$ (**23**)	150
mer-$Ru(etma)_3$ (**24**)	80
$RuCl_3 \cdot 3H_2O$	*c*
cis-$RuCl_2(DMSO)_3(DMSO)$ (**1**)	*c*
$RuCl_2$(BESE)$(metro)_2$ (**19**)	*c*

[a] The concentration range tested was between 0.001 to 2 mM. [b] ±15 %, determined from the error bars of the MTT plot. [c] Not determined because the cell viability did not fall below 50 % within the concentration range tested.

The IC_{50} values of several other Ru complexes are shown in Table 4.1. *Mer*-$Ru(ma)_3$ (**23**) and *mer*-$Ru(etma)_3$ (**24**) have the lowest IC_{50} values (150 and 80 μM, respectively, Figure 4.4), suggesting perhaps that Ru^{III} maltolato complexes are more potent (and toxic) than Ru^{II} maltolato complexes, although the higher content of the maltolato ligands per Ru^{III} (versus those of the Ru^{II} complexes) could also be a factor. Whether the better activity of Ru^{III} versus Ru^{II} is manifested in the activation by a reduction mechanism is unclear; i.e. a reduction of the relatively inert Ru^{III} complexes to more labile Ru^{II} complexes occurs inside the cell, and the latter becomes more active in DNA-binding.[6] A treatment with Ru^{II} complexes may be unsuccessful because the species may be too reactive and decompose before entering the cell. An interesting observation is that the ethylmaltolato complexes (with or without ancillary sulfoxide ligands) exhibit a significantly lower IC_{50} than the analogous maltolato complexes. It is not obvious why a subtle structural difference should give significantly different

References on page 92

anticancer activity. Further *in vivo* testing is encouraged from these preliminary results of Ru maltolato complexes.

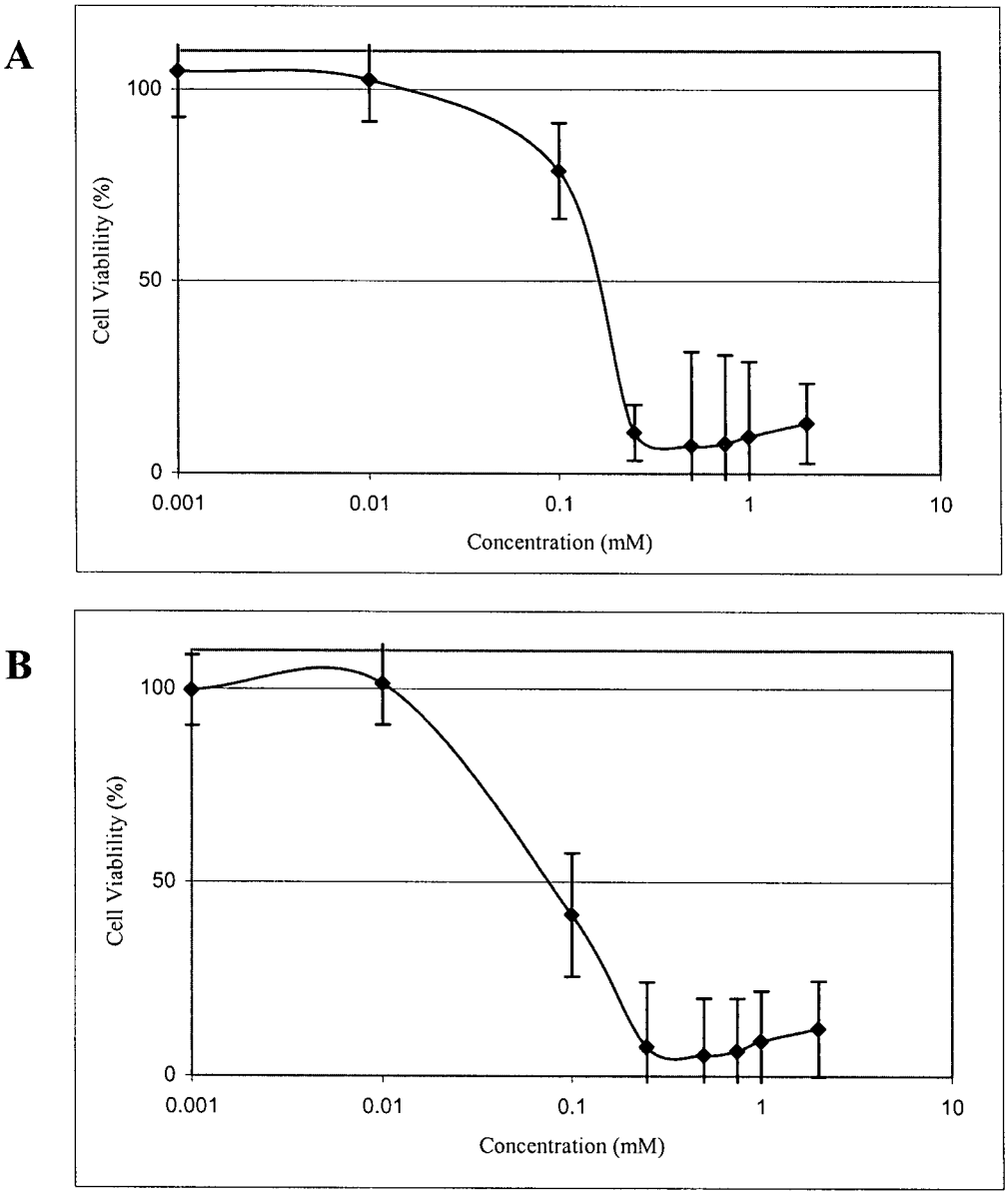

Figure 4.4 The MTT plots for *mer*-Ru(ma)$_3$ (**23**) (A) and *mer*-Ru(etma)$_3$ (**24**) (B), with IC_{50} values equal to 150 and 80 μM, respectively. The error bars indicate one standard deviation of the averaged cell percent viability.

References on page 92

The IC_{50} values for $RuCl_3 \cdot 3H_2O$, *cis*-$RuCl_2(DMSO)_3(DMSO)$ (**1**), and $RuCl_2(BESE)(metro)_2$ (**19**) were not determined, as more than 50 % of the cells remained alive at the highest concentration of 2 mM (Figure 4.5). The percent cell viability of **1** and **19** is ~80 % at 2 mM, while $RuCl_3 \cdot 3H_2O$ is completely inactive showing 100 % cell viability at 2 mM.

The MTT results for *cis*-$RuCl_2(BESE)(DMSO)(DMSO)$, studied previously in this laboratory using human breast cancer cells (MDA-MB-435s), indicate a cell viability greater than 80 % at 3 mM,[7] while *trans*-$RuCl_2(R,R\text{-}BMSE)_2$ and *trans*-$RuCl_2(S,S\text{-}BMSE)_2$ show poor, but better activity with IC_{50} values between 1700 and 1800 μM;[8] MDA435/LCC6 used in this thesis work is a cell line derived from the parental MDA-MB-435.[4] Thus, generally Ru^{II} dichloro-sulfoxide complexes do not appear to be effective against human breast cancer cells, or at least require a higher dosage in order to show any significant activity. However, a Ru^{II} dichloro-(*p*-cymene)-sulfoxide complex, $[RuCl_2(p\text{-cymene})]_2(\mu\text{-BESE})$, shows good anticancer activity (IC_{50} = 345 - 360 μM) against MDA-MB-435s cells.[7]

References on page 92

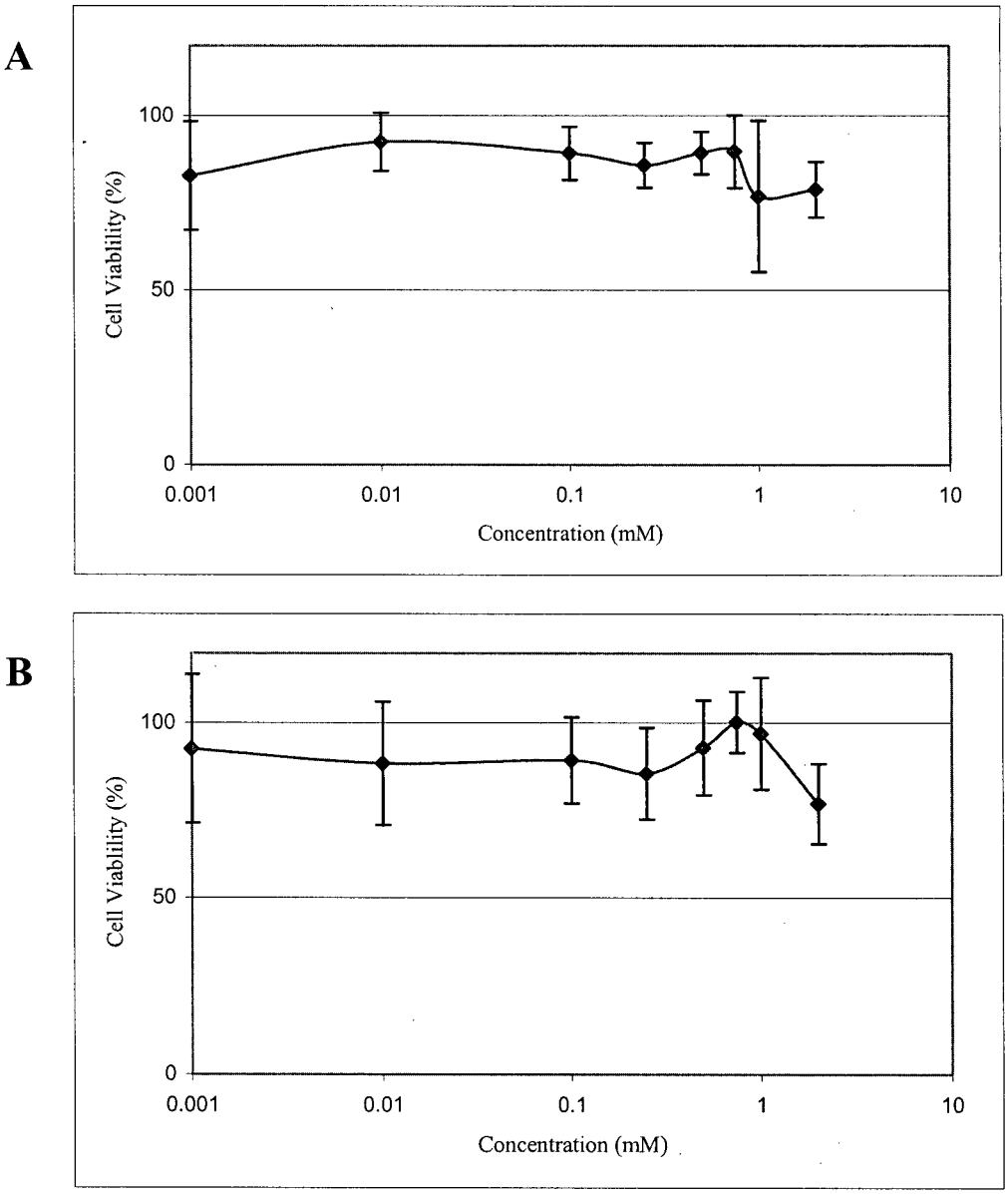

Figure 4.5 The MTT plots for *cis*-$RuCl_2(DMSO)_3(DMSO)$ (**1**) (A) and $RuCl_2(BESE)(metro)_2$ (**19**) (B), both with ~80 % cell viability at 2 mM. The error bars indicate one standard deviation of the averaged cell percent viability.

References on page 92

4.4 References

(1) Alley, M. C.; Scudiero, D. A.; Monks, A.; Hursey, M. L.; Czerwinski, M. J.; Fine, D. L.; Abbott, B. J.; Mayo, J. G.; Shoemaker, R. H.; Boyd, M. R. *Cancer Res.* **1988,** *48,* 589.

(2) Bellamy, W. T. *Drugs* **1992,** *44,* 690.

(3) Carmichael, J.; DeGraff, W. G.; Gazdar, A. F.; Minna, J. D.; Mitchell, J. B. *Cancer Res.* **1987,** *47,* 936.

(4) Leonessa, F.; Green D.; Licht, T.; Wright, A.; Wingate-Legette, K.; Lippman, J.; Gottesman, M. M.; Clarke, R. *Br. J. Cancer* **1996,** *73,* 154.

(5) Mosmann, T. *J. Immunol. Methods* **1983,** *65,* 55.

(6) Clarke, M. J.; Bitler, S.; Rennert, D.; Buchbinder, M.; Kelman, A. D. *J. Inorg. Biochem.* **1980,** *12,* 79.

(7) Huxham, L. A. *The Synthesis and Characterization of Ruthenium Disulfoxide Complexes and Their Preliminary In Vitro Examination as Potential Chemotherapeutic Agents;* M. Sc. Dissertation, University of British Columbia: Vancouver, 2001.

(8) Araujo, C. S.; Khiar, N.; Huxham, L. A.; James, B. R. *Unpublished data; through collaboration with Prof. Khiar's group,* 2001.

CHAPTER 5

Conclusions and Recommendations for Future Work

Water-soluble Ru^{II} bis(maltolato) and bis(ethylmaltolato) complexes with ancillary monodentate and bidentate sulfoxide ligands (DMSO, TMSO, and BESE) have been synthesized and well characterized, as well as a Ru^{II} BESE-metronidazole complex, $RuCl_2(BESE)(metro)_2$. Some Ru^{III} maltolato complexes have also been prepared, and X-ray crystallographic structures were determined for *cis*-$Ru(ma)_2$(*S,R*-BESE) (**17**), *trans*-$RuCl_2$(*R,R*-BESE)$(metro)_2$ (**19**), and *trans*-$[Ru(ma)_2(metro)_2](CF_3SO_3)$ (**25**). The sulfoxide ligands are exclusively S-bonded as observed in the IR and ^1H NMR spectra, and in the first two X-ray structures.

Electrochemical data indicate that the $Ru^{III/II}$ reduction potential of $Ru(ma)_3$ (**23**) is more negative than that of **25,** while the corresponding potentials of $Ru(ma)_2(L)_2$ (L = DMSO, TMSO, or L_2 = BESE) are more positive. Electron-donating, anionic ligands such as maltolato favor coordination to Ru^{III}, while π-accepting S-bonded sulfoxide ligands stabilize the Ru^{II} state. Ru^{II} complexes with anionic maltolato ligands require stabilization by good π-acceptors such as sulfoxides. The $Ru^{III/II}$ reduction potentials of $Ru(ma)_2(L)_2$ (L = DMSO or TMSO) are very similar to that of **17,** strongly suggesting that the DMSO and TMSO complexes exist as the *cis*-isomers as for the BESE complexes.

Of the complexes tested, **23** and $Ru(etma)_3$ (**24**) exhibit the best anticancer activities against human breast cancer cells (MDA435/LCC6) in the *in vitro* MTT assay, in terms of the lowest IC_{50} values of 150 and 80 μM, respectively. The Ru^{II} maltolato-sulfoxide complexes also showed some anticancer activities, with $Ru(etma)_2(DMSO)_2$ (**12**) being the most potent (IC_{50} = 470 μM). The ethylmaltolato complexes are generally more effective than the corresponding maltolato complexes. The promising anticancer activity of the Ru^{III} maltolato and Ru^{II} maltolato-sulfoxide complexes encourages further anticancer testing, both *in vitro* and *in vivo*.

A recommendation for future work includes a study of the radiosensitizing activity of $RuCl_2(BESE)(metro)_2$, for comparison with analogous bis(monodentate-sulfoxide) complexes studied earlier in this group. $RuCl_2(BESE)(metro)_2$ was not effective against the human breast cancer cells in the MTT assay, but its anticancer activity should be determined against other cancer cell lines. Reactions of $[RuCl(H_2O)(BESE)]_2(\mu\text{-}Cl)_2$ with other imidazoles and N-substituted nitroimidazoles should be attempted in order to synthesize further $RuCl_2(BESE)(L)_2$-type complexes (L = imidazoles or nitroimidazoles).

Appendix 1

Crystallographic Experimental Details for

Cis-Ru(ma)$_2$(*S,R*-BESE)·H$_2$O (17)

A. Crystal Data

Empirical Formula	$C_{18}H_{26}O_9S_2Ru$
Formula Weight	551.59
Crystal Color, Habit	orange, prism
Crystal Dimensions	0.15 x 0.10 x 0.05 mm
Crystal System	triclinic
Lattice Type	Primitive
Lattice Parameters	a = 7.5998(3) Å b = 9.8229(4) Å c = 15.3305(4) Å α = 71.618(6)° β = 82.902(8)° γ = 89.238(8)° V = 1077.34(8) Å^3
Space Group	$P\bar{1}$ (#2)
Z value	2
D_{calc}	1.700 g/cm^3
F_{000}	564.00
μ(MoKα)	9.69 cm^{-1}

B. Intensity Measurements

Diffractometer	Rigaku/ADSC CCD
Radiation	MoKα (λ = 0.71069 Å) graphite monochromated
Detector Aperture	94 mm x 94 mm
Data Images	460 exposures @ 35.0 seconds
ϕ oscillation Range (X = -90.0)	0.0 - 190.0°
ω oscillation Range (X = -90.0)	-17.0 - 23.0°
Detector Position	38.77 mm
Detector Swing Angle	-5.53°
$2\theta_{max}$	55.7°
No. of Reflections Measured	Total: 9749 Unique: 4403 (R_{int} = 0.037)
Corrections	Lorentz-polarization Absorption/scaling/decay (corr. factors: 0.7732-1.0000)

C. Structure Solution and Refinement

Structure Solution	Direct Methods (SIR97)
Refinement	Full-matrix least-squares
Function Minimized	$\Sigma\omega(Fo^2 - Fc^2)^2$
Least Squares Weights	$w = 1/[\sigma^2(Fo^2)]$
	$= [\sigma_c^2(Fo^2) + (p^2/4)(Fo^2)]^{-1}$
p-factor	0.0410
Anomalous Dispersion	All non-hydrogen atoms
No. Observations ($1>0.00\sigma(I)$)	4403
No. Variables	271
Reflection/Parameter Ratio	16.25
Residuals (refined on F^2, all data): R; Rw	0.054; 0.076
Goodness of Fit Indicator	0.88
Max Shift/Error in Final Cycle	0.00
No. Observations ($1>3\sigma(I)$)	3396
Residuals (refined on F, $1>3\sigma(I)$): R; Rw	0.029; 0.035
Maximum peak in Final Diff. Map	0.95 $e^-/Å^3$
Minimum peak in Final Diff. Map	-1.17 $e^-/Å^3$

Table A1.1 Atomic coordinates and B_{iso}/B_{eq}.

Atom	x	y	z	B_{eq}
Ru(1)	0.73818(3)	0.27038(2)	0.79054(1)	0.787(5)
S(1)	0.61593(8)	0.36817(8)	0.89380(5)	0.96(1)
S(2)	0.49857(9)	0.13623(8)	0.81780(5)	1.09(1)
O(1)	0.9712(2)	0.4068(2)	0.7460(1)	1.17(4)
O(2)	0.6575(2)	0.4227(2)	0.6747(1)	1.05(4)
O(3)	1.0728(3)	0.6791(2)	0.5235(1)	1.52(4)
O(4)	0.8586(2)	0.1600(2)	0.7030(1)	0.95(4)
O(5)	0.8625(2)	0.1130(2)	0.8874(1)	1.01(4)
O(6)	1.0767(3)	-0.1789(2)	0.7711(1)	1.64(5)
O(7)	0.7186(3)	0.3814(3)	0.9674(1)	1.76(5)
O(8)	0.5079(3)	-0.0211(2)	0.8577(2)	1.87(5)
O(9)	1.0813(3)	0.4678(3)	0.8975(2)	2.56(6)
C(1)	0.9554(3)	0.4975(3)	0.6633(2)	0.98(6)
C(2)	0.7884(3)	0.5034(3)	0.6259(2)	0.98(6)
C(3)	0.7773(4)	0.5996(3)	0.5358(2)	1.41(6)
C(4)	0.9196(4)	0.6807(3)	0.4877(2)	1.58(6)
C(5)	1.0889(4)	0.5910(3)	0.6107(2)	1.34(6)
C(6)	1.2652(4)	0.6057(4)	0.6401(2)	2.06(7)
C(7)	0.9278(3)	0.0414(3)	0.7545(2)	0.87(5)
C(8)	0.9332(3)	0.0209(3)	0.8518(2)	0.90(6)
C(9)	1.0221(4)	-0.1010(3)	0.9026(2)	1.12(6)
C(10)	1.0904(4)	-0.1947(3)	0.8605(2)	1.57(6)
C(11)	0.9952(4)	-0.0622(3)	0.7189(2)	1.19(6)

C(12)	0.9869(4)	-0.0635(4)	0.6230(2)	1.94(7)
C(13)	0.5183(4)	0.5403(3)	0.8500(2)	1.58(7)
C(14)	0.6580(5)	0.6594(4)	0.8088(3)	2.42(8)
C(15)	0.4210(4)	0.2578(3)	0.9538(2)	1.62(6)
C(16)	0.3324(4)	0.2005(4)	0.8897(2)	1.88(7)
C(17)	0.3855(4)	0.1696(4)	0.7160(2)	1.71(7)
C(18)	0.4739(5)	0.0972(5)	0.6494(3)	3.12(9)
H(3)	0.6660	0.6068	0.5087	1.6915
H(4)	0.9116	0.7431	0.4244	1.8908
H(6A)	1.3326	0.6863	0.5937	2.4661
H(6B)	1.3303	0.5171	0.6459	2.4661
H(6C)	1.2489	0.6233	0.7000	2.4661
H(9)	1.0338	-0.1167	0.9679	1.3388
H(10)	1.1524	-0.2778	0.8964	1.8812
H(12A)	0.9139	0.0153	0.5914	2.3257
H(12B)	0.9345	-0.1551	0.6248	2.3257
H(12C)	1.1070	-0.0515	0.5893	2.3257
H(13B)	0.4429	0.5604	0.9009	1.8989
H(13A)	0.4458	0.5375	0.8019	1.8989
H(14B)	0.6011	0.7526	0.7958	2.9098
H(14C)	0.7200	0.6499	0.7511	2.9098
H(14A)	0.7434	0.6527	0.8528	2.9098
H(15B)	0.3367	0.3158	0.9796	1.9414
H(15A)	0.4566	0.1770	1.0043	1.9414
H(16A)	0.2666	0.2772	0.8503	2.2616
H(16B)	0.2503	0.1213	0.9263	2.2616
H(17B)	0.3859	0.2733	0.6844	2.0503
H(17A)	0.2628	0.1329	0.7354	2.0503
H(18A)	0.5946	0.1372	0.6268	3.7468
H(18B)	0.4057	0.1136	0.5969	3.7468
H(18C)	0.4788	-0.0061	0.6812	3.7468
H(19)	0.9864	0.4458	0.9413	1.3929
H(20)	1.0482	0.4358	0.8515	1.3929

$B_{eq} = (8/3)\pi^2(U_{11}(aa^*)^2 + U_{22}(bb^*)^2 + U_{33}(cc^*)^2 + 2U_{12}aa^*bb^* \cos\gamma + 2U_{13}aa^*cc^* \cos\beta + 2U_{23}bb^*cc^* \cos\alpha)$

Table A1.2 Bond lengths (Å).

Atom	Atom	Distance	Atom	Atom	Distance
Ru(1)	S(1)	2.2054(7)	Ru(1)	S(2)	2.1807(7)
Ru(1)	O(1)	2.141(2)	Ru(1)	O(2)	2.082(2)
Ru(1)	O(4)	2.098(2)	Ru(1)	O(5)	2.085(2)
S(1)	O(7)	1.487(2)	S(1)	C(13)	1.798(3)
S(1)	C(15)	1.815(3)	S(2)	O(8)	1.476(2)
S(2)	C(16)	1.812(3)	S(2)	C(17)	1.812(3)

O(1)	C(1)	1.318(3)	O(2)	C(2)	1.281(3)
O(3)	C(4)	1.344(4)	O(3)	C(5)	1.363(4)
O(4)	C(7)	1.328(3)	O(5)	C(8)	1.278(3)
O(6)	C(10)	1.347(4)	O(6)	C(11)	1.365(3)
C(1)	C(2)	1.449(4)	C(1)	C(5)	1.371(4)
C(2)	C(3)	1.418(4)	C(3)	C(4)	1.343(4)
C(5)	C(6)	1.488(4)	C(7)	C(8)	1.446(4)
C(7)	C(11)	1.365(4)	C(8)	C(9)	1.420(4)
C(9)	C(10)	1.346(4)	C(11)	C(12)	1.484(4)
C(13)	C(14)	1.515(4)	C(15)	C(16)	1.502(5)
C(17)	C(18)	1.508(5)	O(9)	H(19)	0.90
O(9)	H(20)	0.92	C(3)	H(3)	0.98
C(4)	H(4)	0.98	C(6)	H(6A)	0.98
C(6)	H(6B)	0.98	C(6)	H(6C)	0.98
C(9)	H(9)	0.98	C(10)	H(10)	0.98
C(12)	H(12A)	0.98	C(12)	H(12B)	0.98
C(12)	H(12C)	0.98	C(13)	H(13B)	0.98
C(13)	H(13A)	0.98	C(14)	H(14B)	0.98
C(14)	H(14C)	0.98	C(14)	H(14A)	0.98
C(15)	H(15B)	0.98	C(15)	H(15A)	0.98
C(16)	H(16A)	0.98	C(16)	H(16B)	0.98
C(17)	H(17B)	0.98	C(17)	H(17A)	0.98
C(18)	H(18A)	0.98	C(18)	H(18B)	0.98
C(18)	H(18C)	0.98			

Table A1.3 Bond angles (°).

Atom	Atom	Atom	Angle	Atom	Atom	Atom	Angle
S(1)	Ru(1)	S(2)	88.27(3)	S(1)	Ru(1)	O(1)	96.63(6)
S(1)	Ru(1)	O(2)	96.74(6)	S(1)	Ru(1)	O(4)	174.52(5)
S(1)	Ru(1)	O(5)	93.59(6)	S(2)	Ru(1)	O(1)	172.93(6)
S(2)	Ru(1)	O(2)	94.04(5)	S(2)	Ru(1)	O(4)	90.30(5)
S(2)	Ru(1)	O(5)	91.87(6)	O(1)	Ru(1)	O(2)	80.37(7)
O(1)	Ru(1)	O(4)	85.28(7)	O(1)	Ru(1)	O(5)	92.89(7)
O(2)	Ru(1)	O(4)	88.64(7)	O(2)	Ru(1)	O(5)	168.24(7)
O(4)	Ru(1)	O(5)	81.17(7)	Ru(11)	S(1)	O(7)	119.68(9)
Ru(1)	S(1)	C(13)	116.9(1)	Ru(1)	S(1)	C(15)	106.4(1)
O(7)	S(1)	C(13)	105.1(1)	O(7)	S(1)	C(15)	105.9(1)
C(13)	S(1)	C(15)	100.9(1)	Ru(1)	S(2)	O(8)	119.96(9)
Ru(1)	S(2)	C(16)	108.4(1)	Ru(1)	S(2)	C(17)	112.1(1)
O(8)	S(2)	C(16)	108.9(1)	O(8)	S(2)	C(17)	106.5(1)
C(16)	S(2)	C(17)	99.0(2)	Ru(1)	O(1)	C(1)	107.9(2)
Ru(1)	O(2)	C(2)	111.1(2)	C(4)	O(3)	C(5)	120.1(2)
Ru(1)	O(4)	C(7)	108.6(2)	Ru(1)	O(5)	C(8)	110.9(2)
C(10)	O(6)	C(11)	119.9(2)	O(1)	C(1)	C(2)	119.5(2)
O(1)	C(1)	C(5)	123.2(3)	C(2)	C(1)	C(5)	117.4(3)

O(2)	C(2)	C(1)	119.4(3)	O(2)	C(2)	C(3)	122.6(2)
C(1)	C(2)	C(3)	118.0(2)	C(2)	C(3)	C(4)	119.9(3)
O(3)	C(4)	C(3)	122.2(3)	O(3)	C(5)	C(1)	122.2(3)
O(3)	C(5)	C(6)	113.0(2)	C(1)	C(5)	C(6)	124.8(3)
O(4)	C(7)	C(8)	119.2(2)	O(4)	C(7)	C(11)	122.3(3)
C(8)	C(7)	C(11)	118.5(3)	O(5)	C(8)	C(7)	119.4(2)
O(5)	C(8)	C(9)	123.2(3)	C(7)	C(8)	C(9)	117.4(3)
C(8)	C(9)	C(10)	119.7(3)	O(6)	C(10)	C(9)	122.6(3)
O(6)	C(11)	C(7)	121.7(3)	O(6)	C(11)	C(12)	113.0(3)
C(7)	C(11)	C(12)	125.3(3)	S(1)	C(13)	C(14)	111.8(2)
S(1)	C(15)	C(16)	111.5(2)	S(2)	C(16)	C(15)	109.6(2)
S(2)	C(17)	C(18)	111.9(2)	H(19)	O(9)	H(20)	103.7
C(2)	C(3)	H(3)	120.1	C(4)	C(3)	H(3)	120.1
O(3)	C(4)	H(4)	118.9	C(3)	C(4)	H(4)	118.9
C(5)	C(6)	H(6A)	109.5	C(5)	C(6)	H(6B)	109.5
C(5)	C(6)	H(6C)	109.5	H(6A)	C(6)	H(6B)	109.5
H(6A)	C(6)	H(6C)	109.5	H(6B)	C(6)	H(6C)	109.5
C(8)	C(9)	H(9)	120.1	C(10)	C(9)	H(9)	120.1
O(6)	C(10)	H(10)	118.7	C(9)	C(10)	H(10)	118.7
C(11)	C(12)	H(12A)	109.5	C(11)	C(12)	H(12B)	109.5
C(11)	C(12)	H(12C)	109.5	H(12A)	C(12)	H(12B)	109.5
H(12A)	C(12)	H(12C)	109.5	H(12B)	C(12)	H(12C)	109.5
S(1)	C(13)	H(13B)	108.9	S(1)	C(13)	H(13A)	108.9
C(14)	C(13)	H(13B)	108.9	C(14)	C(13)	H(13A)	108.9
H(13B)	C(13)	H(13A)	109.5	C(13)	C(14)	H(14B)	109.5
C(13)	C(14)	H(14C)	109.5	C(13)	C(14)	H(14A)	109.5
H(14B)	C(14)	H(14C)	109.5	H(14B)	C(14)	H(14A)	109.5
H(14C)	C(14)	H(14A)	109.5	S(1)	C(15)	H(15B)	109.0
S(1)	C(15)	H(15A)	109.0	C(16)	C(15)	H(15B)	109.0
C(16)	C(15)	H(15A)	109.0	H(15B)	C(15)	H(15A)	109.5
S(2)	C(16)	H(16A)	109.4	S(2)	C(16)	H(16B)	109.4
C(15)	C(16)	H(16A)	109.4	C(15)	C(16)	H(16B)	109.4
H(16A)	C(16)	H(16B)	109.5	S(2)	C(17)	H(17B)	108.9
S(2)	C(17)	H(17A)	108.9	C(18)	C(17)	H(17B)	108.9
C(18)	C(17)	H(17A)	108.9	H(17B)	C(17)	H(17A)	109.5
C(17)	C(18)	H(18A)	109.5	C(17)	C(18)	H(18B)	109.5
C(17)	C(18)	H(18C)	109.5	H(18A)	C(18)	H(18B)	109.5
H(18A)	C(18)	H(18C)	109.5	H(18B)	C(18)	H(18C)	109.5

Table A1.4 Hydrogen-bonding interactions.

Donor-H···Acceptor	D-H (Å)	H···A (Å)	D···A (Å)	D-H···A (°)
O(9)-H(19)···O(7)	0.9004	2.0918	2.868(3)	143.78
O(9)-H(20)···O(1)	0.9193	1.8890	2.797(3)	169.17

Appendix 2

Crystallographic Experimental Details for

Trans-$RuCl_2$(*R,R*-BESE)(metro)$_2$ (19)

A. Crystal Data

Empirical Formula	$C_{18}H_{32}N_6O_8S_2Cl_2Ru$
Formula Weight	696.58
Crystal Color, Habit	orange, platelet
Crystal Dimensions	0.25 x 0.10 x 0.04 mm
Crystal System	orthorhombic
Lattice Type	Primitive
Lattice Parameters	a = 13.4946(7) Å b = 19.628(1) Å c = 20.746(1) Å V = 5495.1(5) Å^3
Space Group	Pbca (#61)
Z value	8
D_{calc}	1.684 g/cm^3
F_{000}	2848.00
μ(MoKα)	9.70 cm^{-1}

B. Intensity Measurements

Diffractometer	Rigaku/ADSC CCD
Radiation	MoKα (λ = 0.71069 Å) graphite monochromated
Detector Aperture	94 mm x 94 mm
Data Images	460 exposures @ 55.0 seconds
ϕ oscillation Range (X = -90.0)	0.0 - 190.0°
ω oscillation Range (X = -90.0)	-17.0 - 23.0°
Detector Position	37.99 mm
Detector Swing Angle	-5.59°
$2\theta_{max}$	55.8°
No. of Reflections Measured	Total: 52041
Corrections	Lorentz-polarization Absorption/scaling/decay (corr. factors: 0.7323-1.0000)

C. Structure Solution and Refinement

Structure Solution	Direct Methods (SIR97)
Refinement	Full-matrix least-squares
Function Minimized	$\Sigma\omega(Fo^2 - Fc^2)^2$
Least Squares Weights	$\omega = 1/(\sigma^2(Fo^2)+(0.0230 \cdot P)^2)$

	where P = (Max(Fo^2,0) + 2·Fc^2)/3
p-factor	0.0000
Anomalous Dispersion	All non-hydrogen atoms
No. Observations (I>0.00σ(I))	6361
No. Variables	366
Reflection/Parameter Ratio	17.38
Residuals (refined on F^2, all data): R; Rw	0.088; 0.099
Goodness of Fit Indicator	0.87
Max Shift/Error in Final Cycle	0.00
No. Observations (I>2σ(I))	3674
Residuals (refined on F, I>2σ(I)): R; Rw	0.042; 0.089
Maximum peak in Final Diff. Map	0.86 $e^-/Å^3$
Minimum peak in Final Diff. Map	-0.99 $e^-/Å^3$

Table A2.1 Atomic coordinates (x 10^4) and equivalent isotropic displacement parameters (A^2 x 10^3). U(eq) is defined as one third of the trace of the orthogonalized Uij tensor.

Atom	x	y	z	U(eq)	occ
Ru(1)	3584(1)	16(1)	1534(1)	18(1)	
Cl(1)	5295(1)	-314(1)	1398(1)	25(1)	
Cl(2)	1889(1)	354(1)	1677(1)	35(1)	
S(1)	3779(1)	837(1)	805(1)	29(1)	
S(2)	3149(1)	-661(1)	727(1)	30(1)	
O(1)	4786(2)	1079(2)	645(2)	37(1)	
O(2)	2094(2)	-881(2)	656(2)	49(1)	
O(3)	3713(2)	-877(2)	4281(2)	34(1)	
O(4)	1885(3)	-2424(2)	3369(2)	62(1)	
O(5)	1099(3)	-2169(2)	2493(2)	71(1)	
O(6)	4616(3)	1059(2)	5022(2)	40(1)	
O(7)	5863(2)	2077(2)	3530(2)	41(1)	
O(8)	6370(2)	1974(2)	2536(2)	47(1)	
N(1)	3362(2)	-791(2)	2212(2)	18(1)	
N(2)	3430(2)	-1530(2)	3016(2)	20(1)	
N(3)	1794(3)	-2102(2)	2860(2)	46(1)	
N(4)	4031(2)	667(2)	2311(2)	18(1)	
N(5)	4269(2)	1187(2)	3256(2)	22(1)	
N(6)	5807(3)	1836(2)	2977(2)	31(1)	0.58(1)
C(1)	2951(5)	1569(4)	821(5)	27(2)	0.58(1)
C(2)	3271(7)	2066(4)	1343(4)	44(3)	
C(3)	3233(4)	511(3)	80(2)	41(1)	
C(4)	3488(4)	-227(2)	1(2)	40(1)	
C(5)	3860(4)	-1428(2)	679(3)	49(2)	
C(6)	3562(5)	-1895(3)	130(3)	73(2)	
C(7)	3906(3)	-1014(2)	2707(2)	18(1)	
C(8)	2539(3)	-1625(2)	2689(2)	27(1)	

C(9)	2518(3)	-1171(2)	2199(2)	29(1)	
C(10)	4886(3)	-752(2)	2916(2)	24(1)	
C(11)	3799(3)	-1877(2)	3592(2)	33(1)	
C(12)	3393(4)	-1554(2)	4197(2)	44(1)	
C(13)	3679(3)	756(2)	2911(2)	20(1)	
C(14)	5025(3)	1370(2)	2839(2)	20(1)	
C(15)	4871(3)	1051(2)	2268(2)	21(1)	
C(16)	2776(3)	444(2)	3196(2)	29(1)	
C(17)	4130(3)	1352(2)	3937(2)	28(1)	
C(18)	4653(3)	839(2)	4374(2)	33(1)	
C(1B)	3269(10)	1650(4)	1064(6)	33(4)	0.42(1)
C(2B)	3613(9)	2225(5)	628(6)	46(4)	0.42(1)

Table A2.2 Bond lengths (Å).

Bond	Length	Bond	Length	Bond	Length
Ru(1)-N(1)	2.139(3)	Ru(1)-N(4)	2.143(3)	Ru(1)-S(2)	2.2174(11)
Ru(1)-S(1)	2.2267(11)	Ru(1)-Cl(2)	2.4006(11)	Ru(1)-Cl(1)	2.4148(10)
S(1)-O(1)	1.477(3)	S(1)-C(3)	1.793(5)	S(1)-C(1B)	1.817(6)
S(1)-C(1)	1.819(6)	S(2)-O(2)	1.495(3)	S(2)-C(5)	1.789(5)
S(2)-C(4)	1.790(5)	O(3)-C(12)	1.410(5)	O(4)-N(3)	1.238(5)
O(5)-N(3)	1.214(5)	O(6)-C(18)	1.414(5)	O(7)-N(6)	1.242(5)
O(8)-N(6)	1.219(5)	N(1)-C(7)	1.337(5)	N(1)-C(9)	1.362(4)
N(2)-C(7)	1.360(5)	N(2)-C(8)	1.393(5)	N(2)-C(11)	1.463(5)
N(3)-C(8)	1.419(5)	N(4)-C(13)	1.343(5)	N(4)-C(15)	1.364(4)
N(5)-C(13)	1.364(5)	N(5)-C(14)	1.385(5)	N(5)-C(17)	1.462(5)
N(6)-C(14)	1.426(5)	C(1)-C(2)	1.521(9)	C(3)-C(4)	1.497(7)
C(5)-C(6)	1.515(7)	C(7)-C(10)	1.483(5)	C(8)-C(9)	1.351(6)
C(11)-C(12)	1.510(6)	C(13)-C(16)	1.488(5)	C(14)-C(15)	1.356(5)
C(17)-C(18)	1.528(6)	C(lB)-C(2B)	1.520(10)		

Table A2.3 Bond angles (°).

Bond	Angle	Bond	Angle
N(1)-Ru(1)-N(4)	89.26(12)	N(1)-Ru(1)-S(2)	90.86(9)
N(4)-Ru(1)-S(2)	179.03(8)	N(1)-Ru(1)-S(1)	177.93(9)
N(4)-Ru(1)-S(1)	92.66(9)	S(2)-Ru(1)-S(1)	87.23(4)
N(1)-Ru(1)-Cl(2)	89.43(8)	N(4)-Ru(1)-Cl(2)	90.62(9)
S(2)-Ru(1)-Cl(2)	90.35(4)	S(1)-Ru(1)-Cl(2)	89.79(4)
N(1)-Ru(1)-Cl(1)	90.69(8)	N(4)-Ru(1)-Cl(1)	88.81(8)
S(2)-Ru(1)-Cl(1)	90.22(4)	S(1)-Ru(1)-Cl(1)	90.11(4)
Cl(2)-Ru(1)-Cl(1)	179.41(4)	O(1)-S(1)-C(3)	107.7(2)
O(1)-S(1)-C(1B)	97.6(5)	C(3)-S(1)-C(1B)	114.0(5)
O(1)-S(1)-C(1)	108.4(3)	C(3)-S(1)-C(1)	92.6(3)
C(1B)-S(1)-C(1)	21.6(4)	O(1)-S(1)-Ru(1)	119.59(14)
C(3)-S(1)-Ru(1)	105.24(16)	C(1B)-S(1)-Ru(1)	112.9(4)

C(1)-S(1)-Ru(1)	119.1(3)	O(2)-S(2)-C(5)	105.2(2)
O(2)-S(2)-C(4)	107.4(2)	C(5)-S(2)-C(4)	102.5(3)
O(2)-S(2)-Ru(1)	119.96(15)	C(5)-S(2)-Ru(1)	113.86(17)
C(4)-S(2)-Ru(1)	106.41(16)	C(7)-N(1)-C(9)	107.2(3)
C(7)-N(1)-Ru(1)	132.1(2)	C(9)-N(1)-Ru(1)	120.7(3)
C(7)-N(2)-C(8)	106.1(3)	C(7)-N(2)-C(11)	124.8(3)
C(8)-N(2)-C(11)	129.0(3)	O(5)-N(3)-O(4)	123.7(4)
O(5)-N(3)-C(8)	117.6(4)	O(4)-N(3)-C(8)	118.7(4)
C(13)-N(4)-C(15)	106.4(3)	C(13)-N(4)-Ru(1)	132.5(3)
C(15)-N(4)-Ru(1)	120.9(2)	C(13)-N(5)-C(14)	105.2(3)
C(13)-N(5)-C(17)	124.8(3)	C(14)-N(5)-C(17)	129.8(4)
O(8)-N(6)-O(7)	124.8(4)	O(8)-N(6)-C(14)	116.9(4)
O(7)-N(6)-C(14)	118.3(4)	C(2)-C(1)-S(1)	110.1(5)
C(4)-C(3)-S(1)	110.0(3)	C(3)-C(4)-S(2)	108.0(3)
C(6)-C(5)-S(2)	114.1(4)	N(1)-C(7)-N(2)	110.2(3)
N(1)-C(7)-C(10)	127.0(3)	N(2)-C(7)-C(10)	122.8(3)
C(9)-C(8)-N(2)	107.3(3)	C(9)-C(8)-N(3)	127.4(4)
N(2)-C(8)-N(3)	125.3(4)	C(8)-C(9)-N(1)	109.2(4)
N(2)-C(11)-C(12)	111.2(4)	O(3)-C(12)-C(11)	112.7(4)
N(4)-C(13)-N(5)	111.2(3)	N(4)-C(13)-C(16)	127.2(4)
N(5)-C(13)-C(16)	121.6(4)	C(15)-C(14)-N(5)	108.2(3)
C(15)-C(14)-N(6)	125.8(4)	N(5)-C(14)-N(6)	125.9(4)
C(14)-C(15)-N(4)	109.0(3)	N(5)-C(17)-C(18)	111.6(3)
O(6)-C(18)-C(17)	110.2(4)	C(2B)-C(lB)-S(1)	111.2(8)

Appendix 3

Crystallographic Experimental Details for

Trans-$[Ru(ma)_2(metro)_2](CF_3SO_3)\cdot C_3H_6O$ (25)

A. Crystal Data

Empirical Formula	$C_{28}H_{34}O_{16}N_6F_3SRu$
Formula Weight	900.74
Crystal Color, Habit	blue, chip
Crystal Dimensions	0.25 x 0.15 x 0.20 mm
Crystal System	triclinic
Lattice Type	Primitive
Lattice Parameters	a = 11.087(1) Å b = 12.511(1) Å c = 13.890(2) Å α = 105.636(4)° β = 97.737(3)° γ = 99.838(4)° V = 1794.6(3) $Å^3$
Space Group	$P\bar{1}$ (#2)
Z value	2
D_{calc}	1.667 g/cm^3
F_{000}	918.00
μ(MoKα)	5.91 cm^{-1}

B. Intensity Measurements

Diffractometer	Rigaku/ADSC CCD
Radiation	MoKα (λ = 0.71069 Å) graphite monochromated
Detector Aperture	94 mm x 94 mm
Data Images	460 exposures @ 27.0 seconds
ϕ oscillation Range (X = -90.0)	0.0 - 190.0°
ω oscillation Range (X = -90.0)	-17.0 - 23.0°
Detector Position	38.14 mm
Detector Swing Angle	-5.60°
$2\theta_{max}$	55.7°
No. of Reflections Measured	Total: 16753 Unique: 7380 (R_{int} = 0.056)
Corrections	Lorentz-polarization Absorption/scaling/decay (corr. factors: 0.7654 - 1.0000)

C. Structure Solution and Refinement

Structure Solution	Patterson Methods (DIRDIF92 PATTY)
Refinement	Full-matrix least-squares
Function Minimized	$\Sigma\omega\,(Fo^2 - Fc^2)^2$
Least Squares Weights	$\omega = 1/\sigma^2(Fo^2) + (0.0665\cdot P)^2$ where $P = (\mathrm{Max}(Fo^2,0) + 2\cdot Fc^2)/3$
p-factor	0.0000
Anomalous Dispersion	All non-hydrogen atoms
No. Observations (I>0.00σ(I))	7380
No. Variables	545
Reflection/Parameter Ratio	13.54
Residuals (refined on F^2, all data): R; Rw	0.085; 0.132
Goodness of Fit Indicator	0.97
Max Shift/Error in Final Cycle	0.00
No. Observations (I>2σ(I))	5075
Residuals (refined on F, I>2σ (I)): R; Rw	0.050; 0.119
Maximum peak in Final Diff. Map	1.16 $e^-/Å^3$
Minimum peak in Final Diff. Map	-0.96 $e^-/Å^3$

Table A3.1 Atomic coordinates (x 10^4) and equivalent isotropic displacement parameters (A^2 x 10^3). U(eq) is defined as one third of the trace of the orthogonalized Uij tensor.

Atom	x	y	z	U(eq)	occ
Ru(1)	0	0	0	16(1)	
Ru(2)	0	0	5000	21(1)	
O(1)	1772(3)	234(2)	816(2)	24(1)	
O(2)	953(3)	628(2)	-931(2)	25(1)	
O(3)	4252(3)	1826(3)	-497(3)	37(1)	
O(4)	562(3)	3497(3)	3807(2)	40(1)	
O(5)	-365(3)	4673(2)	3271(2)	38(1)	
O(6)	-3001(4)	3428(3)	369(3)	41(1)	0.84(1)
O(7)	933(3)	79(2)	3827(2)	30(1)	
O(8)	1358(3)	1372(2)	5750(2)	27(1)	
O(9)	3256(3)	3162(3)	4631(3)	44(1)	
O(10)	-2814(3)	1258(3)	1833(2)	44(1)	
O(11)	-3177(4)	2832(3)	2737(3)	44(1)	
O(12)	-3952(5)	2798(4)	5640(4)	80(2)	
O(13)	-4835(4)	696(3)	3094(3)	58(1)	
N(l)	-114(3)	1627(2)	788(2)	19(1)	
N(2)	-467(3)	3364(2)	1241(3)	22(1)	
N(3)	58(3)	3800(3)	3119(3)	27(1)	
N(4)	-1020(3)	1080(3)	4540(3)	23(1)	
N(5)	-1928(3)	2512(3)	4506(3)	21(1)	

N(6)	-2741(4)	1977(3)	2648(3)	30(1)	
C(l)	2590(4)	690(3)	392(3)	25(1)	
C(2)	2179(4)	950(3)	-511(3)	26(1)	
C(3)	3022(5)	1557(4)	-908(4)	32(1)	
C(4)	4659(5)	1515(4)	318(4)	41(1)	
C(5)	3907(4)	972(4)	782(4)	33(1)	
C(6)	2705(6)	2029(5)	-1747(4)	50(1)	
C(7)	-462(4)	2458(3)	440(3)	23(1)	
C(8)	-82(4)	3085(3)	2110(3)	22(1)	
C(9)	127(4)	2028(3)	1825(3)	20(1)	
C(10)	-742(5)	2395(4)	-641(3)	36(1)	
C(11)	-832(4)	4415(3)	1126(4)	30(1)	
C(12)	-2205(5)	4364(4)	1170(4)	36(1)	
C(13)	1727(4)	1028(4)	4063(3)	29(1)	
C(14)	1924(4)	1756(3)	5078(3)	26(1)	
C(15)	2674(4)	2820(4)	5333(4)	36(1)	
C(16)	3118(5)	2447(5)	3687(5)	49(1)	
C(17)	2411(5)	1396(4)	3368(4)	39(1)	
C(18)	2930(6)	3694(4)	6324(4)	51(2)	
C(19	-1275(4)	2035(3)	5114(3)	22(1)	
C(20)	-2081(4)	1807(3)	3520(3)	23(1)	
C(21)	-1509(4)	942(3)	3550(3)	23(1)	
C(22)	-883(5)	2515(4)	6237(3)	34(1)	
C(23)	-2319(4)	3601(3)	4878(3)	26(1)	
C(24)	-3676(5)	3411(4)	4957(4)	43(1)	
C(25)	-4232(6)	-506(6)	4029(6)	68(2)	
C(26)	-5054(5)	-227(4)	3241(4)	42(1)	
C(27)	-6167(6)	-1106(5)	2626(6)	72(2)	
S(lA)	-2885(2)	4690(2)	8165(3)	72(1)	0.76(1)
O(14A)	-2102(7)	4904(11)	9111(5)	228(9)	0.76(1)
O(15A)	-2266(5)	4828(5)	7379(4)	73(2)	0.76(1)
O(16A)	-3889(7)	3760(5)	7905(7)	246(9)	0.76(1)
C(28A)	-3649(5)	5850(5)	8411(5)	64(3)	0.76(1)
F(lA)	-2847(6)	6796(4)	8595(7)	138(4)	0.76(1)
F(2A)	-4467(7)	5789(7)	7634(8)	140(4)	0.76(1)
F(3A)	-4296(7)	5878(7)	9119(7)	142(4)	0.76(1)
S(lB)	-2670(4)	5263(5)	8491(3)	24(1)	0.24(1)
O(14B)	-2128(18)	6309(8)	9217(8)	73(6)	0.24(1)
O(15B)	-2277(15)	4335(8)	8714(9)	32(4)	0.24(1)
O(16B)	-2676(18)	5259(11)	7482(6)	53(5)	0.24(1)
C(28B)	-4271(9)	5087(11)	8590(10)	41(5)	0.24(1)
F(lB)	-4889(18)	5736(16)	8253(17)	77(6)	0.24(1)
F(2B)	-4365(16)	5306(13)	9533(10)	59(4)	0.24(1)
F(3B)	-4900(15)	4068(11)	8129(12)	70(5)	0.24(1)
O(6B)	-2280(3)	5560(2)	1270(2)	66(9)	0.16(1)

Table A3.2 Bond lengths (Å).

Bond	Length	Bond	Length	Bond	Length
Ru(1)-O(2)#1	2.010(3)	Ru(1)-O(2)	2.010(3)	Ru(1)-O(1)	2.063(3)
Ru(1)-O(1)#1	2.063(3)	Ru(1)-N(1)#1	2.069(3)	Ru(1)-N(1)	2.069(3)
Ru(2)-O(8)#2	2.007(3)	Ru(2)-O(8)	2.007(3)	Ru(2)-O(7)#2	2.060(3)
Ru(2)-O(7)	2.060(3)	Ru(2)-N(4)	2.075(3)	Ru(2)-N(4)#2	2.075(3)
O(1)-C(1)	1.280(5)	O(2)-C(2)	1.350(5)	O(3)-C(4)	1.340(6)
O(3)-C(3)	1.353(6)	O(4)-N(3)	1.221(5)	O(5)-N(3)	1.240(4)
O(6)-C(12)	1.438(6)	O(7)-C(13)	1.283(5)	O(8)-C(14)	1.339(5)
O(9)-C(16)	1.345(7)	O(9)-C(15)	1.360(6)	O(10)-N(6)	1.225(5)
O(11)-N(6)	1.231(4)	O(12)-C(24)	1.404(7)	O(13)-C(26)	1.216(6)
N(1)-C(7)	1.350(5)	N(1)-C(9)	1.363(5)	N(2)-C(7)	1.358(5)
N(2)-C(8)	1.378(5)	N(2)-C(11)	1.481(5)	N(3)-C(8)	1.417(5)
N(4)-C(19)	1.345(5)	N(4)-C(21)	1.362(5)	N(5)-C(19)	1.360(5)
N(5)-C(20)	1.384(5)	N(5)-C(23)	1.481(5)	N(6)-C(20)	1.414(5)
C(1)-C(2)	1.416(6)	C(1)-C(5)	1.434(6)	C(2)-C(3)	1.369(6)
C(3)-C(6)	1.471(7)	C(4)-C(5)	1.327(7)	C(7)-C(10)	1.469(6)
C(8)-C(9)	1.344(5)	C(11)-C(12)	1.523(6)	C(13)-C(14)	1.422(6)
C(13)-C(17)	1.426(7)	C(14)-C(15)	1.370(6)	C(15)-C(18)	1.466(7)
C(16)-C(17)	1.334(8)	C(19)-C(22)	1.485(6)	C(20)-C(21)	1.352(5)
C(23)-C(24)	1.505(6)	C(25)-C(26)	1.483(8)	C(26)-C(27)	1.486(8)
S(1B)-O(14B)	1.396(5)	S(1B)-O(16B)	1.399(5)	S(1B)-O(15B)	1.402(5)
S(1B)-C(28B)	1.779(8)	C(28B)-F(2B)	1.286(6)	C(28B)-F(1B)	1.287(6)
C(28B)-F(3B)	1.287(6)	S(1A)-O(16A)	1.395(5)	S(1A)-O(15A)	1.399(4)
S(1A)-O(14A)	1.406(5)	S(1A)-C(28A)	1.781(7)	C(28A)-F(2A)	1.289(5)
C(28A)-F(3A)	1.290(5)	C(28A)-F(1A)	1.293(5)		

Table A3.3 Bond angles (°).

Bond	Angle	Bond	Angle
O(2)#1-Ru(1)-O(2)	180.0	O(2)#1-Ru(1)-O(1)	97.86(12)
O(2)-Ru(1)-O(1)	82.14(12)	O(2)#1-Ru(1)-O(1)#1	82.14(12)
O(2)-Ru(1)-O(1)#1	97.86(12)	O(1)-Ru(1)-O(1)#1	180.0
O(2)#1-Ru(1)-N(1)#1	90.01(12)	O(2)-Ru(1)-N(1)#1	89.99(12)
O(1)-Ru(1)-N(1)#1	89.12(11)	O(1)#1-Ru(1)-N(1)#1	90.88(11)
O(2)#1-Ru(1)-N(1)	89.99(12)	O(2)-Ru(1)-N(1)	90.01(12)
O(1)-Ru(1)-N(1)	90.88(11)	O(1)#1-Ru(1)-N(1)	89.12(11)
N(1)#1-Ru(1)-N(1)	180.0	O(8)#2-Ru(2)-O(8)	180.0
O(8)#2-Ru(2)-O(7)#2	81.48(12)	O(8)-Ru(2)-O(7)#2	98.52(12)
O(8)#2-Ru(2)-O(7)	98.52(12)	O(8)-Ru(2)-O(7)	81.48(12)
O(7)#2-Ru(2)-O(7)	180.0	O(8)#2-Ru(2)-N(4)	91.92(12)
O(8)-Ru(2)-N(4)	88.07(12)	O(7)#2-Ru(2)-N(4)	93.18(13)
O(7)-Ru(2)-N(4)	86.82(13)	O(8)#2-Ru(2)-N(4)#2	88.07(12)
O(8)-Ru(2)-N(4)#2	91.93(12)	O(7)#2-Ru(2)-N(4)#2	86.82(13)
O(7)-Ru(2)-N(4)#2	93.18(13)	N(4)-Ru(2)-N(4)#2	179.999(1)

C(1)-O(1)-Ru(1)	110.7(3)	C(2)-O(2)-Ru(1)	109.7(3)
C(4)-O(3)-C(3)	120.1(4)	C(13)-O(7)-Ru(2)	110.6(3)
C(14)-O(8)-Ru(2)	109.3(2)	C(16)-O(9)-C(15)	120.1(4)
C(7)-N(1)-C(9)	107.0(3)	C(7)-N(1)-Ru(1)	130.1(3)
C(9)-N(1)-Ru(1)	122.8(3)	C(7)-N(2)-C(8)	106.6(3)
C(7)-N(2)-C(11)	123.4(4)	C(8)-N(2)-C(11)	130.0(3)
O(4)-N(3)-O(5)	123.0(3)	O(4)-N(3)-C(8)	117.5(3)
O(5)-N(3)-C(8)	119.4(4)	C(19)-N(4)-C(21)	107.9(3)
C(19)-N(4)-Ru(2)	128.4(3)	C(21)-N(4)-Ru(2)	123.6(3)
C(19)-N(5)-C(20)	106.3(3)	C(19)-N(5)-C(23)	124.2(3)
C(20)-N(5)-C(23)	129.5(3)	O(10)-N(6)-O(11)	123.8(4)
O(10)-N(6)-C(20)	116.6(3)	O(11)-N(6)-C(20)	119.6(4)
O(1)-C(1)-C(2)	118.6(4)	O(1)-C(1)-C(5)	124.2(4)
C(2)-C(1)-C(5)	117.3(4)	O(2)-C(2)-C(3)	122.1(4)
O(2)-C(2)-C(1)	118.5(4)	C(3)-C(2)-C(1)	119.3(4)
O(3)-C(3)-C(2)	120.8(4)	O(3)-C(3)-C(6)	113.9(4)
C(2)-C(3)-C(6)	125.2(5)	C(5)-C(4)-O(3)	123.3(5)
C(4)-C(5)-C(1)	118.8(5)	N(1)-C(7)-N(2)	109.5(4)
N(1)-C(7)-C(10)	124.6(3)	N(2)-C(7)-C(10)	125.9(4)
C(9)-C(8)-N(2)	108.0(3)	C(9)-C(8)-N(3)	126.8(4)
N(2)-C(8)-N(3)	125.2(3)	C(8)-C(9)-N(1)	108.9(4)
N(2)-C(11)-C(12)	111.0(3)	O(6)-C(12)-C(11)	111.9(4)
O(7)-C(13)-C(14)	117.6(4)	O(7)-C(13)-C(17)	124.0(4)
C(14)-C(13)-C(17)	118.4(4)	O(8)-C(14)-C(15)	122.4(4)
O(8)-C(14)-C(13)	118.3(4)	C(15)-C(14)-C(13)	119.3(4)
O(9)-C(15)-C(14)	120.3(4)	O(9)-C(15)-C(18)	113.2(4)
C(14)-C(15)-C(18)	126.5(5)	C(17)-C(16)-O(9)	124.0(5)
C(16)-C(17)-C(13)	117.7(5)	N(4)-C(19)-N(5)	109.5(3)
N(4)-C(19)-C(22)	125.5(4)	N(5)-C(19)-C(22)	125.0(3)
C(21)-C(20)-N(5)	108.2(3)	C(21)-C(20)-N(6)	127.0(4)
N(5)-C(20)-N(6)	124.8(3)	C(20)-C(21)-N(4)	108.2(3)
N(5)-C(23)-C(24)	111.6(3)	O(12)-C(24)-C(23)	112.7(4)
O(13)-C(26)-C(25)	121.5(5)	O(13)-C(26)-C(27)	120.1(5)
C(25)-C(26)-C(27)	11.8.4(5)	O(14B)-S(1B)-O(16B)	114.6(5)
O(14B)-S(1B)-O(15B)	114.2(5)	O(16B)-S(1B)-O(15B)	113.6(5)
O(14B)-S(1B)-C(28B)	102.9(10)	O(16B)-S(1B)-C(28B)	104.0(10)
O(15B)-S(1B)-C(28B)	105.9(9)	F(2B)-C(28B)-F(1B)	104.4(15)
F(2B)-C(28B)-F(3B)	107.5(14)	F(1B)-C(28B)-F(3B)	105.2(14)
F(2B)-C(28B)-S(1B)	109.6(11)	F(1B)-C(28B)-S(1B)	116.9(13)
F(3B)-C(28B)-S(1B)	112.7(11)	O(16A)-S(1A)-O(15A)	116.0(3)
O(16A)-S(1A)-O(14A)	115.8(3)	O(15A)-S(1A)-O(14A)	114.8(3)
O(16A)-S(1A)-C(28A)	101.7(4)	O(15A)-S(1A)-C(28A)	103.7(4)
O(14A)-S(1A)-C(28A)	101.6(6)	F(2A)-C(28A)-F(3A)	102.9(8)
F(2A)-C(28A)-F(1A)	106.3(7)	F(3A)-C(28A)-F(1A)	111.6(7)
F(2A)-C(28A)-S(1A)	111.8(5)	F(3A)-C(28A)-S(1A)	114.0(5)
F(1A)-C(28A)-S(1A)	109.9(5)		

Table A3.4 Hydrogen-bonding interactions.

Donor-H···Acceptor	D-H (Å)	H···A (Å)	D···A (Å)	D-H···A (°)
O(12)-H(12)···O(15A)	0.8400	2.3611	3.104(8)	147.71
O(12)-H(12)···O(16A)	0.8400	2.2755	3.037(11)	150.84

Appendix 4

A Typical MTT Drug Dilution Sheet

Table A4.1 Stock solution preparation for $Ru(ma)_2(DMSO)_2$ **(11)**.

Complex	$Ru(ma)_2(DMSO)_2$
Molecular weight (g/mol)	507.543
Compound used (mg)	15
Diluent	PBS
Diluent volume (mL)	5
Initial working concentration (mM)	5.911
Total working volume (mL)	5
Amount per well (μL)	100
Dilution factor (200 μL total/100μL drug volume)	2

Table A4.2 Serial dilution data of $Ru(ma)_2(DMSO)_2$ **(11)**.

Final conc. (mM)	Volume of working solution (mL)	Volume of diluent (medium, mL)	Volume remaining for addition to MTT plate (mL)
2	3.38	1.62	2.50
1	2.50	2.50	1.25
0.75	3.75	1.25	1.67
0.5	3.33	1.67	2.50
0.25	2.50	2.50	3.00
0.1	2.50	3.00	4.50
0.01	0.50	4.50	4.50
0.001	0.50	4.50	5.00

Appendix 5

The MTT Plots for the Ruthenium Complexes

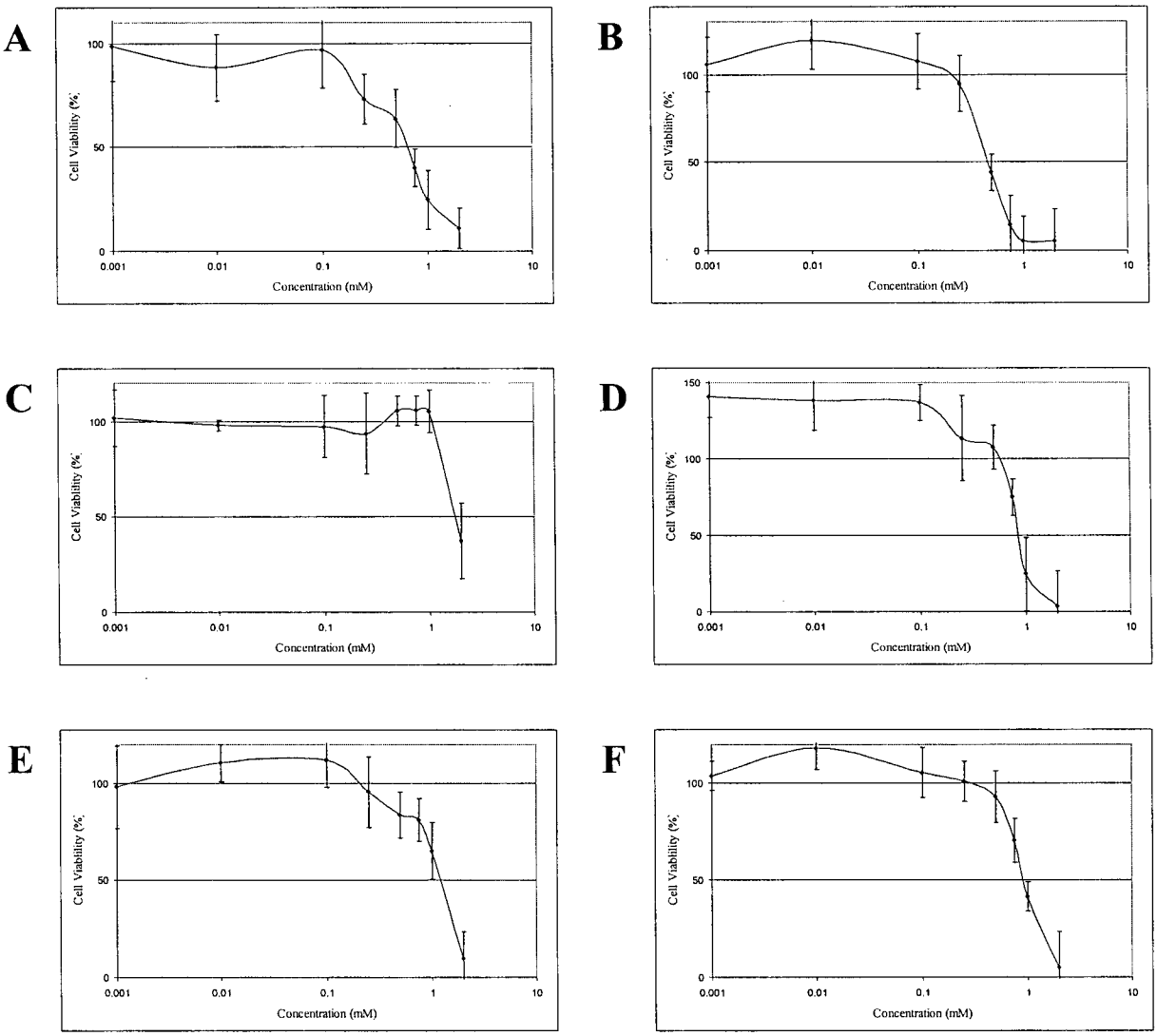

Figure A5.1 The MTT plots for $Ru(ma)_2(DMSO)_2$ (**11**) (A), $Ru(etma)_2(DMSO)_2$ (**12**) (B), $Ru(ma)_2(TMSO)_2$ (**13**) (C), $Ru(etma)_2(TMSO)_2$ (**14**) (D), *cis*-$Ru(ma)_2(BESE)$ (**17**) (E), and *cis*-$Ru(etma)_2(BESE)$ (**18**) (F).

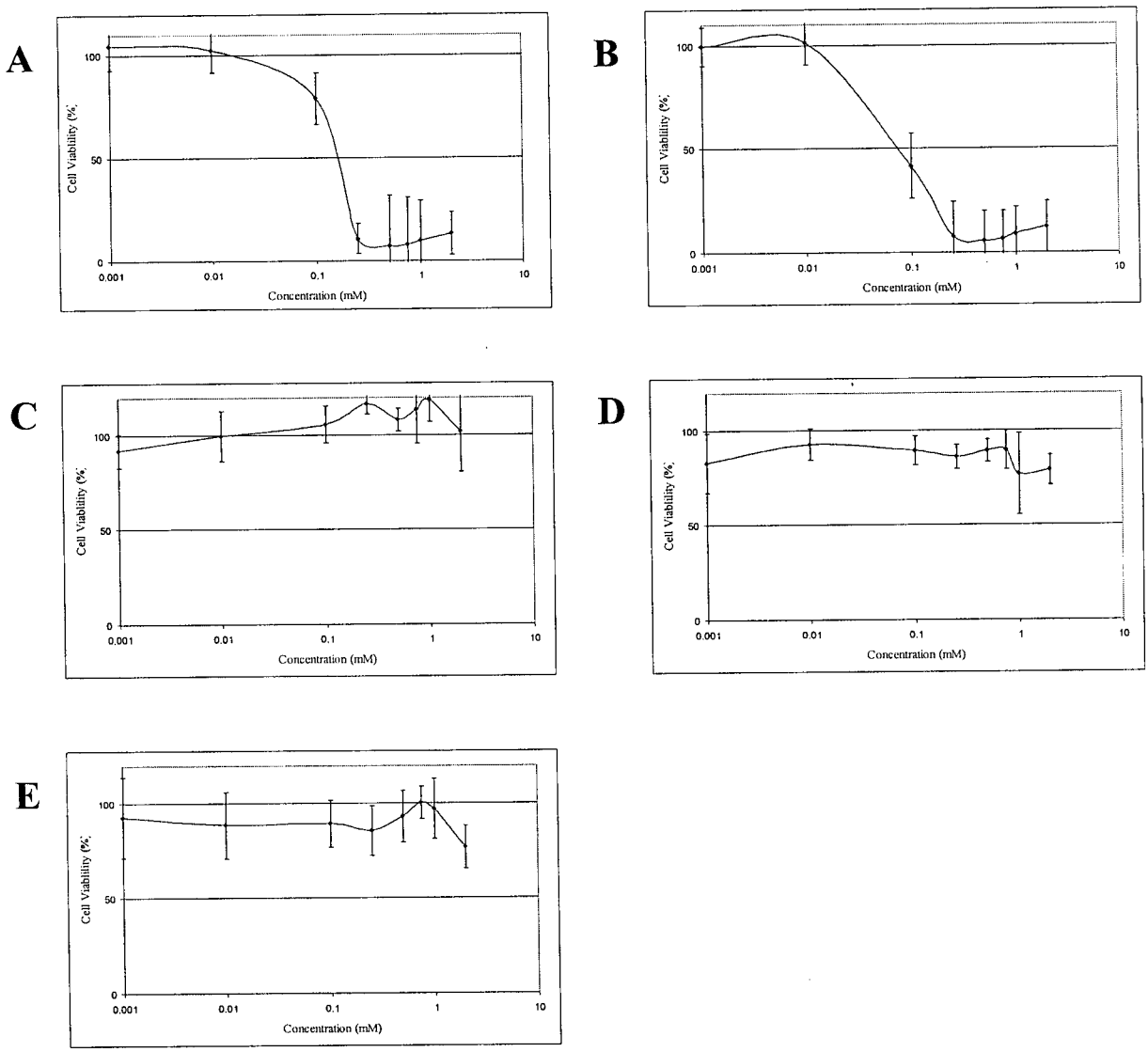

Figure A5.2 The MTT plots for *mer*-Ru(ma)$_3$ (**23**) (A), *mer*-Ru(etma)$_3$ (**24**) (B), $RuCl_3 \cdot 3H_2O$ (C), *cis*-$RuCl_2(DMSO)_3(DMSO)$ (**1**) (D), and $RuCl_2(BESE)(metro)_2$ (**19**) (E).